

## CHARACTERISATION AND MODEL COMPOUND STUDIES ON Pd AND Ni/Mo HYDROUS TITANIUM OXIDES

Lindsey E. Hayes, Colin E. Snape and Stanley Affrossman  
University of Strathclyde, Dept. of Pure & Applied Chemistry,  
Thomas Graham Building, 295 Cathedral St., Glasgow G1 1XL, UK

**Keywords:** Hydrogenation mechanism, characterisation, activity.

### ABSTRACT

Pd and Ni/Mo exchanged hydrous titanium oxides (HTOs) have high activities for hydrogenation and hydroprocessing reactions, respectively which arise principally from the effective dispersion of the active phases and the acidity of the substrate. This paper covers (i) the use of deuterated substrates to investigate the mechanism of pyrene hydrogenation with Pd-HTOs, (ii) the use of XPS and EXAFS to investigate the dispersion of the Pd and Ni/Mo and (iii) the impact of ion-exchange procedures on the activity of Ni/Mo-HTOs for hydrodesulphurisation (HDS) and hydrodenitrogenation (HDN). The deuteration experiments indicated that acidic hydrogen on the HTO does not participate in hydrogenation despite the broad correlation of activity with the substrate acidity. XPS and EXAFS indicated that the Pd and sulphided Mo phases on HTOs are smaller than on other substrates, such as  $\gamma$ -alumina where impregnation procedures are used. Indeed, EXAFS has provided evidence for the existence of a mixed 'Ni-Mo-S' phase. Hydrogenation and hydrogenolysis activities and selectivities in HDS of dibenzothiophene and quinoline vary considerably as a function of substrate surface area, preparation procedure and calcination temperature.

### INTRODUCTION

Hydrous metal oxide ion-exchange compounds of Ti, Zr, Nb and Ta were developed originally for the preparation of ceramic materials [1] and the decontamination of aqueous nuclear wastes [2]. However, the high surface areas and ion-exchange capacities, variable acidities and relatively good thermal stability make these amorphous materials ideal substrates for transition metal, metal oxide and metal sulphide catalysts. Indeed, research to date has shown that Pd-hydrous titanium oxides (HTOs, the cheapest hydrous metal oxide to prepare) have considerably higher activities than Pd- $\gamma$ -alumina catalysts for the hydrogenation of polynuclear aromatic compounds, such as pyrene [3]. Active carbon is the only widely-used support for Pd that has been found to give comparable activities to the HTOs [4]. Moreover, activities of Ni/Mo-HTOs have been found to be broadly comparable to their  $\gamma$ -alumina counterparts for hydroprocessing coal tars [5] and heavy coal liquids [6] and they do not undergo rapid deactivation. However, there are a large number of variables involved in the preparation of HTOs and their compositions, particularly in relation to catalytic activity, remain important topics for research.

In this paper, the following aspects of structure and reactivity of HTOs are addressed.

- (i) The use of X-ray photoelectron spectroscopy (XPS) and extended X-ray adsorption fine structure (EXAFS) to investigate the dispersions of Pd and sulphided Ni/Mo, respectively.
- (ii) The use of deuterated substrates to investigate whether acidic hydrogen participates in the mechanism for pyrene hydrogenation with Pd-HTOs.
- (iii) The impact of ion-exchange and calcination procedures on activity and selectivity in hydrodesulphurisation (HDS) and hydrodenitrogenation (HDN).

### EXPERIMENTAL

#### Catalyst preparation

Sodium hydrous titanium oxide substrates (Na-HTOs) were prepared as described [3-6] previously by hydrolysing the soluble intermediate formed from titanium tetraisopropoxyl and a methanolic solution of sodium hydroxide. The atomic ratio of Na to Ti was 0.5 for all the substrates used in this investigation. To increase the surface areas of the HTOs, about 15% w/w of silica was incorporated into the substrates using the appropriate amount of silicon tetraethyl in the preparation [7]. Pd was ion-

exchanged onto the Na-HTOs to give nominal loadings in the range 1-20% w/w using two procedures. In the first, Pd was dissolved in a mixture of concentrated nitric and hydrochloric acids and diluted to a pH of 1. Following ion-exchange with the appropriate volume of solution, the Pd-HTO was filtered, washed with acetone/water and dried under vacuum. In the second method, the Na-HTO was contacted with an aqueous solution of  $\text{Pd}(\text{NH}_3)_4\text{Cl}_2 \cdot \text{H}_2\text{O}$  and, after filtration and washing, the catalyst was acidified with phosphoric acid to a pH of 3-4. All the Pd-HTOs were calcined at 350°C for 10 minutes. For deuteration experiments, Pd-HTOs were prepared by these two methods but using the corresponding deuterated mineral acids.

A series of Ni/Mo-HTOs were prepared with a nominal loading of 10% Mo and the Ni concentration was varied between 1 and 7% w/w. Table 1 summarises the variables in the preparation procedure which included the substrate surface area, the order of ion-exchanging Ni and Mo in conjunction with substrate acidity, calcination temperature and whether or not the HTO was calcined in between ion-exchanging Ni and Mo. The nickel was loaded from nickel nitrate solution at a pH of 4 and Mo from ammonium heptamolybdate solution at the same pH. Sulphuric acid was used to acidify the HTOs in all the preparation stages.

#### Characterisation

Nitrogen BET surface areas of most of the HTOs were determined and typical values are summarised in Table 2. Incorporating silica into the substrate and exchanging Pd for Na greatly increased the surface area from the typical baseline value of  $80 \text{ m}^2 \text{ g}^{-1}$  for the Na-HTO. Mo concentrations were determined directly from XRF and indirectly by AA using the ammonium heptamolybdate solutions after ion-exchange.

The Pd and Ni/Mo HTOs have been analysed using XPS at each stage in their preparation procedures. The spectrometer comprised a Vacuum Science Workshop 100 mm hemispherical analyser with an Al anode as the X-ray source giving  $\text{AlK}_\alpha$  radiation at 1486.6 eV. The powdered samples were adhered to conventional SEM stubs with double-sided cello tape and evacuated to  $10^{-6}$  torr before transfer from the entry to the main chamber for analysis. Ni EXAFS was carried out at the Daresbury laboratory using station 7.1. with monochromatic X-rays having a wavelength of  $1.488 \text{ \AA}$ .

#### Activity measurements

Pyrene was hydrogenated at 100°C and 10 bar pressure using stainless steel tubing bomb microreactors (TBM) immersed in a fluidised sandbath and agitated via a flask shaker and ball bearings in the reactors [3]. 0.1g of pyrene was used with n-hexadecane as an inert diluent and 20mg of catalyst. After the desired reaction period, the TBMs were quenched in water and the reaction mixture was recovered for gas chromatographic (GC) analysis.

HDS and HDN activities of the Ni/Mo catalysts were assessed using dibenzothiophene and quinoline respectively. For purposes of comparison, tests were also carried out with a commercially available Ni/Mo- $\gamma$ -alumina catalyst (Akzo 153). The catalysts were pre-sulphided at 400°C prior to the tests using a large stoichiometric excess of hydrogen sulphide in hydrogen. Both the HDS and HDN tests were conducted at 350°C and 70 bar pressure (cold) in TBMs. These were loaded with 20 mg of catalyst and  $1 \text{ cm}^3$  of 0.06 molar solutions of dibenzothiophene and quinoline in n-decane or n-hexadecane containing a different n-alkane as internal standard [8]. After the desired reaction period, the solutions were recovered and the product distributions were determined by GC.

## **RESULTS AND DISCUSSION**

#### Hydrogenation activity and XPS characterisation of Pd-HTOs

The hydrogenation of pyrene to di- and tetrahydropyrenes can be conveniently modelled as a pseudo first order reaction [3]. The rate constants on a weight of catalyst basis are presented in Figure 1 for the two methods used to ion-exchange Pd onto the HTOs. As the Pd concentration is increased from 1 to 20% (maximum ion-exchange capacity of Pd is about 23% w/w of dry catalyst), the rate constants increase linearly, i.e. they remain virtually constant with respect to the weight of Pd. However, the activities of the HTOs prepared from Pd dissolved in aqua regia are vastly higher than those prepared from the tetra-amine salt. Apart from a possible inhibiting effect from the amine ligands, the key difference in the two methods is that with the tetra-amine salt, the catalyst is acidified after rather than during ion-exchange. As reported previously [3], activity does broadly correlate with substrate acidity

as demonstrated by the fact that the neutral Pd-HTO gave an extremely low conversion, but other more subtle effects such as the Pd precursor used can also be important. For a given preparation method, the hydrogenation activity has been found to broadly correlate with the substrate BET surface area [4].

Figure 2 presents the surface atomic Pd/Ti ratios for the two methods used to prepare the Pd-HTOs. For the method employing the tetraamine salt as the Pd precursor, the Pd/Ti increases linearly with Pd concentration up to the highest loading used of 20% w/w in accord with the increase in the rate constant for pyrene hydrogenation (Figure 1) and suggesting that the dispersion of the Pd does not vary markedly. In contrast, for the method using Pd dissolved in aqueous regia, the Pd/Ti ratios plateau at approximately 5% Pd despite the hydrogenation rate constant increasing linearly with Pd concentration. Up to a loading of 5% Pd, both methods give the same Pd/Ti ratio. It is proposed that this apparent difference arises from a kinetic effect with much faster ion-exchange of Pd occurring on the HTO surface when the Pd is dissolved in acid.

The results above and previous work [3] suggest that the acidic protons on the HTOs may participate in the hydrogenation reaction in much the same way as with super acids. To test this ascription, the Pd-HTOs deuterated acids were used instead of the corresponding mineral acids in the preparations of the Pd-HTOs. Moreover, the reactions with deuterium-labelled Pd-HTOs were carried out under conditions where the concentrations of acidic deuterium on the catalyst were vastly in excess of the amount of hydrogen required. GC-MS analyses of the hydrogenated pyrenes indicated that the acidic deuterium had not been incorporated in measurable quantities and, therefore, it is suggested that the primary role of the acidic substrate in hydrogenation and indeed, also in HDS and HDN, is to facilitate the adsorption of aromatic species.

#### Characterisation of Ni/Mo HTOs

Figure 3 presents the XPS-determined surface Mo concentrations for two Mo- and a Ni/Mo-HTO, together with that for the commercial  $\gamma$ -alumina catalyst. The surface Mo concentrations increase linearly with the bulk concentration up to a loading of 20% w/w. For nominal bulk loadings of about 10% Mo, the surface concentration is higher on the HTOs (Figure 3). EXAFS provides evidence that the dispersion of Ni is also superior on the HTOs than on  $\gamma$ -alumina. In the EXAFS transforms for supports containing only sulphided Ni, the characteristic Ni-Ni peak at about 3.0 Å was virtually absent for the HTOs whereas it was a prominent feature for  $\gamma$ -alumina. For the Ni/Mo catalysts, the peak due to the mixed Ni-Mo-sulphide phase at about 2.8 Å was less pronounced for the HTO than for the commercial  $\gamma$ -alumina catalyst (Figure 4). However, this difference is attributed to the fact that the HTO was calcined in between ion-exchanging Ni and Mo and that the Ni concentration was higher (5 cf 2.5 %) meaning that a smaller proportion of the Ni is likely to be in the mixed phase.

#### Hydrodesulphurisation and hydrodenitrogenation

Figures 5 and 6 summarise the product distributions obtained from the HDS and HDN tests on dibenzothiophene and quinoline, respectively with the Ni/Mo HTOs (M1A-M7A, Table 1) and the commercial  $\gamma$ -alumina catalyst. The highest activities for the HTOs were observed for those samples not calcined between ion-exchanging the Ni and Mo (M2A and M7A) possibly due to maximising the concentration of the catalytically active mixed Ni-Mo-sulphide phase. Indeed, the activities of these HTOs were comparable to that of the  $\gamma$ -alumina catalyst for HDS (Figure 5) and superior for HDN where higher concentrations of propylcyclohexane and propylbenzene were obtained (Figure 6). However, it should be pointed out that the activities of commercial  $\gamma$ -alumina catalysts can vary considerably and the HDN activity of Akzo 153 may be less than that of other corresponding samples.

All the HTOs discussed above were calcined at 500°C because results for thiophene indicated that HDS activity increased markedly as the calcination temperature is increased above 400°C. Figures 7 and 8 present the variations in HDS and HDN activity for dibenzothiophene and quinoline, respectively as the calcination temperature is increased from 350 to 550°C. For HDS, the activity increases considerably and the extent of hydrogenation as indicated by the concentrations of bicyclohexyl decreases. Similarly for HDN, an increase in hydrogenolysis activity for removal of the heteroatom is observed. Interestingly, these significant changes in activity with increasing temperature must be accompanied by increasing amounts of the amorphous HTOs being converted into crystalline titania (primarily anatase as indicated by XRD).

## ACKNOWLEDGEMENTS

The authors thank SERC for financial support (Grant no. GR/T/03226 and studentship for LEH), Mr. C. Saenz and Ms. L. Stephen for helping to carry out the experimental programme and Dr. H.P. Stephens and colleagues at Sandia National Laboratories for many helpful discussions.

## REFERENCES

1. Dosch, R.G. and O'Neill, W.M., US Patent 3,699,044, 1972.
2. Dosch, R.G., Headley, T.J. and Hlava, P.F., *J. Am. Chem. Soc.*, 1984, 67, 354.
3. Stephens, H.P. and Dosch, R.G., Proc. of 4th Int. Symp. on the Scientific Bases for the Preparation of Heterogeneous Catalysts, Belgium, Eds. Delman, B. and Yales, J.T., 1987, p271.
4. Hayes, L.E., Ph.D thesis, University of Strathclyde, in preparation.
5. Stephens, H.P., Bolton, C. and Snape, C.E., *Fuel*, 1989, 68, 161.
6. Stohl, F.V., Dosch, R.G. and Stephens, H.P., *Proc. Direct Liquefaction Contractors Review meeting*, Pittsburgh, Oct. 1988, p490.
7. Dosch, R.G., Stohl, F.V. and Richardson, J., *Prepr. Am. Chem. Soc. Div. Fuel Chem.*, 1989, 34(4), 1415.
8. Moreau, C., Durand, R., Zmimita, N. and Geneste, P., *J. Catal.*, 1988, 112, 411.

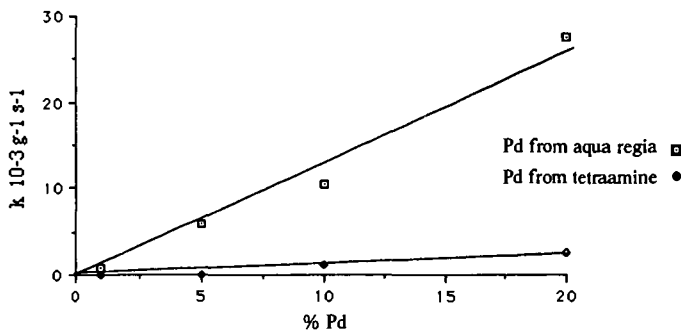


FIGURE 1 RATE CONSTANTS FOR PYRENE HYDROGENATION

**Table 1 Typical BET surface areas of the HTOs**

Type of HTO	Surface area m <sup>2</sup> g <sup>-1</sup>
Na-HTO ( atomic Na/Ti ratio = 0.5)	98
Na-HTO/silica (about 15% w/w silica)	204
10% Pd-HTO	170
10% Pd-HTO/silica	310
Ni/Mo-HTO (about 3% Ni, 10% Mo)	73
Ni/Mo-HTO/silica	270

**Table 2 Summary of high surface area Ni/Mo HTO/silica catalysts prepared**

Designation	Ion-exchange sequence		No. of calcinations <sup>a</sup>	Removal of Na <sup>b</sup>
M1A	1. Mo	2. Ni	2	No
M2A	1. Mo	2. Ni	1	No
M3A	1. Ni	2. Mo	2	No
M4A	1. Mo	2. Ni	2	No
M5A	1. Mo	2. Ni	2	Yes (pH 2.5)
M6A	1. Mo	2. Ni	2	Yes (pH 4)
M7A	1. Ni	2. Mo	1	No

<sup>a</sup> = two corresponds to calcining between the ion-exchange steps.

<sup>b</sup> = sodium removed via acidification prior to ion-exchange of Mo.

The pH of the molybdate solution was adjusted to 4 except for M1A where it was 2.5.

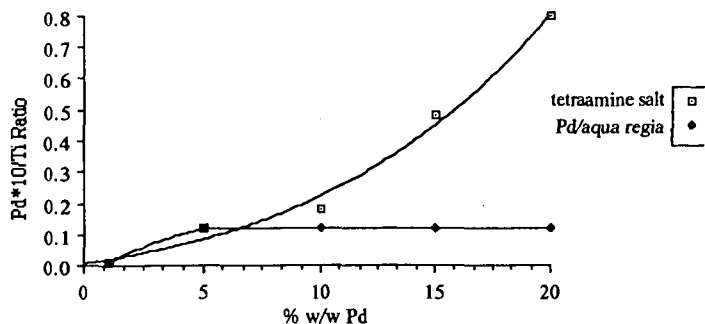


FIGURE 2 Pd/Ti RATIOS VS. BULK Pd CONCENTRATIONS

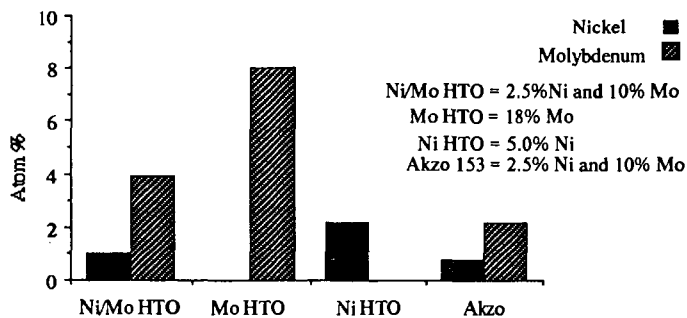


FIGURE 3 XPS-DETERMINED SURFACE CONCENTRATIONS

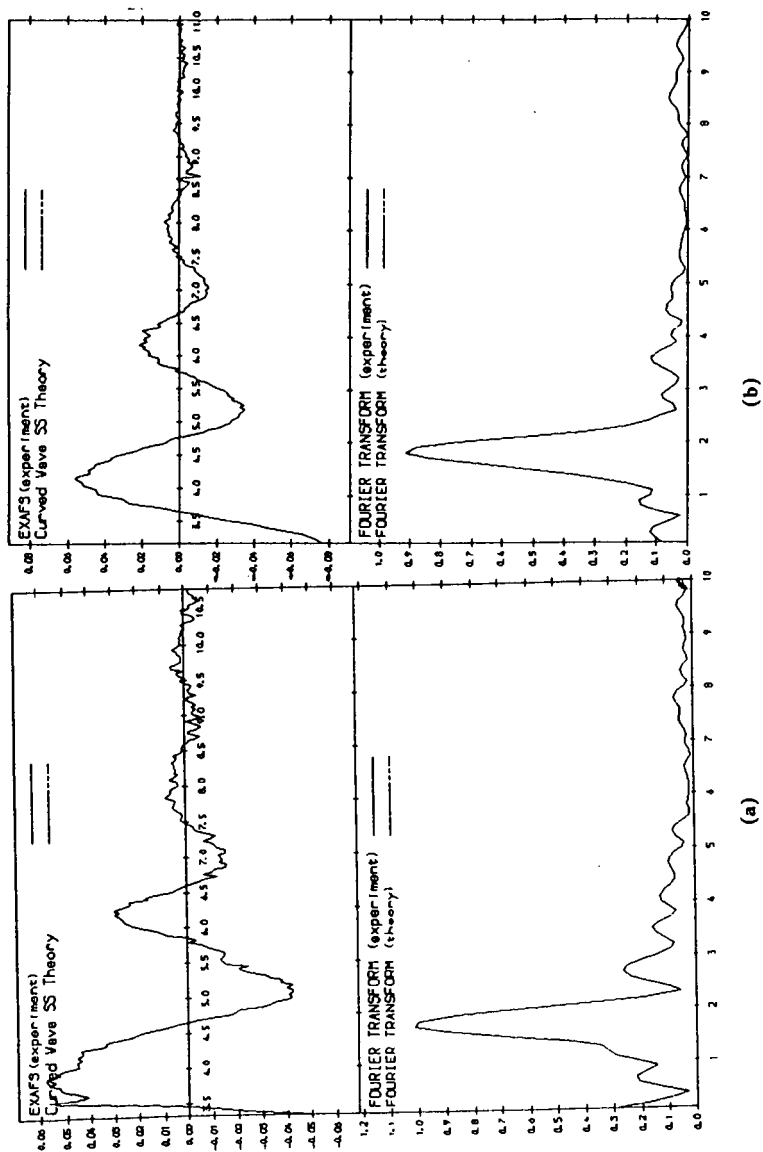


FIGURE 4 RAW AND TRANSFORMED Ni EXAFS DATA FOR Ni/Mo (a)  $\gamma$ -ALUMINA AND (b) HTO CATALYSTS

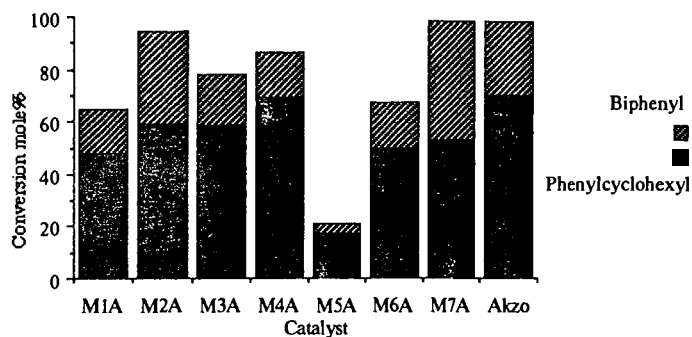


FIGURE 5 HDS OF DIBENZOTHIOPHENE

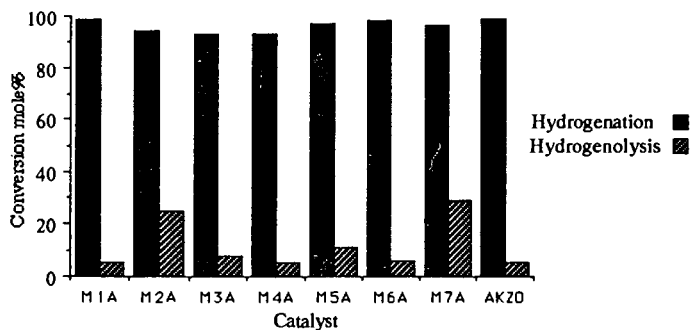


FIGURE 6 HDN OF QUINOLINE



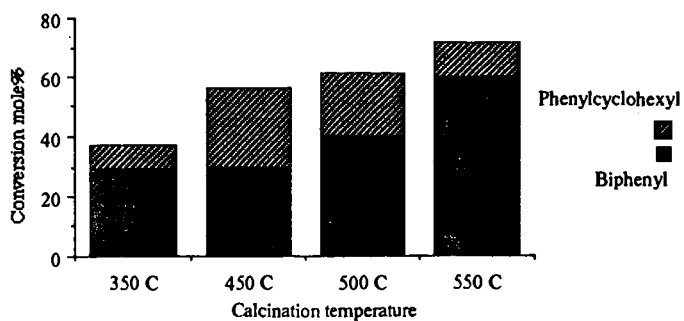


FIGURE 7 EFFECT OF CALCINATION TEMP. ON HDS ACTIVITIES

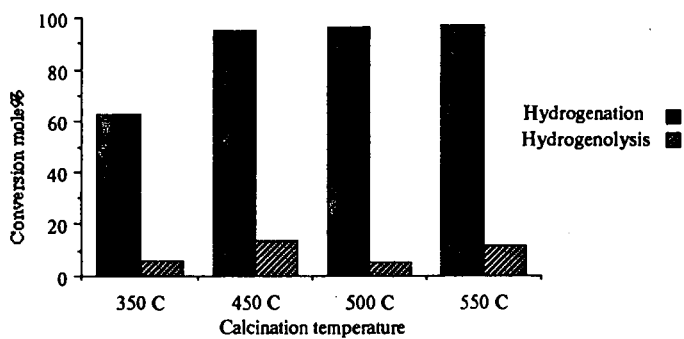


FIGURE 8 EFFECT OF CALCINATION TEMP. ON HDN ACTIVITIES

## REACTIONS OF PROPANE ON HYDROUS METAL OXIDE-SUPPORTED CATALYSTS

Zhentao Feng and Rayford G. Anthony  
Department of Chemical Engineering, Texas A&M University  
College Station, TX 77843

Keywords: propane, dehydrogenation, metal oxide

### INTRODUCTION

There are strong economical incentives today to develop catalysts for the selective conversion of light paraffins, especially propane. Formation of propylene, aliphatics or aromatics is favorable. Previous work has shown catalytic conversion of propane on HZSM-5 (Inui and Okazumi, 1984; Kitagawa et al., 1986; Scurrrell, 1988). The main products are benzene, toluene and xylenes. In this work, a relatively new type of catalyst is prepared for the reaction of propane, i.e., hydrous metal oxides.

Hydrous metal oxides were first used for waste water treatment and direct coal liquefaction (Stephens et al., 1985). Research on these materials identified several properties that might make hydrous metal oxides useful as catalyst supports. They include high surface area, large ion exchange capacity, dual ion exchange properties for cation and anion, and strong thermal stability (Lehto, 1987). This study employed hydrous metal oxides as catalyst supports for the synthesis of catalysts for the propane transformation.

### EXPERIMENTAL

**Catalysts.** Sol-gel method was used to prepare two different types of hydrous metal oxides, i.e., hydrous silicon titanium oxide and hydrous zirconium oxide. The main procedure followed the patent by Dosch et al. (1985):

Tetraisoethyl titanate was mixed with tetraorthoethyl silicate to get a clear solution. Then slowly add the alkoxide mixture into a 10 wt% methanol solution of sodium hydroxide to get a very thick soluble intermediate. The intermediate was rapidly added to a solution of 1:10 water and acetone. The slurry was continuously stirred until it was homogenized. Filter the mixture and rinse with acetone. Collect the precipitate and dry it in vacuum at 80 °C overnight. This procedure was used to prepare hydrous silicon titanium oxide.

Hydrous zirconium oxide was synthesized by the same procedure, except that zirconium propoxide and potassium hydroxide were used. These two types of hydrous metal oxides were incorporated with Mo, Ni, Pd or Zr via ion exchange. After ion exchange, the catalysts were treated with sulfuric acid and then calcined in air at 540 °C.

**Activity Tests.** Activities of the catalysts were determined by their performance in the reactions of propane. Reactions were carried out isothermally in a Pyrex reactor under atmospheric pressure. Reaction temperature was 600 °C. The feed was 20% propane in nitrogen. Propane weight hour space velocity was 1.5 to 1.9. Composition of products was obtained with two GCs using a flame ionization detector and a thermal conductivity detector, respectively.

## RESULTS

*Characterization of Catalysts.* Hydrous metal oxides as prepared were amorphous materials with 30% to 35% volatile. The surface areas of hydrous silicon titanium oxide and hydrous zirconium oxide were 390 m<sup>2</sup>/g and 260 m<sup>2</sup>/g, respectively. The pore volume was 0.6 cc/g with pore diameters in the range of mesopores. After ion exchange, the weight percent of Pd, Mo, Ni and Zr in the catalysts were 0.52%, 15%, 1.4% and 14% respectively based on dry weight. After calcination, hydrous silicon titanium oxide and hydrous zirconium oxide changed to their oxide forms, i.e., silica, titania and zirconia. X-ray diffraction showed that titania was predominately anatase with a small amount of rutile, while the phase of zirconia was cubic.

NaOH titration and temperature programmed desorption of ammonia experiments showed that the catalysts synthesized were weak acidic materials. Zirconia supported catalysts had higher acidity than the corresponding silica titania catalysts. Figure 1 is the ammonia TPD of Pd on zirconia and Pd on silica titania. Most of the ammonia desorbed below 250 °C, which indicates the absence of strong acid sites.

*Activity Tests.* Figure 2 is the summary of the activity tests on the catalysts. Dehydrogenation was the main reaction of propane and propylene was the largest reaction product. The change of propylene selectivity at different levels of propane conversion is shown on the figure. For silica titania supported catalysts, propane conversion ranged from 10% to 20% and propylene molar selectivity from 55% to 70%. For most zirconia supported catalysts, the conversion of propane was higher, up to 30% to 47%.

Besides propylene, the product consisted of methane, ethane, ethylene, small amounts of aromatics and C<sub>4</sub> to C<sub>6</sub> aliphatics. Figure 3 is the product distribution of propane reaction on silica titania supported molybdenum. Molar selectivities to light hydrocarbons ranged from 5% to 15% without significant change with time on stream.

Figure 4 shows the effects of active metals on propane conversion. The three catalysts were Pd, Mo and Ni supported on zirconia. The comparison indicated that palladium was the most active among these three metals.

## DISCUSSION

From thermodynamic equilibrium point of view, propane converts to light hydrocarbons (methane, ethane, etc.) and aromatics much more favorably than to propylene. The results of this study showed just the opposite. Propylene was the main reaction product. Previous work (Riley and Anthony, 1986) on alkane transformation over HZSM-5 showed the formation and reactions of carbonium ions on the catalysts surface. On strong acid sites, carbonium ions would undergo cracking and aromatization reactions forming methane, ethane and aromatics. However, the catalysts in this study are weak acidic materials, consequently the formation and reactions of carbonium ions are less favorable. The mechanisms of propane

reaction on these catalysts are hydride abstraction on the dispersed metals. Hydride abstraction of propane produces propylene and hydrogen. Palladium has relatively strong interactions with hydrides and hence shows higher activity, which coincides with the experimental results. Beside hydride abstraction, carbonium ion formation and reactions, though not as important as that on zeolite, also contributes to the reaction. Zirconia supported catalysts have stronger acidity than titania supported ones, and hence higher amount of light hydrocarbons and aromatics are produced.

The equilibria conversion of propane to propylene at 600 °C is about 45%. Some catalysts in this study achieved about 35% to 45% conversion. Most catalysts showed high selectivity to propylene (about 60%). Therefore, hydrous metal oxides show considerable potential for the synthesis of catalysts for propane dehydrogenation.

#### ACKNOWLEDGEMENTS

The synthesis of the palladium catalysts by Dr. R.G. Dosch of Sandia National Laboratories is very much appreciated. The financial support of Texaco, Inc for the Texas A&M Research Foundation Project 6448 is also gratefully appreciated.

#### REFERENCES

1. Dosch, R.G., H.P. Stephens, and F.V. Stool, U.S. Patent 4,511,455, 1985.
2. Feng, Z., M.S. Thesis, Texas A&M University, 1991.
3. Inui, T., and Okazumi, "Propane Conversion to Aromatic Hydrocarbons on Pt/H-ZSM-5 Catalysts," *Journal of Catalysis*, 90, 366, 1984.
4. Kitagawa, H., Y. Sendoda, and Y. Ono, "Transformation of Propane into Aromatic Hydrocarbons over ZSM-5 Zeolites," *Journal of Catalysis*, 101, 12, 1986.
5. Lehto, J., "Sodium Titanate for Solidification of Radioactive Waste - Preparation, Structure and Ion Exchange Properties," Academic Dissertation, Department of Radiochemistry, University of Helsinki, 1987.
6. Riley, M.G., and R.G. Anthony, "Transition-State Selectivity in the Cracking of N-Heptane over Modified ZSM-5 Catalysts," *Journal of Catalysis*, 100, 322, 1986.
7. Scurrell, M.S., "Factors Affecting the Selectivity of the Aromatization of Light Alkanes on Modified ZSM-5 Catalysts," *Applied Catalysis*, 41, 89, 1988.
8. Stephens, H.P., R.G. Dosch, and F.V. Stool, "Hydrous Metal Oxide Ion Exchangers for Preparation of Catalysts for Direct Coal Liquefaction," *I&EC Proc. Res. Dev.*, 24, 15, 1985.

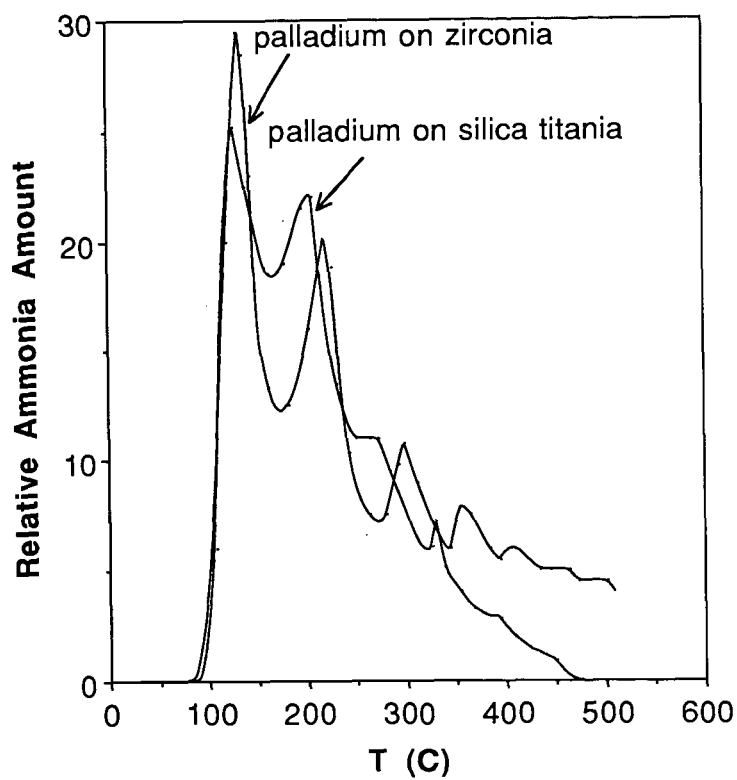
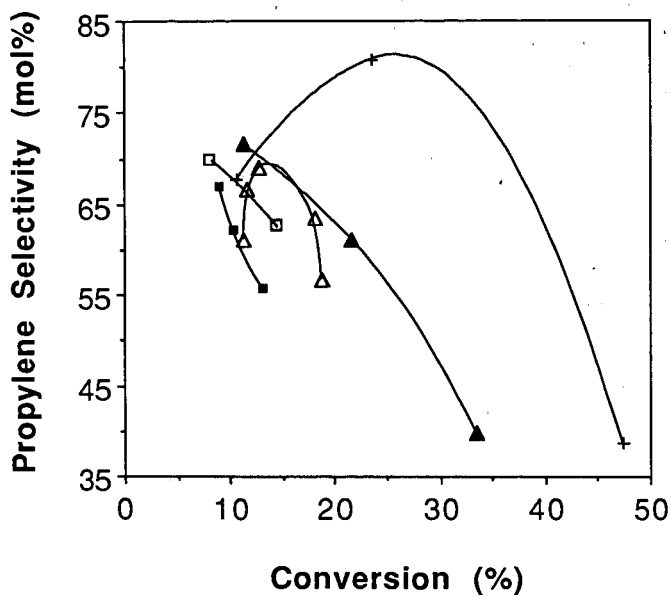


Figure 1. Ammonia TPD of Catalysts



- + Pd on zirconia    Δ Pd on silica titania  
 ▲ Mo on zirconia    ■ Mo and Zr on silica titania  
 ◻ Ni on zirconia

Figure 2. Propylene Selectivity at Different Levels of Propane Conversion

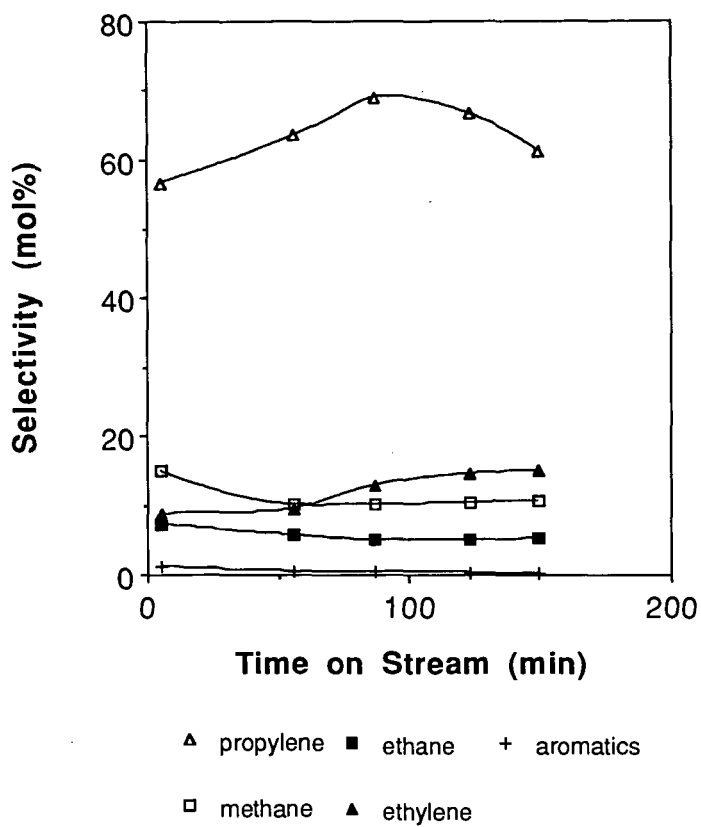


Figure 3. Product Distribution of Propane Transformation for Mo on silica titania

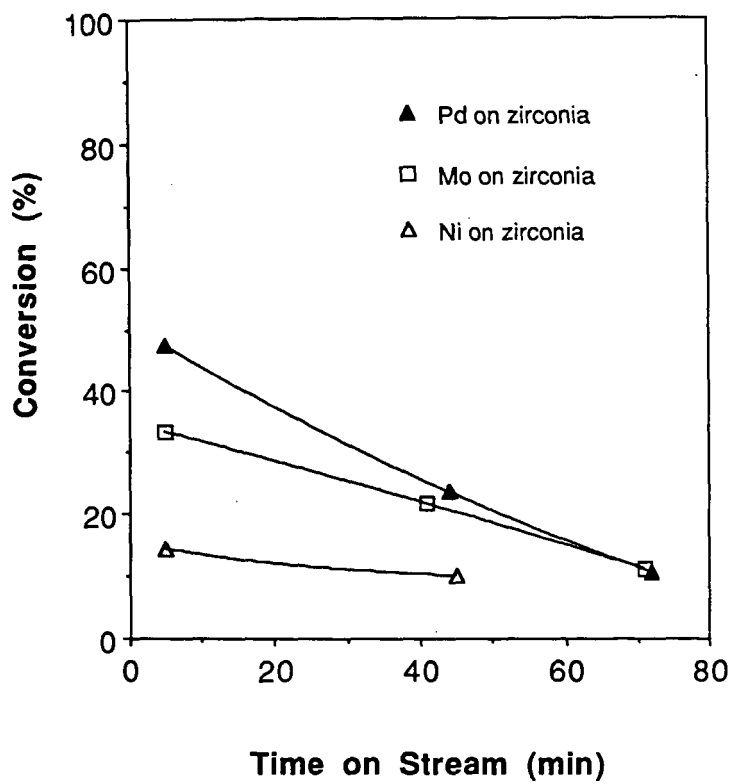


Figure 4. Comparison of Different Active Metals



## H-D EXCHANGE DURING SELECTIVE BENZENE HYDROGENATION TO CYCLOHEXENE

M. A. Richard, D. J. Taube, D. K. Yee, D. O. Durieux,  
J. C. De Deken, P. Alcalá, and H. Moreno

Catalytica, Inc.  
430 Ferguson Drive  
Mountain View, CA 94043

Keywords: benzene, hydrogenation, H-D exchange

### INTRODUCTION

Ruthenium catalyzed hydrogenation of benzene to a mixture of cyclohexene and cyclohexane has been studied in gas phase (1-4) and slurry phase (5-9) reactions. The highest yields of cyclohexene, on the order of 30-40%, have been observed in a four-phase slurry system consisting of a liquid benzene/cyclohexene/cyclohexane phase, an aqueous phase containing a dissolved transition metal salt, a solid heterogeneous ruthenium catalyst, and gas phase hydrogen. The presence of water and a transition metal promoter are generally required to achieve high selectivity to cyclohexene. There has been limited speculation on the role that water (1,2,4,8) and other promoters play in enhancing selectivity to cyclohexene. We have investigated the hydrogenation of benzene- $d_6$  with  $H_2$  to probe mechanistic aspects of the four-phase slurry reaction. We have determined the extent of H-D exchange in the benzene feed and analyzed the H-D distributions in the products, cyclohexene and cyclohexane, at increasing benzene conversions.

### EXPERIMENTAL

Benzene- $d_6$  hydrogenation was carried out in a 1 liter teflon-lined stirred reactor (Autoclave Engineers) at 150°C and 650 psig total pressure. A supported ruthenium catalyst (10) was reduced at 400°C in flowing hydrogen; a sample of the reduced catalyst was suspended in 150 cc of an aqueous solution of cobalt sulfate at 150°C in the teflon-lined reactor. Benzene- $d_6$  (250 cc) was preheated to 150°C and charged to the reactor. The total pressure was adjusted to 650 psig and maintained at 650 psig during hydrogenation. The reactor was sampled periodically and the organic phase composition determined by standard gas chromatographic methods. The H-D ratios and distributions in the organic components were determined by GC/MS.

### RESULTS

Hydrogenation - Cyclohexene yield and selectivity vs. conversion are shown in Figure 1. Full conversion was reached after 100 minutes.

H-D Exchange in Benzene- $d_6$  - Less than 5% of the deuterium in benzene- $d_6$  was exchanged after 75 minutes (88% conversion). While the amount of hydrogen incorporated into the feed was very low, the amount increased as residence time in the reactor increased. The net make of benzene- $h_6$  increased from 0.2% after 11 minutes to 0.9% after 75 minutes.

H/D Ratios in Cyclohexane and Cyclohexene - The H/D ratios in the products, cyclohexane and cyclohexene, were determined at increasing benzene conversions by deconvolution and integration of the MS signals of the individual components. The ratios are shown in Table 1. We estimate that the error in these ratios is less than 5%. The expected ratios are 1.0 and 0.67 for cyclohexane ( $C_6H_6D_6$ ) and cyclohexene ( $C_6H_4D_6$ ), respectively, if one assumes no hydrogen incorporation by H-D exchange from  $H_2$  or  $H_2O$ .

H-D Distributions in Cyclohexane and Cyclohexene - The distributions of H and D in cyclohexane and cyclohexene were determined by deconvolution of the GC/MS signals. The major products were  $C_6H_6D_6$  and  $C_6H_4D_6$ ; however there was significant scrambling of H and D giving the isotopic distributions shown in Figures 2 and 3.

## DISCUSSION

Hydrogenation of benzene- $d_6$  was zero-order in benzene- $d_6$  up to 95% conversion; this is consistent with saturation of the catalytic sites with benzene- $d_6$ . We were surprised to find no significant H-D exchange in the benzene- $d_6$  feed. This observation has two implications. First, it is unlikely that benzene adsorbs dissociatively. And second, cyclohexene disproportionation to benzene/cyclohexane does not occur to any measurable extent.

The data in Table 1 show that no H-D exchange occurred during hydrogenation of benzene- $d_6$  to cyclohexane and cyclohexene. However, the isotopic distributions in cyclohexane and cyclohexene (Figures 2 and 3) show that considerable intermolecular H-D exchange occurs with conservation of deuterium. The exchange of H and D between cyclohexene molecules to give the distributions observed supports the view that cyclohexene must adsorb and desorb numerous times so that the molecules can present both sides of the ring to the surface randomly. We believe that the key intermediate for the scrambling reaction is cyclohexene dissociatively adsorbed at the allylic position. As the reaction time in the reactor increases, the average residence time of the cyclohexene increases (it is continuously produced from benzene and continuously disappears as cyclohexane; thus, the residence time distribution of the cyclohexene molecules broadens as reaction time increases) and this results in increased scrambling with time as shown by the broadening of the distributions for cyclohexene in Figure 3. The less pronounced broadening of the cyclohexane distribution with time is consistent with little or no intermolecular exchange for the fully hydrogenated product; this is consistent with adsorption of cyclohexane being very weak relative to the adsorption strengths of benzene and cyclohexene.

The lack of a net hydrogen (H) incorporation into cyclohexene (or cyclohexane) is very surprising in view of the rampant scrambling that occurs. We believe that this is conclusive evidence supporting the view that the catalyst surface is hydrogen "starved" despite the very high hydrogenation rate (turnover frequency on the order of  $10 \text{ sec}^{-1}$  per exposed ruthenium site).

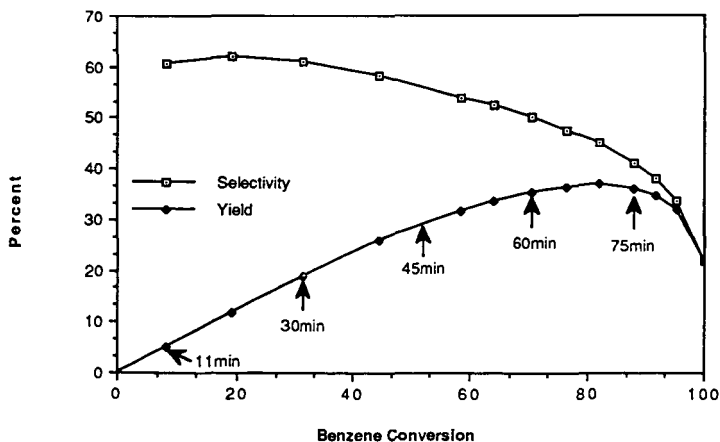
## REFERENCES

1. Don, J. A. and Scholten, J. J. F. Faraday Disc., Chem. Soc. 1982, 72, 145.
2. van der Steen, P. J. and Scholten, J. J. F. Proceedings of the 8th International Congress on Catalysis 1984, 2, 659.

3. Schoenmaker-Stolk, M. C., Verwijs, J. W., Don, J. A., and Scholten, J. J. F. Appl. Catal. 1987, 29, 73.
4. van der Steen, P. J. and Scholten, J. J. F. Appl. Catal. 1990, 58, 281, 291.
5. Niwa, S., Mizukami, F., Isoyama, S., Tsuchiya, T., Shimizu, K., Imai, S., and Imamura, J. J. Chem. Tech. Biotechnol. 1986, 36, 236.
6. Niwa, S., Lopez Salinas, E., Mizukami, F., and Toba, M., Yukagaku 1989, 38(11), 938.
7. Niwa, S., Mizukami, F., Toba, M., Tsuchiya, T., Shimizu, K., and Imamura, J. Shokubai 1989, 31(6), 421.
8. Niwa, S. Mizukami, F., Imamura, J., and Itabashi, K. Sekiyu Gakkaishi 1989, 32(6), 299.
9. Nagahara, H., et al. US 4,734,536 (1988), JP 63-243038 (1988), JP 63-88139 (1988), all assigned to Asahi Kasei Kogyo K. K.
10. Details of catalyst preparation and characterization will be given in subsequent publications.

**TABLE 1. H/D Ratios in Cyclohexane and Cyclohexene**

<u>Reaction Time, min</u>	<u>H/D, Cyclohexane</u>	<u>H/D, Cyclohexene</u>
11	0.94	0.71
30	0.98	0.65
45	0.97	0.66
60	0.98	0.68
75	0.98	0.71



**FIGURE 1.** Cyclohexene selectivity and yield vs. benzene conversion. Note that the only products were cyclohexene and cyclohexane. The times noted correspond to the samples analyzed for H/D ratios and distributions.

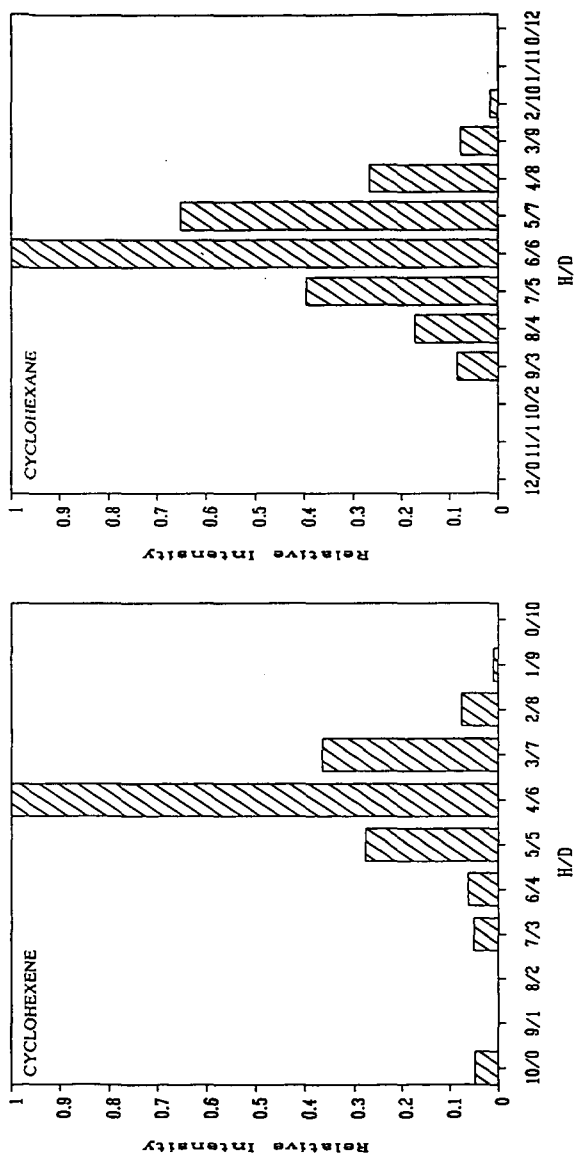


FIGURE 2. Isotopic distributions in cyclohexane and cyclohexene; 11 min sample.

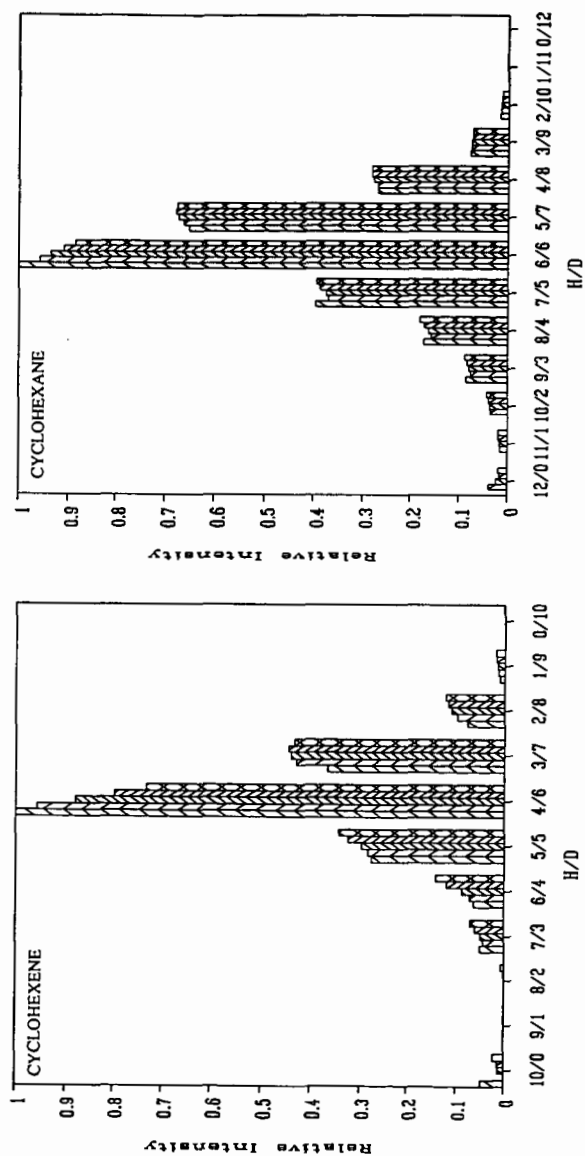


FIGURE 3. Isotopic distributions in cyclohexane and cyclohexene; reaction time increases from left-to-right (11, 30, 46, 60, 75 minutes) in each bar cluster.

## Catalyst Selectivity in Hydrocarbon Reactions: Ethylene on Ru/SiO<sub>2</sub> and M-Ru/SiO<sub>2</sub>

M. PRUSKI<sup>α</sup>, D.K. SANDERS<sup>β,α</sup>, X. WU<sup>β,α</sup>, S.-J. HWANG<sup>γ,α</sup>, T. S. KING<sup>β,α</sup>,  
and B.C. GERSTEIN<sup>γ,α</sup>

<sup>α</sup>Ames Laboratory, USDOE, and Departments of <sup>β</sup>Chemical Engineering, and <sup>γ</sup>Chemistry,  
Iowa State University, Ames, IA 50011

The nuclear spin dynamics of <sup>1</sup>H in adsorbed hydrogen, and <sup>13</sup>C in adsorbed ethylene on Ru/SiO<sub>2</sub> and M-Ru/SiO<sub>2</sub> (M=Cu, Ag or Au) catalysts are used to probe surface concentrations of Ru and M, reactive intermediates, and selectivity in hydrocarbon conversion reactions. The temperature and exposure dependence of ethylene reaction on Ru/SiO<sub>2</sub> is investigated via various <sup>13</sup>C NMR techniques, as well as via <sup>1</sup>H multiple quantum coherence. Comparisons between monometallic and bimetallic catalysts are made.

### Introduction.

Solid state NMR is becoming an increasingly important tool in the study of heterogeneous catalysis. The ability to directly study phenomena on the surfaces of dispersed metal particles is one advantage offered by NMR. This is contrasted with mainstay ultrahigh vacuum techniques requiring single crystal surfaces, which may not always be good models for real catalysts. The objective of this paper is to demonstrate the application of several solid state NMR techniques to study the fundamental processes associated with hydrocarbon conversion over supported bimetallic catalysts. To this end, the interaction of hydrogen with M-Ru/SiO<sub>2</sub> (M=Cu, Ag or Au) is used to probe catalyst surface composition. An investigation of ethylene reaction on mono- and bimetallic catalysts at various temperatures, exposures and M composition is presented.

### Experimental.

Catalyst samples were prepared as described previously.<sup>1,2</sup> <sup>1</sup>H NMR was performed on a 220 MHz homebuilt spectrometer, equipped with an 8-bit digital phase shifter.<sup>3</sup> Multiple quantum coherence was developed using a single quantum propagator.<sup>4</sup> <sup>13</sup>C NMR experiments were carried out on another homebuilt spectrometer operating at 100.06 MHz for <sup>1</sup>H and 25.16 MHz for <sup>13</sup>C. Transient techniques included cross polarization (CP) and direct excitation (Bloch decay), both of which were done with and without magic angle spinning (MAS) and proton decoupling. Special procedures were developed for low temperature (85-300K) experiments whereby samples were prepared, sealed, transferred to the spectrometer, and measured using CP/MAS without rise in temperature at any time.<sup>5</sup>

### Results and Discussion.

#### NMR of Adsorbed Hydrogen: Establishing the Surface Composition of Bimetallic Catalysts

Studies on Cu-Ru/SiO<sub>2</sub> have shown that, at room temperature, hydrogen undergoes fast exchange between the two metals such that the observed lineshift,  $\delta_{\text{obs}}$ , may be expressed as:

$$\delta_{\text{obs}} = X_{\text{Ru}}\delta_{\text{Ru}} + X_{\text{Cu}}\delta_{\text{Cu/Ru}}$$

where  $X_i$  is the surface concentration of metal  $i$ ,  $\delta_{\text{Ru}}$  and  $\delta_{\text{Cu/Ru}}$  are the lineshifts for hydrogen chemisorbed on Ru/SiO<sub>2</sub> and the asymptotic limit as  $X_{\text{Cu}}$  approaches unity in Cu-Ru/SiO<sub>2</sub>, respectively.<sup>6</sup> Thus, the surface composition of the bimetallic catalyst can be obtained from <sup>1</sup>H spectra (Fig. 1).

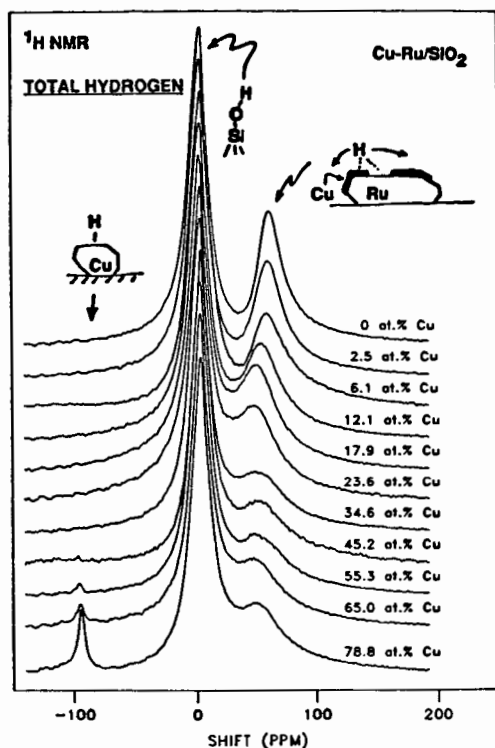


Fig. 1. NMR of adsorbed hydrogen on Cu-Ru/SiO<sub>2</sub> as a function of Cu concentration. The first moment of the upfield peak establishes the surface concentration of Ru.

Peak shifts in Fig. 1 demonstrate that  $X_{Ru}$  decreases quickly as the total Cu concentration increases from 0 to 20 at.%, before levelling off at ca. 35 at.%, and approaches zero at ca. 80 at.%, where complete masking of Ru is concluded. These trends suggest that Cu forms a thin monoatomic layer on Ru particles, until near complete coverage, after which 3-d Cu islands and/or pure particles begin to form, as evidenced by the emergence of a downfield peak indicative of hydrogen chemisorbed on bulk Cu (cf. Figure 1). Hydrogen uptake and <sup>1</sup>H NMR studies on Ag-Ru/SiO<sub>2</sub> and Au-Ru/SiO<sub>2</sub> indicate a higher tendency for these metals to form three dimensional aggregates.<sup>2</sup>

NMR of Adsorbed Ethylene: Weakly and Strongly Adsorbed Intermediates and Products  
Ethylene on Ru/SiO<sub>2</sub>



Transient NMR techniques were used to probe the development of intermediates and products as  $^{13}\text{C}$ -labelled ethylene reacted over  $\text{Ru}/\text{SiO}_2$  to establish:

- (i) concentrations of weakly and strongly adsorbed species (Bloch decay),
- (ii) possible identities of strongly adsorbed intermediates (Bloch decay, CP/MAS, dipolar dephasing), and
- (iii) identities of weakly adsorbed products (liquid state NMR techniques).

Intensity measurements indicated that no significant amounts of  $^{13}\text{C}$  nuclei remain undetected in the Bloch decay studies. Assignments of weakly adsorbed species could be made unambiguously based on chemical shifts, relative intensities of the various peaks, and, in some cases, J-splittings. These experiments were performed at a high magnetic field (300 MHz), using slow MAS to remove broadening due to magnetic susceptibility. The identification of strongly adsorbed species based solely on NMR shifts is not straightforward. Although MAS can remove the effect of anisotropies of chemical shift, Knight shift, and magnetic susceptibility, considerable line broadening often remains due to the distribution of sites across the metal particles. The extent to which isotropic Knight shifts affect the identification of  $^{13}\text{C}$  resonances of hydrocarbon species on highly dispersed, supported Ru is debatable. Dipolar dephasing and multiple quantum NMR were also used to probe possible identities of the strongly adsorbed species.

Selectivity and product distributions are strong functions of temperature and surface coverage. Fig. 2 shows an example of the temperature dependence of  $^{13}\text{C}$  CP/MAS spectra of ethylene dosed on  $\text{Ru}/\text{SiO}_2$  at 78K. The exposures ( $\epsilon$ ) were 0.5 and 1.5 ethylene molecules per surface Ru atom, and spectra were accumulated at 85K, at 185 K after reaction at that temperature for 2 days, and at 300 K after reaction at 300 K for 1 day.<sup>7</sup>

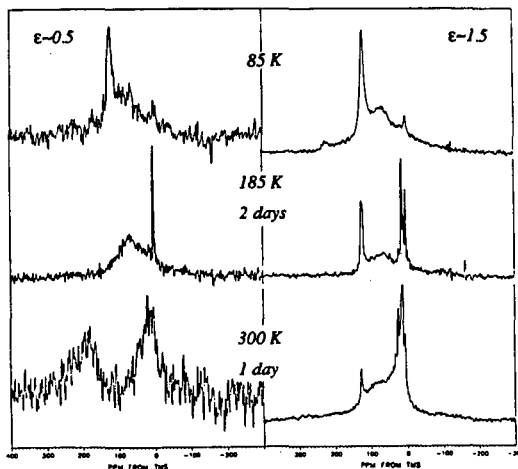


Fig. 2. NMR of  $^{13}\text{C}$  in ethylene adsorbed on  $\text{Ru}/\text{SiO}_2$  as a function of exposure ( $\epsilon = 0.5$  and  $1.5$ ), and temperature ( $85\text{K} \leq T \leq 300\text{K}$ ).

Both exposures give similar spectra at 85K. Peaks are assigned to weakly and strongly adsorbed ethylene, the strongly adsorbed species being either  $\pi$ , or di- $\sigma$  bonded to the metal surface. To distinguish between the  $\pi$  and di- $\sigma$  bound species, bond length measurements may be performed using the homonuclear dipolar coupling between  $^{13}\text{C}$  nuclei. This work is in progress.

At 185K and  $\epsilon = 0.5$ , only ethane is observed in the weakly adsorbed layer. Changes in the spectrum also suggest a strongly bound  $\text{C}_2\text{H}_2$  species in addition to the strongly bound  $\text{C}_2\text{H}_4$ . For  $\epsilon = 1.5$ , the increase in temperature leads to the development of weakly bound cis- and trans-butenes.

At 300K, for  $\epsilon = 0.5$ , broad peaks are observed at ca. 185 and 10 ppm, which are tentatively assigned to the  $>\text{C}-$  and  $-\text{CH}_3$  carbons of ethylidyne, although experiments are underway to further investigate this assignment. At  $\epsilon = 1.5$ , the weakly adsorbed species were identified as ethane, butenes, and butane. Surface attached alkyl groups and acetylide are inferred to be present in the strongly bound layer.<sup>1</sup>

Evolution of weakly adsorbed products is shown in Fig. 3, for an  $\epsilon = 5$  sample. At 140K,

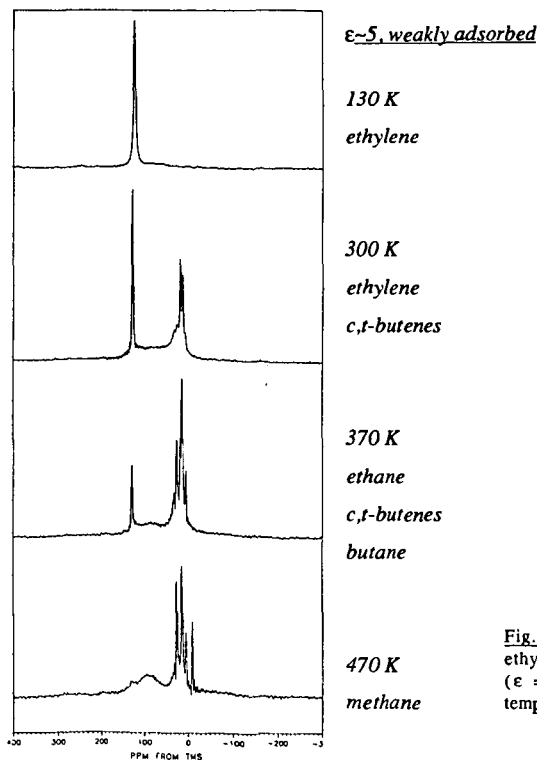


Fig. 3.  $^{13}\text{C}$  CP/MAS NMR of ethylene adsorbed on  $\text{Ru}/\text{SiO}_2$  ( $\epsilon = 5$ ) as a function of temperature.

only ethylene is observed. When the temperature is raised to 300K, cis- and trans- butenes are formed. Butadiene is observed as a transient during this temperature rise. Increasing temperature to 370K results in the formation of ethane and butane. At 470K only the fully hydrogenated products, methane, ethane and butane, are observed. The appearance of methane indicates that C-C bond cleavage has already occurred at or below 470K.

As a means of further establishing identities of the strongly adsorbed species, multiple quantum spin counting was used.<sup>4</sup> Under the conditions imposed in this experiment for the development of multiple quantum coherence, the number of coupled spins is  $k_{\max} + 1$ , where  $k_{\max}$  is the highest order of observed coherence. The silanol protons of the support, separated by ca. 4Å, only develop double quantum coherence in a period sufficient to see  $k > 8$  for the infinitely coupled ensemble of spins in adamantane. Fig. 4 shows the multiple quantum spectrum of the strongly adsorbed species resulting from ethylene adsorption on Ru/SiO<sub>2</sub>.  $k_{\max}$  sharply cuts off at a value of 5, indicating that species with no more than 6 strongly coupled protons are present in the sample. One possible candidate for the fragment with 6 coupled protons is metalocyclic (Ru)CH<sub>2</sub>CH=CHCH<sub>2</sub>(Ru), which may be a participant in the formation of butenes. Small concentrations of this species cannot be excluded on the basis of <sup>13</sup>C NMR data.

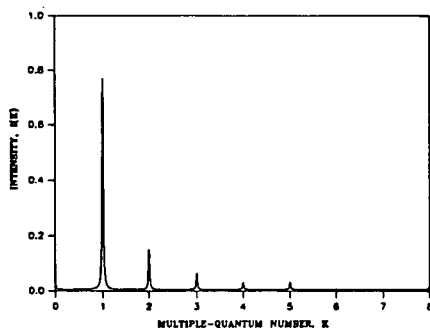


Fig. 4. Multiple quantum spectrum of strongly bound species from reaction of ethylene with Ru/SiO<sub>2</sub>.

#### Ethylene on M-Ru/SiO<sub>2</sub>

Unlike the extensive reaction of ethylene on Ru/SiO<sub>2</sub>, no reaction is observed on Cu/SiO<sub>2</sub> at 300K. The bimetallic Cu-Ru/SiO<sub>2</sub> differs from the monometallic Ru/SiO<sub>2</sub> in that the ability of the catalyst to produce hydrogenated products is reduced. At room temperature, the intermediate, butadiene, is stabilized in the bimetallic system.<sup>8</sup> This is evidenced by Fig. 5, which shows the CP/MAS spectrum of <sup>13</sup>C in ethylene adsorbed on a 15 at. % Cu bimetallic catalyst.

Cu and Ru are known to be immiscible in the bulk.<sup>9</sup> Monte-Carlo simulations<sup>10</sup> indicate Cu-Ru bimetallic particles to be polyhedra in which the Cu selectively populates high coordination edge and corner sites, and then forms islands on the particle faces as Cu content increases. The equilibrium structure for a Cu-Ru particle with 15 at. % Cu, as predicted by Monte Carlo simulations, is shown in Fig. 5. It is therefore postulated that the selectivity towards highly

hydrogenated products is affected by the availability of edge and corner Ru sites, which become blocked by the adsorption of Cu.

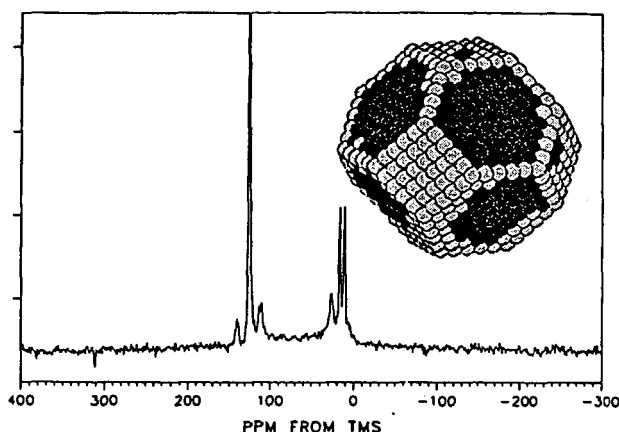


Fig. 5. NMR of  $^{13}\text{C}$  adsorbed on Cu-Ru/SiO<sub>2</sub> at room temperature. Total metal loading = 4%, Cu = 15% of total metal.

Ethylene reaction on Ag-Ru/SiO<sub>2</sub> shows reduced hydrogenation<sup>2</sup> as compared to Ru/SiO<sub>2</sub>, but not as much as for Cu-Ru/SiO<sub>2</sub>. Although Ag tends to aggregate on Ag-Ru/SiO<sub>2</sub>, this result suggests that it does block edge and defect-like sites to some extent, consistent with Monte Carlo simulations of Ag-Ru particles.<sup>10</sup> Preliminary  $^{13}\text{C}$  data on Au-Ru/SiO<sub>2</sub> indicate that the hydrogenation capability is also reduced. This is a surprising result, since, of the three metals studied, Au has the least tendency to efficiently cover the Ru surface.

#### Conclusions.

Product distributions, reaction intermediates, and surface metal concentrations are very important clues in understanding the mechanistic details of heterogeneous catalytic reactions. This paper demonstrates the wealth of information available via solid state NMR, illustrated by the study of ethylene reaction on mono and bimetallic catalysts. On Ru/SiO<sub>2</sub>, this reaction is a complex function of both temperature and exposure. For example, the evolution of weakly adsorbed C<sub>4</sub> species is observed only at higher exposures, whereas the strongly bound species tentatively identified as ethylidyne is only observed at low exposures. Hydrogenation reaction is extensive on Ru/SiO<sub>2</sub>. The addition of Cu, Ag or Au to the catalyst generally reduces hydrogenation activity, presumably by the blockage of catalytically active edge and corner sites.

**Acknowledgement.** This work is supported by the U. S. Department of Energy, Office of Basic Energy Sciences, Contract Number W-7405-ENG-82.

# References

1. Pruski, M., Kelzenberg, J.C., Gerstein, B.C., and King, T.S., J. Am. Chem. Soc. 1990, 112, 4232.
2. Wu, X., Gerstein, B. C., and King, T. S., J. Catal. 1990, 123, 43.
3. Gerstein, B.C., Han, J.-W., Hwang, S.-J., Pan, H.-J., and Skank, H., Rev. Sci. Instr. 1990, 61, 2349.
4. Hwang, S.-J., and Gerstein, B.C., "Spin Counting in Dipolar Coupled Spin 1/2 Systems by Multiple Quantum Coherence", in NMR: Basic Principles and Progress, Springer-Verlag (Berlin) (in press).
5. Pruski, M., Sanders, D. K., King, T. S., and Gerstein, B.C., J. Magn. Res. (submitted).
6. Wu, X., Gerstein, B. C., and King, T. S., J. Catal. 1990, 121, 271.
7. Sanders, D. K. Gerstein, B. C. King, T. S., and Pruski, M., manuscript in preparation.
8. Sprock, M., Pruski, M., Gerstein, B. C., and King, T. S., Catal. Lett. 1990, 5, 395.
9. Hansen, M., Constitution of Binary Alloys, 2nd ed., McGraw-Hill, New York, 1958, p. 620.
10. Strohl, J. K., and King, T. S., J. Catal. 1989, 116, 540.

## SELECTIVE PARTIAL OXIDATION OF METHANE BY CATALYTIC SUPERCRITICAL WATER OXIDATION

Catherine N. Dixon and Martin A. Abraham  
Department of Chemical Engineering  
The University of Tulsa  
Tulsa, Oklahoma 74104

### ABSTRACT

The product spectrum obtained from catalytic partial oxidation in supercritical water has been compared to that obtained from catalytic oxidation in the gas phase. The presence of supercritical water inhibits the methane conversion but promotes the yield of methanol. The effect of oxygen concentration on the reaction in supercritical water has also been considered. High oxygen concentrations apparently inhibit the conversion reaction and decrease the yield of methanol. These results are considered in terms of consistent reaction pathways.

Keywords: Methane, Partial Oxidation, Supercritical Water

### INTRODUCTION

Abundant supplies of natural gas exist within the United States. Methane, the major component of natural gas, is useful primarily as a fuel and, because it is difficult to transport, primarily at the wellhead. Partial oxidation to methanol or formaldehyde, or oxidative coupling to ethylene or other higher hydrocarbons, would greatly enhance the usability of methane both as a fuel source and as a raw material. Unfortunately, it is easier to convert partial oxidation products such as methanol to complete oxidation products than it is to form the partial oxidation products in the first place.

Research has centered on the identification of a selective catalyst which will provide high selectivity to partial oxidation products. Limited success has been obtained using selected metal-oxide catalysts, namely  $\text{MoO}_3$  and  $\text{Cr}_2\text{O}_3$  [Pitchai & Klier, 1986]. However, in these cases low conversion must be maintained so that the desired methanol product is not further converted to undesired complete oxidation products. The complete oxidation products, CO and  $\text{CO}_2$ , have little economic value. Low oxygen concentrations also have been used to increase the selectivity to partial oxidation products. Reports also indicate that, independent of the catalyst, the addition of water decreased the rate of methane conversion but increased the selectivity to methanol [Pitchai & Klier, 1986].

The use of supercritical water as a reaction solvent has previously been shown to alter the reaction pathways and thereby the product spectrum. Kinetic studies for the thermal oxidation of carbon monoxide, ammonia, and ethanol in supercritical water [Helling & Tester, 1987; Helling & Tester, 1988] revealed that secondary reaction pathways can be created through the addition of the supercritical fluid. Thermal oxidations of methane and methanol were accomplished in supercritical water [Rofer &

Streit, 1989] and a mechanism, modified from the gas-phase free radical mechanism, approximately described the kinetics. Extrapolation of the kinetics obtained from these experiments reveals that high methanol yields should be obtained from thermal oxidation in supercritical water [Dixon & Abraham, 1991].

Several investigators have also demonstrated that the addition of a supercritical fluid in a catalyzed reaction can influence the mechanism through which conversion is obtained. In one particular effort of interest, Dooley & Knopf [1987] selectively converted toluene to benzaldehyde through oxidation over  $\text{CoO}/\text{Al}_2\text{O}_3$  in supercritical  $\text{CO}_2$ . In the oxidation of cumene hydroperoxide, Suppes & McHugh [1989] have shown that the addition of the catalyst can promote specific steps in a free-radical mechanism relative to others, which led to an observed change in the product selectivity.

Within the current paper, we present evidence to indicate that oxidation of methane in the presence of supercritical water can be used to promote the formation of the desired partial oxidation product, methanol. Gas phase catalytic oxidation is compared with catalytic oxidation in supercritical water, in terms of both methane conversion and methanol yield. Secondly, the influence of oxygen concentration on the conversion and methanol yield is considered.

## EXPERIMENTAL

Batch reactions were used to determine the influence of supercritical water on the product spectrum of catalytic oxidation of methane. All reactions were carried out in separate 1.26 mL batch reactors, which have been described in detail elsewhere [Jin & Abraham, 1990]. Each reactor was loaded at room temperature with 0.8 mg of  $\text{Cr}_2\text{O}_3$  catalyst [Aldrich Chemical]. For the reactions with supercritical water, 0.4 g deionized water was also added to the reactor. After the reactors were sealed, oxygen, methane, and nitrogen were added to the reactor in the desired proportions to a total pressure of 51.7 bar; for the high oxygen concentration study, a gas mixture containing 1.83% methane, 18.4%  $\text{O}_2$  and the balance nitrogen [Scott Specialty Gases] was used. All materials were commercially available and used as received.

After loading, the reactors were placed into a high temperature fluidized sandbath (Tecam SBL-2), which had been pre-heated to the desired temperature. After the desired reaction time, the reactor was quenched by placing it into a cold water bath. Insertion into the sandbath and into the cold water bath corresponded to zero and the measured reaction time, respectively. Each experiment was repeated at least twice and the resulting values averaged to obtain the reported data. Heatup time for these reactors was approximately 1 minute, short compared to ultimate reaction times of up to 40 minutes.

The small reactor size, combined with the high temperature and pressure at the reaction conditions made measurement of the actual reaction pressure unfeasible. However, it was possible to estimate the actual pressure of the gas phase reaction using the assumption of the ideal gas law; this provided an estimate of the pressure as 118.8 bar. For the reactions in supercritical water, the actual pressure at the reaction temperature of 400 °C was greater than the gas phase reactions. Steam tables could be used to estimate the partial pressure of water at the reaction conditions as 325 bar, and then assuming Dalton's Law allows estimation of the total pressure as 444 bar.

Product analysis was accomplished by gas chromatography. For the gas analysis, an Hewlett Packard 5840 gas chromatograph with gas sampling valve, 30 ft Haysep DB packed column, and thermal conductivity detector, was used in temperature programmed mode. Liquid analysis was accomplished with the HP 5840 instrument, using capillary column injection, 10 m DB-5 capillary column, and flame ionization detector. In both cases, product identification was accomplished by injection of pure component samples of the suspected material. Quantification was accomplished by comparison of peak areas with that of a standard, calibrated by injection of known amounts of materials. Inert nitrogen introduced with oxygen as air was the standard for the gas phase products while added naphthalene was used as a liquid phase standard.

## RESULTS AND DISCUSSION

The conversion of methane is reported as a function of time in Figure 1, in which the gas phase conversion is compared directly with catalytic oxidation in supercritical water. Conversion increased monotonically with time in both cases. For the gas phase catalysis, approximately 0.6 conversion was achieved at 40 minutes, compared with approximately 0.3 conversion for the supercritical water case. At any given reaction time, the conversion achieved from gas phase catalysis was approximately twice that obtained from the reaction in supercritical water.

Experiments were accomplished at 400 °C and initial concentrations of oxygen and methane of 6.32 mol/L and 0.627 mol/L, respectively. The stoichiometry of the complete combustion reaction



indicates that only 2 moles of oxygen are required for complete conversion of methane to  $\text{CO}_2$  and water. Thus, initial experiments were accomplished with greater than 500% excess of oxygen and should be well-represented by assuming that the kinetics are independent of oxygen concentration. Pseudo-first order kinetics for methane conversion provides

$$dx/dt = k(1-x) \quad (2)$$

which upon integration reveals

$$x = 1 - \exp(-kt) \quad (3)$$

Best fit analysis of the data of Figure 1 in terms of equation 3 provides estimated values of the rate constants as  $0.0233 \text{ min}^{-1}$  and  $0.0115 \text{ min}^{-1}$  for gas and supercritical water phase reaction, respectively. The solid lines in Figure 1 represent the predictions of the first order approximation and indicate the quality of the fit of the data.

Methanol yield is compared for the two cases in Figure 2. Essentially no methanol was observed for the gas phase catalysis at any reaction time. For the case of oxidation in supercritical water, the methanol yield ( $y_{\text{MeOH}} = C_{\text{MeOH}}/C_{\text{CH}_4,0}$ ) was also low, however, a maximum of approximately 0.7% yield was obtained at 5 minutes. The concentration decreased at longer reaction times, owing to subsequent conversion of methanol to complete combustion products  $\text{CO}_2$  and water. Although the oxygen



concentration was in substantial excess, thereby favoring the production of total oxidation products, the yield of methanol was increased by more than one order of magnitude through the presence of the water. The lines in Figure 2 do not represent kinetics predictions but are used to more clearly indicate the trends in the data.

The presence of supercritical water serves to inhibit the initial conversion of methane, as evidenced by the data of Figure 1. This may occur by inhibiting adsorption of either methane or oxygen (or both), thereby decreasing the available concentration of the reactants. Alternatively, water may compete with the reactants for catalytic sites, or may poison some sites, limiting the effectiveness of the catalyst. It is not clear, however, what effect the water has on the reaction of methanol to  $\text{CO}_2$  and water. Certainly, the presence of water promotes the formation of methanol, as indicated in Figure 2. From this observation, it would be suspected that the presence of water inhibits conversion of methanol to  $\text{CO}_2$  and water, as well. The mechanism of this inhibition, while not determined within this study, could be attributed to the same factors used in understanding the inhibition of the methane conversion reaction.

Initial experiments were accomplished at high oxygen concentration, which would be expected to promote methane conversion but inhibit the formation of methanol. Several experiments were then accomplished to determine the effect of oxygen concentration on methane conversion and methanol yield. In these cases, the molar ratio of oxygen to methane is indicated in terms of the initial loading in the reactor,  $\theta = \text{C}_{\text{O}_2}/\text{C}_{\text{CH}_4}$ . Based on this definition and the stoichiometry of equation 1,  $\theta = 2$  would correspond to stoichiometric oxygen.

Figure 3 reveals the effect of oxygen concentration on the methane conversion. At very low oxygen concentration,  $\theta = 0.071$ , conversion increased to approximately 0.1 after 5 minutes, and then remained steady at longer reaction times. In this case, the maximum conversion based on the stoichiometry and the oxygen loading should be approximately 0.035. However, if only methanol is produced, the reaction stoichiometry is



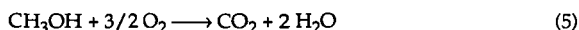
and, given the oxygen loading, 0.14 conversion could be expected. Thus, it was likely that this low oxygen concentration reaction was oxygen-limited.

For oxygen concentration  $0.6 < \theta < 0.8$ , conversion increased steadily with reaction time, reaching approximately 0.25 conversion at 20 minutes. Little discrimination in conversion could be observed between the 3 experimental runs attempted within this concentration range. The high oxygen concentration data is repeated from Figure 1 for comparison purposes and reveals that conversion was slightly lower at  $\theta = 8.72$  than at the lower concentration conditions. Although this was not expected, it is possible that the high concentration of oxygen inhibited methane conversion by preferential adsorption of oxygen onto the catalytic sites.

The effect of oxygen concentration on the yield of methanol is indicated in Figure 4. In all cases, a maximum in methanol yield was observed at a reasonable short reaction time. The highest yield was observed for  $\theta = 0.071$ , with a maximum yield of approximately 0.035 at 10 minutes. Considering that methane conversion was only 0.12 at this reaction time, the selectivity to methanol ( $s = y/x$ ) was approximately 30%. As

the oxygen concentration was increased, the maximum yield of methanol decreased. For the intermediate range of oxygen,  $0.6 < \theta < 0.8$ , the maximum yield was approximately 0.015 at 15 minutes, and the maximum methanol yield was 0.005 for the high oxygen concentration case.

These observations for methanol yield are consistent with a series of reaction pathways described by equation 4 above followed by further reaction of methanol to  $\text{CO}_2$  and water,



From Figure 4, this reaction is likely to be dependent upon the oxygen concentration, with higher concentrations of oxygen promoting methanol conversion. The data of Figure 3 suggests that the initial conversion of methane to methanol is essentially independent of oxygen concentration, although at high concentration, oxygen apparently inhibits the initial conversion. Under all conditions, reaction 5 is more facile than is reaction 4, leading to low methanol yield in all cases. However, the yield of methanol is greater in all cases where supercritical water was present than when the reaction was accomplished within the gas phase.

## CONCLUSIONS

Methane oxidation was inhibited by the presence of supercritical water, with the rate of reaction being approximately one-half of that observed for gas phase oxidation.  $\text{CO}_2$  and water were always the primary products of the reaction, but methanol was formed as an intermediate in low to moderate yield. The presence of supercritical water increased the yield and selectivity of methanol by approximately one order of magnitude compared to reaction in the gas phase. Little effect of increasing oxygen concentration was observed on the methane conversion reaction occurring within supercritical water, although inhibition was observed at very high oxygen concentration. At all oxygen concentrations, increasing oxygen led to a decrease in the maximum yield of methanol.

## REFERENCES

- Dixon, C. N., Abraham, M. A., "Direct Conversion of Methane to Methanol by Reaction with Supercritical Water", submitted to *Chem. Eng. Commun.*, 1991.
- Dooley, K.M.; Knopf, F.C.; *I&EC Research*, 26(9):1910-16, 1987.
- Helling, R.K.; Tester, J.W.; *Energy & Fuels*, 1(5):417-23, 1987.
- Helling, R.K.; Tester, J.W.; *Environ Sci Tech*, 22(1):1319-24, 1988.
- Jin, L., Shah, Y. T., Abraham, M.A.; *J. Supercritical Fluids*, 3(4):233-9, 1990.
- Pitchai, R.; Klier, K.; *Catal. Rev. - Sci. Eng.*, 28:13, 1986.
- Rofer, C.K.; Streit, G.E.; US DOE Hazardous Waste Remedial Actions Program, LA-11700-MS DOE/HWP-90, 1989.
- Suppes, G.J.; McHugh, M.A.; *I&EC Research*, 28(8):1146-52, 1989.

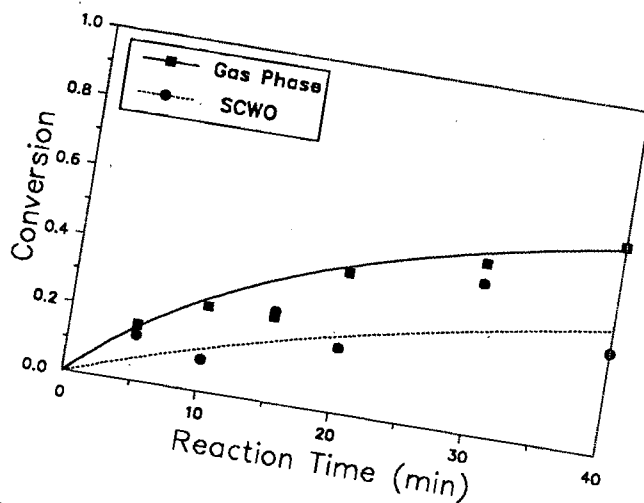


Figure 1: Comparison of methane conversion obtained from gas phase and supercritical water catalytic oxidation at 400 °C.

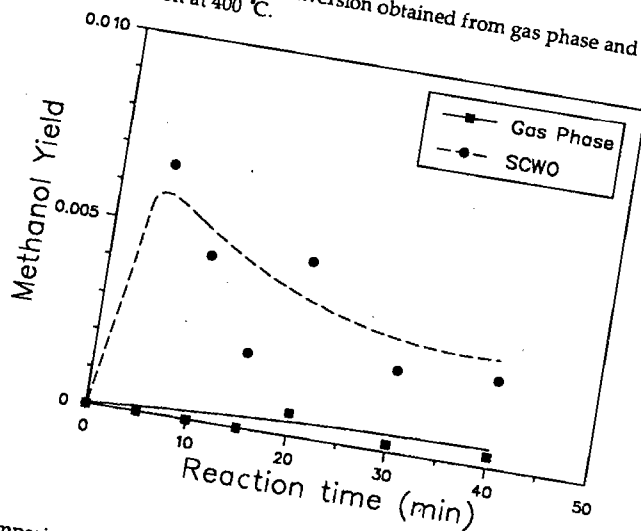
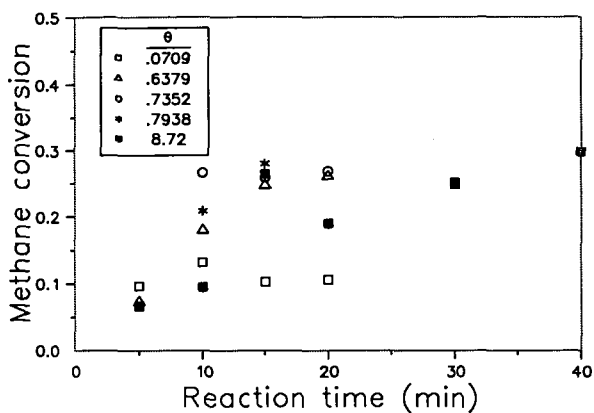
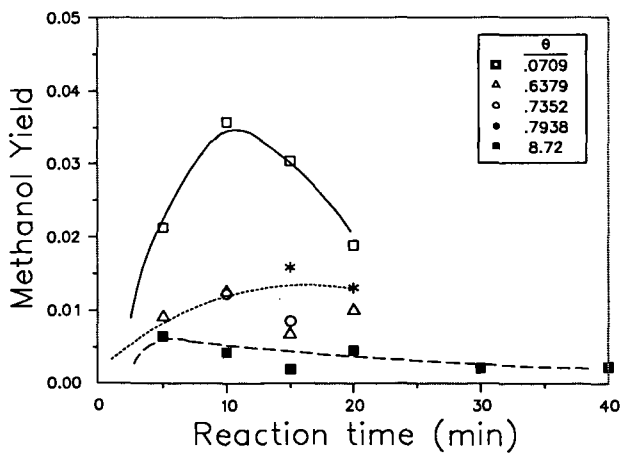


Figure 2: Comparison of methanol yield obtained from gas phase and supercritical water catalytic oxidation at 400 °C.



**Figure 3:** Influence of oxygen concentration on the temporal variation of methane conversion during catalytic oxidation in supercritical at 400 °C.



**Figure 4:** Influence of oxygen concentration on the temporal variation of methanol yield during catalytic oxidation of methane in supercritical at 400 °C.

## Selectivity of $\gamma$ - $\text{Al}_2\text{O}_3$ supported vanadium catalysts in the Hydrometallisation (HDM) of Ni-TPP and VO-TPP.

**R.L.C. Bonn , P. van Steenderen and J.A. Moulijn<sup>(1)</sup>**

*Department of Chemical Engineering, University of Amsterdam, Nieuwe Achtergracht 166, 1018 WV Amsterdam (The Netherlands).*

*(1) Present address: Faculty of Chemical Technology and Materials Science, Delft University of Technology, Julianalaan 136, 2628 BL Delft (The Netherlands).*

### abstract

The HDM reactions of nickel-tetraphenylporphin (Ni-TPP) and vanadyl-tetraphenylporphin (VO-TPP) over sulfided  $\text{V}/\gamma\text{-Al}_2\text{O}_3$  catalysts have been studied in the liquid phase. Kinetic analysis revealed that both Ni-TPP and VO-TPP are demetallised through a reversible sequential mechanism via hydrogenated intermediate porphinic compounds. For the hydrogenation of the porphins a single site model, in which atomic hydrogen and porphins are adsorbed on the same type of sites, applies with a Langmuir-Hinshelwood type of kinetics for hydrogen. Hydrogenolysis is achieved on a different type of sites.

The HDM reactions of both Ni-TPP and VO-TPP are structure sensitive: increasing the vanadium loading of the catalysts initially results in an increased hydrogenation activity. The presence of crystalline materials on the catalysts suppresses the hydrogenation activity of the catalysts. Hydrogenolysis is not influenced by the presence of crystalline material but decreases almost linearly with increasing vanadium loading of the catalysts.

### Introduction

Today's oil refining is facing major changes. The world's supplies of relatively easily refinable petroleum are decreasing whereas demands for clean refinery products (e.g. transportation fuels) are increasing. As a consequence, ever increasing quantities of low quality crude oils have to be processed, resulting in vast amounts of economically invaluable residual oils. The alternative which is rapidly becoming more important is to upgrade the residual oils into the desired products composition. In doing this, not only the C/H ratio of the feed has to be improved but a more thorough removal of hetero-atoms (sulfur, nitrogen and metal compounds) has to be achieved as well in order to protect 'down-stream' catalysts from rapid deactivation and to meet with stricter environmental legislations.

Unlike HDS and HDN, hydrometallisation (HDM) generates deposits of metal sulfides (mainly nickel and vanadium sulfides) on the catalysts, leading to an alteration of selectivity and eventually to an irreversible deactivation of the catalysts. Furthermore, the metallic constituents of petroleum tend to concentrate in the heavy fractions which makes the upgrading of residual oils even more cumbersome. In the improvement of existing processes and the development of new processes, kinetic data are highly desirable. Also the development of new types of catalysts with improved selectivity toward demetallisation as well as large metal storage capacity is to a large extent based on kinetics.

The objective of the current investigation is to relate structural aspects and sulfiding behavior of  $\gamma\text{-Al}_2\text{O}_3$  supported vanadium catalysts to their activity and selectivity in the HDM of model metal compounds.

### Experimental

#### 1) Catalysts.

A listing of the catalysts applied in this study is given in table 1. All catalysts were prepared by pore volume impregnation of a wide-pore, high purity  $\gamma\text{-Al}_2\text{O}_3$  support (Rh ne-Poulenc SCM

99XL, specific surface area  $156 \text{ m}^2/\text{g}$ , pore volume  $1.2 \cdot 10^{-6} \text{ m}^3/\text{g}$  and mean pore radius 13 nm). 75-150  $\mu\text{m}$  particles were used. Further details on the preparation of the catalysts are given elsewhere [1].

**Table 1. Catalysts applied**

catalyst	vanadium loading wt% V	atoms V/nm <sup>2</sup>
V(0.9)/Al <sub>2</sub> O <sub>3</sub>	1.25	0.94
V(1.4)/Al <sub>2</sub> O <sub>3</sub>	1.79	1.35
V(1.8)/Al <sub>2</sub> O <sub>3</sub>	2.33	1.77
V(3.0)/Al <sub>2</sub> O <sub>3</sub>	3.93	2.98

Prior to the activity measurements, the catalysts were sulfided at 673 K in a gas mixture consisting of 15 vol% H<sub>2</sub>S in H<sub>2</sub> (total flow rate: 13.67  $\mu\text{mol/s}$ ). The sulfiding mechanism of the catalysts is discussed in detail elsewhere [2]. The sulfiding procedure was as follows:

- Purging with Ar at 293 K to remove air.
- Isothermal sulfiding at 293 K in H<sub>2</sub>S/H<sub>2</sub> for 1.8 ks.
- Temperature programmed heating (0.167 K/s) in H<sub>2</sub>S/H<sub>2</sub> to 673 K.
- Isothermal sulfiding at 673 K in H<sub>2</sub>S/H<sub>2</sub> for 7.2 ks.
- Purging with Ar at 673 K for 1.8 ks.
- Cooling down to 293 K in Ar.

## 2) HDM-activity measurements.

Vanadyl-meso-Tetraphenylporphyrin (VO-TPP) and Nickel-meso-Tetraphenylporphyrin (Ni-TPP) were used as model metal compounds. The HDM-activity measurements were performed in the liquid phase. The solvent employed in this study was o-Xylene (Janssen Chimica, p.a. grade). Because of the poor solubility of the model compounds at room temperature and their reactivity towards oxygen at elevated temperatures [3], they were dissolved under argon in refluxing o-Xylene for 7.2 ks. The porphyrin solutions thus obtained contained approximately 0.3 mol/m<sup>3</sup> VO-TPP or Ni-TPP and were stored under Ar or used immediately.

HDM-activity measurements of the presulfided catalysts were performed in a  $2 \cdot 10^{-4} \text{ m}^3$  stirred batch autoclave. The reactor was equipped with a sampling device from which samples were taken at regular intervals. After thoroughly purging the autoclave with argon, about 100 g of model compound solution was loaded into the reactor. The reactor was then evacuated and approximately 0.1 g of catalyst was introduced from a catalyst loader that had been mounted on the reactor to prevent the presulfided catalyst from contact with air. After purging with H<sub>2</sub> and subsequent evacuation the reactor was pressurised to approximately 0.3 MPa with a gas mixture containing 15 vol% H<sub>2</sub>S in H<sub>2</sub>. The H<sub>2</sub>S/H<sub>2</sub> mixture was used as received. The reactor was further pressurised to 3 MPa with H<sub>2</sub> (99.9 %) which had been prepurified to remove traces of oxygen and water. After completing the loading and pressurising, the autoclave was closed and heated to 573 K while stirring its contents.

With each metalporphyrin, six runs were carried out at 573 K. In four of these runs the vanadium loading of the catalysts was varied while the liquid phase concentration of hydrogen was kept constant. The effect of the liquid phase concentration of hydrogen at 573 K was evaluated in three runs with the V(1.8)/Al<sub>2</sub>O<sub>3</sub> catalyst. An overview of the HDM experiments with Ni-TPP and VO-TPP is given in table 2.

In each run 8-10 liquid samples of approximately 0.5 g were taken at various reaction times from the sampling port and analysed immediately with a Philips PU 8725 rapid scanning UV/VIS spectrophotometer. Porphyrins and metalporphyrins are known to have distinct and intense absorption maxima in the visible range. The concentrations of the porphyrins and their

hydrogenated intermediates were calculated from the UV/VIS spectra by applying Beer's law. The specific absorptions of each compound were corrected for overlap with other absorption bands in the spectra.

**Table 2. Overview of HDM experiments with Ni-TPP and VO-TPP over sulfided V/ $\gamma$ -Al<sub>2</sub>O<sub>3</sub> catalysts**

catalyst	run	Ni-TPP		run	VO-TPP	
		[H <sub>2</sub> ] (mol/m <sup>3</sup> )	[H <sub>2</sub> S] (mol/m <sup>3</sup> )		[H <sub>2</sub> ] (mol/m <sup>3</sup> )	[H <sub>2</sub> S] (mol/m <sup>3</sup> )
V(0.9)/Al <sub>2</sub> O <sub>3</sub>	Ni-1	365.50	13.17	V-1	396.55	13.63
V(1.4)/Al <sub>2</sub> O <sub>3</sub>	Ni-2	388.78	13.51	V-2	381.02	13.40
V(1.8)/Al <sub>2</sub> O <sub>3</sub>	Ni-31	255.87	13.81	V-31	236.30	13.39
V(1.8)/Al <sub>2</sub> O <sub>3</sub>	Ni-32	381.02	13.40	V-32	404.31	13.73
V(1.8)/Al <sub>2</sub> O <sub>3</sub>	Ni-33	536.45	13.32	V-33	532.57	13.28
V(3.0)/Al <sub>2</sub> O <sub>3</sub>	Ni-4	400.43	13.68	V-4	392.67	13.57

In order to check for the presence in the liquid samples of metal compounds not detected by UV/VIS spectrometry, the total metal content of several samples was determined by Graphite Furnace Atomic Absorption Spectrometry (GFAAS, Perkin-Elmer HGA 500/560).

The actual concentrations of H<sub>2</sub> and H<sub>2</sub>S at reaction conditions were calculated with the Peng-Robinson equation of state. Binary interaction parameters for H<sub>2</sub> and o-Xylene were obtained from literature [4]. Interaction parameters for H<sub>2</sub>-H<sub>2</sub>S and for H<sub>2</sub>S-Xylene were set to zero. Also the density of the liquid phase at the reaction conditions was calculated with the Peng-Robinson equation of state. This made accurate calculation of the concentration of model compounds at these conditions possible.

### 3) Kinetic analysis.

Intrinsic kinetic parameters were obtained by evaluation of the concentration versus time curves with a non-linear regression programme (NLS). The objective function, defined as the sum of squares of deviations (residuals) between experimental and calculated concentrations, was minimised by using a combination of the Simplex and Levenberg-Marquardt methods.

With the NLS programme, several reaction mechanisms were tested. A fourth order Runge-Kutta method was used to numerically solve the sets of coupled differential equations for each kinetic model. Zero reaction time was taken at the moment the desired reaction temperature was reached. During the heating of the reactor and its contents some conversion of the reactants already occurred. In order to overcome this problem, concentrations of reactants and intermediates in the sample taken at zero reaction time were used as the initial concentrations in the kinetic analysis of the experiments.

## Results

Typical concentration versus reaction time plots for HDM experiments with Ni-TPP and VO-TPP at 573 K are shown in figures 1 (run Ni-32) and 2 (run V-32). The experimentally obtained concentrations of reactants and hydrogenated intermediates are represented by markers. Solid lines represent calculated concentrations.

Ni-TPP has been shown to demetallise through a reversible sequential mechanism via the hydrogenated intermediate species Ni-TPC and Ni-TPiB [5-7]. In analogy with Ni-TPP, VO-TPP appears to demetallise through a similar sequential mechanism. The concentration of VO-TPP as a function of reaction time rapidly drops while the concentrations of VO-TPC and VO-TPiB

build up and then, after reaching a maximum, slowly decline indicating that these hydrogenated species are rather stable intermediates in the course of the HDM reaction of VO-TTP. No other vanadium containing species and metal-free porphins were detected in the liquid samples. Similar trends were observed in all the other HDM-experiments with VO-TTP, irrespective of vanadium-loading of the catalysts, liquid phase concentration of hydrogen and reaction temperature.

It can be seen clearly from figures 1 and 2 that VO-TTP is much more reactive than Ni-TTP at the conditions applied. Not only the concentration of VO-TTP drops faster and the concentration levels of hydrogenated intermediate species are much higher, but also the total content of vanadium in the liquid phase decreases faster than is the case with nickel.

Since the concentrations of reactants, reaction intermediates, hydrogen and hydrogen sulfide could be calculated at the reaction conditions applied, detailed kinetic analysis of the HDM reactions of both Ni-TTP and VO-TTP was possible.

Various kinetic models were tested which were all based on sequential reaction mechanisms. The most successful model is depicted in figure 3. In this model, which applies for both Ni-TTP and VO-TTP, the initial porphin is hydrogenated reversibly to its intermediates M-TPC and M-TPiB ( $M = \text{Ni, VO}$ ). The intermediate M-TPiB then goes through a series of reactions, leading to the deposit of a metal sulfide on the catalyst and the fragmentation of the porphin macrocycle. The hydrogenolysis process is lumped into one irreversible step, represented by an apparent rate constant  $k_5$ .

It was carefully checked if inhibition by porphinic species occurs. No evidence was found for this at the conditions applied. Also in separate experiments with a flow reactor, in which the initial concentration of reactants as well as reaction temperatures were varied over large intervals, no evidence was obtained for inhibition of the HDM reactions by porphinic species.

Kinetic analysis of the HDM reactions of Ni-TTP and VO-TTP with respect to the liquid phase concentration of hydrogen revealed that both the hydrogenation reactions (1 and 3) and the hydrogenolysis step (5) exhibit fractional orders in hydrogen. The dehydrogenation reactions (2 and 4) appeared to be zeroth order in hydrogen. Similar results were obtained by Van Steenderen et al. [8] for the HDM reactions of Ni-TTP over a sulfided  $\text{Mo}/\gamma\text{-Al}_2\text{O}_3$  catalyst at 613 K. The kinetic orders with respect to the liquid phase concentration of hydrogen are given in table 3. For comparison, the results obtained by Van Steenderen et al. are included.

Table 3. Kinetic orders with respect to the liquid phase concentration of hydrogen

catalyst	porphin	T (K)	$\alpha$	$\beta$
V(1.8)/Al <sub>2</sub> O <sub>3</sub>	Ni-TTP	573	0.80	1.89
V(1.8)/Al <sub>2</sub> O <sub>3</sub>	VO-TTP	573	1.01	1.51
Mo(1.2)/Al <sub>2</sub> O <sub>3</sub>	Ni-TTP	613	0.73	1.78

The kinetic order in hydrogen of the hydrogenation reactions is represented by  $\alpha$ .  $\beta$  represents the order in hydrogen of the hydrogenolysis step.

The fractional orders in hydrogen concentration indicate a Langmuir-Hinshelwood type of kinetics. Two kinetic models were considered based on the fact that no inhibition occurs by porphins and their hydrogenated intermediates or products. In the first model, adsorbed molecular hydrogen reacts with the porphins and their hydrogenated intermediates. In the second model, the porphinic species are thought to react with dissociatively adsorbed hydrogen. In both the models hydrogenolysis was considered to take place on either the same type of sites as



hydrogenation and dehydrogenation or on a different type of sites.

Although all models considered fitted reasonably well with the experimental data, for both Ni-TPP and VO-TPP the best results were obtained with the model of dissociatively adsorbed hydrogen with different types of sites for hydrogenation/dehydrogenation and hydrogenolysis. With this model, a value of  $K_H = 7.49 \cdot 10^{-5} \text{ m}^3/\text{mol}$  was obtained. The hydrogenation and dehydrogenation rate constants were not introduced as variables but the ratios  $k_1/k_2$  and  $k_3/k_4$  were kept constant. They are in fact the equilibrium constants which were estimated from non-catalytic experiments and from various catalytic experiments in which liquid phase concentrations of hydrogen and hydrogen sulfide were widely varied. The estimated equilibrium constants at 573 K are given in table 4.

**Table 4. Equilibrium constants of Ni-TPP and VO-TPP at 573 K**

	Ni-TPP	VO-TPP
$K_{1,2} = k_1/k_2$	$3.147 \cdot 10^{-3}$	$7.983 \cdot 10^{-3}$
$K_{3,4} = k_3/k_4$	$8.919 \cdot 10^{-4}$	$2.949 \cdot 10^{-3}$

Plots of intrinsic rate constants for the HDM reactions of Ni-TPP and VO-TPP as a function of vanadium content of the catalysts are shown in figures 4 and 5, respectively.

It can be seen from figures 4 and 5 that VO-TPP is much more reactive than Ni-TPP. In both cases, the HDM reactions appear to be structure sensitive. This effect is for both Ni-TPP and VO-TPP most pronounced in the secondary hydrogenation rates ( $k_3$ ). The (lumped) rate constant of hydrogenolysis ( $k_5$ ) decreases almost linearly with increasing vanadium loading.

### Discussion

The results obtained from the current investigation have demonstrated that the HDM of VO-TPP and Ni-TPP proceed through identical pathways. In both cases the initial porphin is reversibly hydrogenated to its chlorin, which in turn is reversibly hydrogenated to yield a metal-isobacteriochlorin.

Kinetic analysis of the hydrogen dependence of the HDM reactions revealed that both the hydrogenation and hydrogenolysis reactions exhibit fractional orders in the liquid phase concentration of hydrogen (table 3) whereas zeroth order applies for the dehydrogenation reactions. The non-integer orders in hydrogen indicate a Langmuir-Hinshelwood type of kinetics. It was shown that a single site model for hydrogenation and dehydrogenation reactions, in which porphinic species and atomic hydrogen are adsorbed on the same type of sites, fitted best with the experimental data, irrespective of the porphin used. The fact that the value for  $K_H$  is very low shows that the HDM reactions of both Ni-TPP and VO-TPP are only slightly inhibited by hydrogen at 573 K.

At present it is not clear whether the metal is removed from the metal-isobacteriochlorin, at which a very unstable metal-free porphinic molecule is formed, or metal removal takes place after destruction of the porphin macrocycle by e.g a combination of hydrogenation and cracking reactions. Fact is however that the hydrogenolysis reactions leading to the removal of metals from Ni-TPP and VO-TPP have fractional orders in hydrogen greater than 1 indicating that demetallisation is achieved via a sequence of reactions.

The HDM reactions of Ni-TPP and VO-TPP over sulfided  $\text{V}/\text{Al}_2\text{O}_3$  catalysts are clearly demanding. Primary as well as secondary hydrogenation rates initially increase with increasing vanadium loading of the catalysts, the effect being most pronounced with the secondary hydrogenation rates. The catalyst with a vanadium loading of 3 atoms/nm<sup>2</sup> has a significantly lower

activity toward the hydrogenation reactions. Increasing of the vanadium loading of the catalysts has a dramatic impact on the hydrogenolysis step. Whereas hydrogenation rates initially increase with increasing vanadium loading, the hydrogenolysis rate decreases linearly with the vanadium content of the catalysts. This observation nicely confirms the conclusions that hydrogenation and hydrogenolysis are achieved on different types of sites.

It has been reported [1,2] that with  $V/Al_2O_3$  catalysts prepared by pore volume impregnation with vanadium loadings up to 2 atoms/nm<sup>2</sup> the alumina surface contains an ill defined two-dimensional structure of vanadium oxide. At very low loadings the alumina surface contains species of tetrahedrally coordinated vanadium which, on increasing the vanadium loading, are transformed into octahedrally coordinated species. Further increasing of the vanadium loading is thought to result in an expanding of these relatively small clusters due to polymerisation into larger structures of octahedrally coordinated vanadium with a relatively less intimate interaction with the alumina surface than the former ones. At vanadium loadings exceeding 2 atoms/nm<sup>2</sup>,  $V_2O_5$  crystallites are present on the catalysts.

As for the sulfidability of  $V/Al_2O_3$  catalysts, it was shown [2] that catalysts lacking crystalline  $V_2O_5$  are nearly completely sulfided at 673 K whereas the major part of the sulfiding process of crystalline  $V_2O_5$  takes place at temperatures well above 673 K. At temperatures up to 673 K, crystalline  $V_2O_5$  is reduced to  $V_2O_3$ .

The ease with which the catalysts are sulfided and the observed sulfiding mechanism are indicative for the preservation of the characteristics (e.g. dispersion and support interaction) of the active phase. Also the temperature at which the sulfiding of the catalysts was performed is too low for solid state transformations or solid state diffusion processes to occur.

From the above, the impact of the vanadium loading of  $V/Al_2O_3$  catalysts on the HDM of Ni-TPP and VO-TPP reactions can be rationalised as follows. The relatively low hydrogenation activities of  $V(0.9)/Al_2O_3$  may be the result of the presence of the active phase in small clusters with a strong interaction with the support. On increasing the vanadium content, these clusters expand to larger structures which have a weaker interaction with the support. Due to this weaker interaction sulfur vacancies, which are thought to be the active sites for porphyrin adsorption and hydrogenation, may be formed with more easily. Also edges of the clusters of the active phase may contribute to the hydrogenation activity of the catalysts. It appears that after reaching a maximum with the  $V(1.4)/Al_2O_3$  catalyst, the rate constants of hydrogenation slowly decline. This may be the result of the presence of larger clusters, formed out of small clusters, of the active phase with a relatively lower ratio of edges/mol V. The presence of crystalline material on the  $V(3.0)/Al_2O_3$  catalyst results in a lowering of the hydrogenation activity for both Ni-TPP and VO-TPP. From this it is tentatively concluded that crystalline  $V_2O_3$  has no hydrogenation capacity and, through coverage of the active sites, causes a lowering of the hydrogenation activity of  $V/Al_2O_3$  catalysts.

The fact that the hydrogenolysis activity for both Ni-TPP and VO-TPP decreases linearly with increasing vanadium loading of the catalysts indicates that hydrogenolysis is to a large extent independent of the characteristics of the different phases in which the active material is present and supports the idea that hydrogenolysis is achieved on another type of sites.

As in hydrogenation, sites located at the edges of the active phase clusters apparently play an active role in the hydrogenolysis. Upon increasing the vanadium loading of the catalysts small clusters expand through polymerisation to larger clusters with a relatively lower ratio of edges/mol V resulting in a lowering of the hydrogenolysis activity.

## Conclusions

- HDM of Ni-TPP and VO-TPP proceeds through a reversible sequential mechanism via hydrogenated intermediate compounds of similar nature: metal-tetraphenylchlorin and metal-tetraphenylisobacteriochlorin. VO-TPP is more reactive than Ni-TPP with respect to hydrogenation which can be seen from the faster decline of the concentration of VO-TPP and the substantially larger amounts of hydrogenated intermediates formed.

- A two-site mechanism is found to apply for the HDM reactions of both Ni-TPP and VO-TPP. In the hydrogenation and dehydrogenation reactions porphins, intermediates and atomic hydrogen are adsorbed on the same type of sites which are thought to consist of sulfur vacancies. Hydrogenolysis is achieved on another type of sites in which hydrogen sulfide is thought to play an important role.
- The HDM reactions of both Ni-TPP and VO-TPP are first order in porphins and hydrogenated intermediates. Hydrogenation reactions are approximately first order in the liquid phase concentration of hydrogen whereas dehydrogenation reactions are zero order in hydrogen. The hydrogenolysis reactions exhibit fractional orders in hydrogen greater than one.
- The fact that for hydrogenolysis, hydrogen orders are greater than one indicates the demetallisation of the porphins to proceed through a sequence of fast reactions.
- The HDM reactions of both Ni-TPP and VO-TPP over sulfided  $V_7Al_2O_3$  catalysts are clearly structure sensitive. With increasing vanadium loading of the catalysts hydrogenation rates for both Ni-TPP and VO-TPP increase until, at loadings exceeding 2 atoms V/nm<sup>2</sup>, crystalline  $V_2O_3$  is present on the catalysts. The presence of crystalline  $V_2O_3$  results in a loss of hydrogenation activity probably caused by coverage of active sites by crystalline material. The hydrogenolysis rate is not affected by the presence of crystalline  $V_2O_3$ .

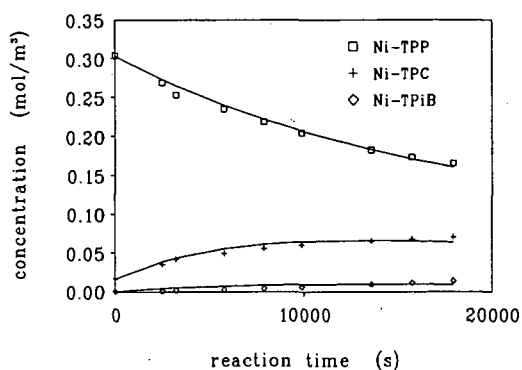
#### Acknowledgements

The authors thank Dr. F. Luck of Rhône-Poulenc for the donation of the various porphins. This study was supported by the Netherlands Foundation for Chemical Research (SON) with financial aid from the Netherlands Organisation for the Advancement of Pure and Applied Research (NWO) and the European Economic Committee (EEC).

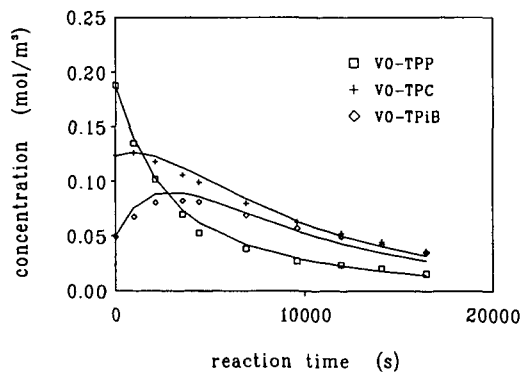
#### Literature cited

1. Bonné, R.L.C., van Langeveld, A.D., Kieboom, M.N.H., and Moulijn, J.A., in preparation.
2. Bonné, R.L.C., van Duin, A.C.T., van Langeveld, A.D., and Moulijn, J.A., in preparation.
3. Agrawal, R., and Wei, J., Ind. Eng. Chem., Process Des. Dev. **23**, 505 (1984).
4. Moysan, J.M., Huron, M.J., Paradowski, H., and Vidal, J., Chem. Eng. Sci. **38**, 1085 (1983).
5. Hung, C.W., and Wei, J., Ind. Eng. Chem., Process Des. Dev. **19**, 250 (1980).
6. Ware, R.A., and Wei, J., J. Catal. **93**, 100 (1985).
7. Ware, R.A., and Wei, J., J. Catal. **93**, 122 (1985).
8. Van Steenderen, P., Bonné, R.L.C., and Moulijn, J.A., in preparation.

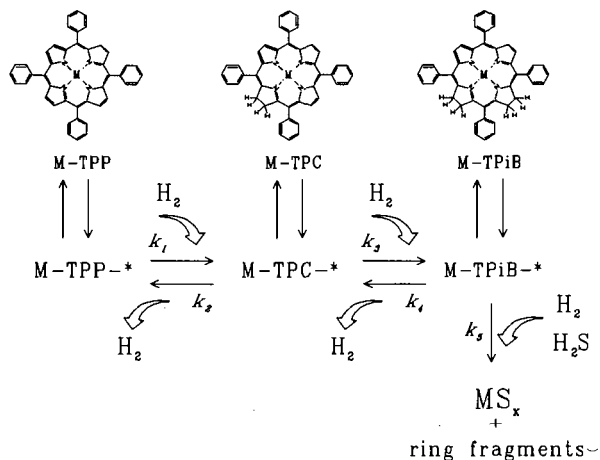
**Figure 1.** Concentration versus reaction time plot of a HDM experiment with Ni-TPP at 573 K (run Ni-32). Experimental values are represented by markers. Solid lines represent calculated values.



**Figure 2.** Concentration versus reaction time plot of a HDM experiment with VO-TPP at 573 K (run V-32). Experimental values are represented by markers. Solid lines represent calculated values.



**Figure 3.** Reversible sequential reaction model for the HDM of M-tetraphenylporphyrins (M=Ni,VO). Deposited metal sulfides are represented by  $MS_x$ .



**Figure 4.** Intrinsic rate constants for the HDM of Ni-TPP at 573 K as a function of the vanadium loading of the catalysts ( $k_2, k_4$  omitted).

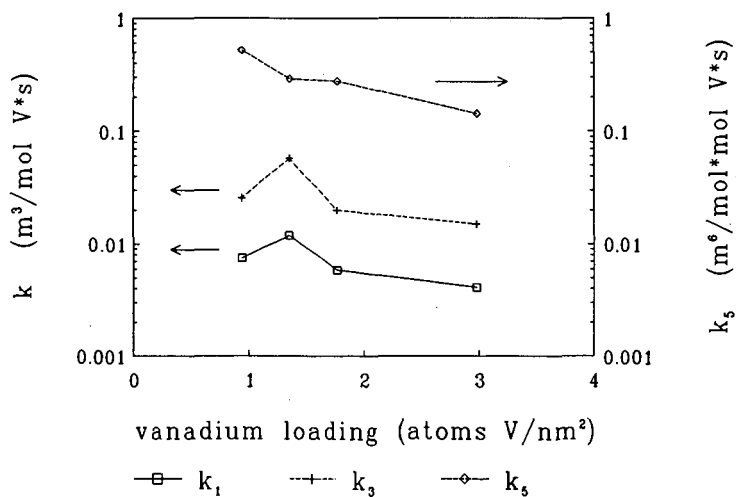
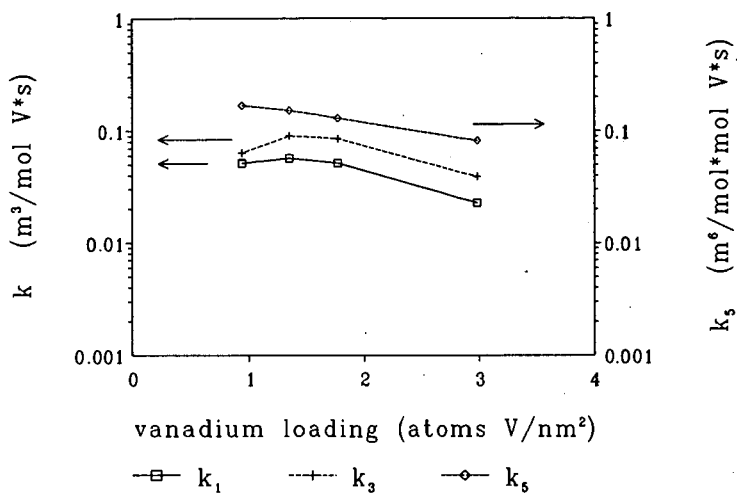


Figure 5. Intrinsic rate constants for the HDM of VO-TPP at 573 K as a function of the vanadium loading of the catalysts ( $k_2$ ,  $k_4$  omitted).



## CRACKING PROPERTIES OF SAPO-37 AND FAUJASITES

M. BRIEND, A. LAMY, D. BARTHOMEUF, Laboratoire de Réactivité de Surface et Structure, URA 1106, Université P. et M. Curie, 4 place Jussieu, 75252, Paris Cédex 05.

Keywords : SAPO-37, stability, acid catalysis

### Abstract :

SAPO-37 materials with Si atomic fraction from 0.12 to 0.22 are studied for their thermal stability, their acidity and their cracking activity. Most of the acid sites have a medium acid strength. A very small number of sites is very strong. The materials are thermally stable up to high temperatures. After pretreatment at 1175 K they are as active as an ultrastable faujasite in the cracking of n-octane.

### INTRODUCTION

SAPO-37, isotype of faujasite, is an active catalyst for cracking reactions (1,2). The present paper compares the properties of this material with those of faujasites.

### EXPERIMENTAL

The samples are synthesised as described in (3) for sample Si-0.12 and Si-0.13 and in (4) for the other solids. The chemical analysis gives results in table 1.

XRD is used to determine the unit cell parameter of the as-synthesised samples. The heating chamber of a Guinier Lenné camera is employed to follow the changes in crystallinity and to determine the temperature for the loss of crystal structure.

TPD of  $\text{NH}_3$  is followed using a quadrupole mass spectrometer Quadrupac PGA 100 Leybold-Heraeus.

The desorption of pyridinium ions from the H-SAPO-37 samples is followed by infrared spectroscopy.

The catalytic activity in the cracking of n-octane at 725 K is studied in a microreactor with  $\text{H}_2$  as carrier gas.

### RESULTS AND DISCUSSION

#### Si incorporation in the framework

The incorporation of Si in the SAPO-37 framework is seen by the decrease of the unit cell parameter  $a_0$  (table 1) as the materials contain more Si.

The mechanism II of substitution of Si for P in a theoretical  $\text{AlPO}_4$  framework creates isolated Si atoms (1). Each Si atom generates one proton. According to mechanism III, 2 Si replace a pair Al-P in the  $\text{AlPO}_4$  framework. In the case of SAPOP-37, Si containing islands are formed (2-5,7). This decreases the potential number of protons formed if no Al is included in those Si islands (5). Alternatively some Si-Al faujasite phase has been described (2,7). The table 1 shows that the Al fraction is often less than the theoretical value 0.50 which suggests the existence of Si islands. The difference from 0.50 increases as the Si content rises (except for the sample Si-0.20 which in fact contains some impurities of SAPO-20). This corresponds to an increasing amount of Si in islands. This is confirmed by the simultaneous decrease in the amount of occluded template (table 1) which indicates that a smaller number of charges have to be neutralized.

### Thermal stability

The stability of the crystal structure studied in the heating XRD chamber is very high (table 1). In a flow of dry O<sub>2</sub> or of oxygen saturated with water at room temperature the structure collapses near 1200-1300 K which is similar to the case of the ultrastable LZ-82 zeolite (8). Nevertheless the SAPO-37 structure is not stable in ambient conditions for the template free samples (table 2). The instability occurs when the template free sample is contacted with water at temperatures lower than around 350 K. It probably results from the attack of Al-O-P bonds (8).

### Acidity

The TPD of ammonia and of pyridine (table 3) gives one broad peak for all the SAPO-37 materials (free of template) located near 500 K or 665 K for the two bases respectively. Examples are given for Si-0.13 and Si-0.20 in table 3. The same experiment gives for HY and for a dealuminated sample (HYD) 2 peaks indicating two main average acid strength distributions. The mean acid strength of SAPO-37's is intermediate between the two which exist in faujasites (9). A detailed infrared study of the acid strength of protons followed by the limit temperature to evacuate the pyridinium ions shows (table 3) that higher temperatures are required (i.e. stronger acid present) for the SAPO-37 material than for HY or even than the dealuminated HYD compared to Si-0.13. This suggests the presence of very strong acid sites which infrared study showed to be in a very small amount (6).

The TPD peaks related to the medium acid strength which is the main source of acidity very likely reflects the protonic acidity associated to isolated Si-O-Al species. The very strong sites evidenced by infrared would be the Si-O-Al centers at the border of Si islands.

### CATALYTIC ACTIVITY

The n-octane cracking carried at 725 K gives the results of table 4. After a pretreatment at 875 K for SAPO-37 and 675 K for HY (in order to avoid structure collapse) the % conversion and selectivities are reported in table 4. The very active HY had to be tested at a higher flow rate in order to decrease the % conversion to the SAPO's range. With a similar flow rate HY would be 15 to 20 times more active. The table 4 shows that similar products are formed with all the catalysts. Looking at the ratios olefin/paraffin, values of 1.9, 1.9 and 1.6 are obtained for Si-0.16, Si-0.20 and Si-0.22 while HY gives 1.2. This suggests lower hydrogen transfer reactions for SAPO's which might result from a higher distance between close sites than in Si-Al faujasites. For the branched to non branched hydrocarbons ratios, SAPO's give 0.6, 0.5 and 0.6 in the same order of materials as above and HY 0.65.

Increasing the pretreatment temperature up to 1225 shows that HY loses its activity near 1075 K and the SAPO's together with the ultrastable LZ-82 material near 1175 K. The table 5 compares the changes in per cent conversion for Si-0.22 and LZ-82. It shows that after pretreatment at 1175 K Si-0.22 is even more active than LZ-82. This stability for the catalytic properties at high temperatures may be related to the high thermal stability described above in tables 1 and 3.

In conclusion the main influence of phosphorus in SAPO's compared to Si-Al faujasites is an increased thermal stability which maintain catalytic properties after heating at high temperatures. It also give rise to a higher olefin to paraffin ratio suggesting a lower hydrogen transfer activity.



## REFERENCES

- 1 E.M. Flanigen, R.L. Patton, S.T. Wilson, Innovation in Zeolite Materials Science (P.J. Grobet et al., eds), Stud. Surf. Sci. Catal., 1988, **37**, 13.
- 2 J.A. Martens, P.J. Grobet, P.A. Jacobs, J. Catal., 1990, **126**, 299.
- 3 B.M. Lok, C.A. Messina, R.L. Patton, R.T. Gajek, T.R. Cannan, E.M. Flanigen, US Pat. 4 440 871 (1984).
- 4 G.C. Edwards, J.P. Gilson, V. Mc Daniel, US Pat. 4 681 864 (1987).
- 5 P.P. Man, M. Briend, M.J. Peltre, A. Lamy, P. Beaunier, D. Barthomeuf, Zeolites, 1991, in press.
- 6 S. Dzwigaj, M. Briend, A. Shikholeslami, M.J. Peltre, D. Barthomeuf, Zeolites, 1990, **10**, 157.
- 7 L. Maistriau, N. Dumont, J.B. Nagy, Z. Gabelica, E.G. Derouane, Zeolites, 1990, **10**, 243.
- 8 M. Briend, A. Shikholeslami, M.J. Peltre, D. Delafosse, D. Barthomeuf, J. Chem. Soc. Dalton Trans., 1989, 1361.
- 9 M. Briend, A. Lamy, S. Dzwigaj, D. Barthomeuf, Proceed. Int. Zeol. Symp., Prague, 1991.

Table 1. Characteristics of SAPO-37 materials

	Si 0.12	Si 0.13	Si 0.16	Si 0.20	Si 0.22
Si <sub>x</sub> <sup>(a)</sup>	0.12	0.13	0.16	0.20	0.22
Al y	0.50	0.49	0.48	0.50	0.46
Pz	0.38	0.49	0.36	0.30	0.32
Occluded templates % <sup>(b)</sup>	22.3	20.7	21.9	19.7	18.5
a <sub>0</sub> (Å) <sup>(c)</sup>	24.76	24.76	24.74	24.70	24.71
Thermal stability (O <sub>2</sub> ) (K)	nd <sup>(d)</sup>	1270 ± 30	nd	nd	1320 ± 30
O <sub>2</sub> + H <sub>2</sub> O (K)	nd	1275 ± 30	nd	nd	1240 ± 30

a : x, y, z molar fraction

b : weight %

c : as-synthesised samples

d : not determined

Table 2. Thermal stability

With template	stable	template decomposition	stable
template free no water	stable		
template free + water	unstable	stable	
RT	~ 350 K	~ 850 K	1200-1300 K

Table 3. Acidity of SAPO-37 materials

	TPD NH <sub>3</sub>	TPD Py	T desorption pyridinium
Si-O.13	500 (a)	665 (b)	723 (c)
Si-O.20	500	665	673
HY	455 520	545 735	623
HYD	455 520	545 735	673

a, b peak (K) of the maxima in TPD of ammonia (a) or pyridine (b)

c evacuation temperature (K) for the complete disappearance of the pyridinium ion (infrared spectroscopy)

Table 4. Selectivities (mole %) in the cracking of n-octane at 725 K

Products	Si-0.16(a)	Si-0.20	Si-0.22	HY (a)
methane (b)	4.4	3.9	3.8	3
ethylene (b)	2.8	2.2	2.1	1.7
ethane	7.9	5.9	6.7	4.7
propene + propane	24.8	23.0	24.9	25.4
iso-butane	3.1	5.2	5.2	7.1
n-butane	9.2	12.4	9.7	9.8
iso-butene	9.6	6.8	9.7	10.5
n-butene	3.9	5.0	4.4	4.1
cis-butene	4.8	5.7	5.0	4.9
trans-butene	6.7	7.9	6.8	6.8
iso-pentane	2.5	4.1	4.1	4.8
n-pentane	5.7	4.7	5.4	5.5
1-pentene	0.8	1.0	0.7	0.6
3-methyl-butene	0.3	0.4	0.4	0.5
trans-2-pentene	1.8	2.2	1.9	1.9
cis-2-pentene	5.4	3.6	3.2	3.5
2-methyl-2-butene	6.1	6.0	6.0	5.2
conversion %	1.3	1.3	1.6	2.7

(a) Flow rate 13 ml/min for SAPO's and 56.2 ml/min for HY

(b) Thermal cracking

Table 5. % conversion in n-octane cracking at 725 K

	1075	1175	1225
Si-0.22	1.7	2.4	~ 0
LZY-82	> 6	1.5	~ 0

## Carbon Materials - Activity and Selectivity in Hydrocracking Reactions.

M. Farcaiu, C.M. Smith, E.P. Ladner  
U.S. Department of Energy  
Pittsburgh Energy Technology Center  
P.O. Box 10940, Pittsburgh, PA 15236

A.P. Sylwester  
Sandia National Laboratory, Albuquerque, NM 87185

Keywords: carbon materials, hydrocracking catalysts, selectivity.

### INTRODUCTION

The use of carbon materials in catalytic systems has been traditionally associated with their properties as supports (1). There are, however, some literature data describing their use as catalysts. It was reported that, after activation with ammonia, some carbon blacks are good oxidation catalysts (2) and that some activated carbons are active in the cracking of hydrocarbons (3). Our data (4,5), as well as recent data by Grunewald and Drago (6), show that some carbon materials could act as catalysts for specific reactions. Thus, a high surface area carbon molecular sieve was active for oxidative dehydrogenation reactions at temperatures of about 2300C (6). We have used carbon materials with variable surface area as catalysts for C-C cleavage in a reductive medium and at temperatures above 3200C (4,5).

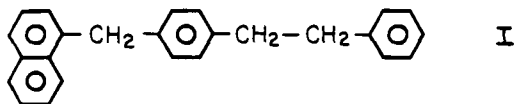
In this paper, we describe a systematic study of the catalytic activity of carbon blacks of different surface area and origin and also the catalytic activity of carbon materials obtained by the pyrolysis of polymers such as resorcinol - formaldehyde and polyacrylonitrile.

### EXPERIMENTAL

**Materials and Analytical Procedures.** 9,10-Dihydrophenanthrene (9,10-DHP) was obtained from Aldrich Chemical Co. Black Pearls 2000, Monarch, Mogul and Regal carbon blacks were provided by Cabot Corporation; graphite powder -325 mesh was supplied by ALFA. The carbon materials from the carbonization of polyacrylonitrile and resorcinol-formaldehyde polymers were prepared at Sandia National Laboratory and their methods of preparation have been described previously (7-11). The results of the analyses performed on different carbon materials used in this work are given in Tables 1, 2, and 3.

The elemental analyses were performed by Huffman Laboratories, Golden, CO, and at the Pittsburgh Energy Technology Center. The surface area of various carbon materials was measured in Prof. D. Smith's laboratories at the University of New Mexico in Albuquerque and at Sandia for the carbon materials from the polymer pyrolyses.

4(1-Naphthylmethyl)bibenzyl, I, was prepared in Prof. Paul Dowd's laboratory at the University of Pittsburgh and completely characterized, as previously reported (5). Dichloromethane was stored over 4A molecular sieves.



Glass reaction tubes were made of Pyrex tubing, 5 x 7 mm (i.d. x o.d.). Sealed sample tubes were approximately 75 mm long.

Gas chromatographic analyses were carried out on a Hewlett Packard Model 5890 gas chromatograph equipped with an SE-30 60m capillary column. Gas chromatography/Mass spectra (GC/MS) were obtained on a Hewlett Packard GC/MS Model 5985 instrument equipped with a 30 m SE-52 capillary column.

Identification of reaction products was accomplished by GC/MS analysis and, when possible, by GC comparison with authentic samples. Reported product yields and overall conversion of I are based on capillary GC.

**General Experimental Procedure.** The reaction components (9,10 DHP, ca. 100 mg, I, ca. 25 mg, and catalysts) were weighed into open-ended glass reaction tubes. The tubes were flame-sealed, and no precaution was taken to exclude air. Warm water was used to melt the hydrogen donor and ensure the mixing of the reactants. The samples were placed upright in a temperature-equilibrated Lindberg muffle furnace and heated at the indicated temperatures for given times. The samples were removed from the oven, cooled to room temperature, and diluted with ca. 0.5 mL of dichloromethane. The samples were filtered through a plug of  $MgSO_4$  and glass wool. An additional 0.5 mL of dichloromethane was used to wash the filter and, in the catalytic reaction, the carbon black catalyst. An aliquot of the resulting solution was analyzed by gas chromatography. The recovery was checked for selected experiments with an internal standard.

**Catalytic Activity.** As a measure of the catalytic activity, we determined: the overall conversion (thermal + catalytic), the catalytic conversion, and the selectivity of the catalytic conversion toward cleavage of the C-C bond between the naphthalenic ring and the adjacent aliphatic carbon. The selectivity of the above-described cleavage is calculated as the percent of the catalytic conversion only.

**Deactivation, Recovery and Reuse of Black Pearls 2000.** Black Pearls 2000 was recovered from several different reactions, washed, and dried for reuse. In a typical procedure, the catalyst was recovered from a reaction using compound I and 9,10 DHP, which had been run at 420°C for 1 h. The samples were prepared as described above in the general procedure. At the end of the reaction time, the tubes were cooled to room temperature. The reaction mixture was filtered through a filter paper and the retained catalyst was washed with dichloromethane and cyclohexane. The catalyst was washed

exhaustively until the GC analysis indicated only the presence of the solvent. The Black Pearls was dried in vacuo at 105°C for 4 h. Surface area determination and elemental analyses of the used catalyst are presented in Table 1.

## RESULTS AND DISCUSSION

Soon after observing the catalytic activity of carbon blacks for the cleavage of C-C bonds, we found that not all carbon materials act as a catalyst. Therefore, we initiated a study to determine what features make some carbon materials active. Obvious candidates were chemical composition, surface area, and the structure of the carbon skeleton. As a first step of this study, we looked at several carbon materials of different origin and properties and tested their catalytic activity for reactions of compound I in presence of 9,10 dihydrophenanthrene as H-donor.

**Cabot Carbon Blacks as Catalysts** We used four carbon blacks (Table 1) obtained from Cabot Corp. and found that all four were active as catalysts for selective cleavage of C-C bonds. Their catalytic activity was proportional to their surface area. When the Cabot carbon blacks were present in quantities that provided equivalent surface area their catalytic activity and selectivity were very similar (Table 4). We found, however, that another commercial carbon black Norit (1300 m<sup>2</sup>/g) exhibits only about 77% of the activity of BP2000 for equivalent surface area.

For comparison, Alpha graphite does not exhibit any catalytic activity under our reaction conditions.

**Carbon Materials from Carbonization of Organic Polymers** A variety of carbon materials can be obtained by carbonization of organic polymers under controlled conditions (7-11). We investigated the carbonization products of polyacrylonitrile and of resorcinol-formaldehyde foams prepared at Sandia NL.

- a. **Carbonized Polyacrylonitrile Polymers (PAN) as Catalysts** Polymers pyrolyzed at various temperatures (Table 2) were tested for their hydrocracking activity (Table 5). They have substantially lower surface area and catalytic activity than the Cabot Carbon Blacks, but exhibit the same selectivity. After 1h at 422°C, the catalytic conversion of Ig of I is 1.65 %/ m<sup>2</sup> catalyst for carbon black BP2000 but only 1.1 %/ m<sup>2</sup> catalyst for PAN 410. Also, while the surface area of PAN 410 (pyrolyzed at 1200°C) is almost twice as large as that of PAN 1448 (pyrolyzed at 2000°C), the catalytic conversion of I is ~ four times larger with PAN 410 than with PAN 1448. Obviously, surface area is one, but not the only, factor in the activity of carbon materials.
- b. **Carbonized Resorcinol-Formaldehyde Foams (CRF) as Catalysts** A systematic study of carbon materials as catalysts was possible because carbon materials could be obtained by controlled pyrolysis of resorcinol-formaldehyde foams (9). For each pyrolysis temperature, several surface areas of carbon material could be obtained (10). The samples used in this paper are described in Table 3 and their catalytic activity is presented in Table 6. It can be seen that for materials pyrolyzed at the same temperature the activity is

proportional to the surface area, while for materials with the same surface area, the activity depends on the pyrolysis temperature (Fig.1). The CRF materials are the most active catalysts among the materials we have investigated so far. The catalytic conversion at 400°C in 1h for Ig of I is 0.54%/m<sup>2</sup> of CRF (pyrolyzed at 1050°C) and only 0.34 % /m<sup>2</sup> of BP2000.

**Activity of the Reused Carbon Materials** We have conducted some preliminary experiments in which carbon black BP2000 was recovered after reaction and re-used (see experimental part, Tables 1 and 7). These experiments showed that the reactivated BP2000 has an elemental composition different from the initial material and its surface area is reduced by ~30%. The catalytic activity of the recovered material is also reduced by 30%, but the selectivity remains the same.

**Charge Distribution Analysis of Carbon Materials** Charge Distribution Analysis (CDA) is a new method, invented by F.Freund (12), which makes possible the determination of the charge on the surface of solids as a function of temperature. Several of the carbon materials used as catalysts in this work have been studied by F.Freund by CDA. In all cases, the carbon materials that are acting as catalysts started to develop positive charges on their surface when heated in an inert gas at temperatures around 3000°C. We have shown that carbon black BP2000 becomes catalytically active for the C-C cleavage reaction at ~ 3200°C, and we have discussed possible mechanistic implications (4,5). Further work is being carried out to determine whether the selectivity of carbon materials for the cleavage of C-C bond adjacent to a condensed polyaromatic structures is related to this positive charge on the surface of the catalyst.

## CONCLUSIONS

Our results show that no simple relationship exists between the catalytic activity of some carbon materials for selective cleavage of carbon-carbon bonds adjacent to condensed polyaromatic rings and the elemental composition or surface area of these materials. The activity is dependent, however, upon the precursor used to generate the carbon material. Moreover, for a given precursor the activity is determined by the method of conversion to the carbon material. It remains to be established what elements of structure are responsible for the observed activity in carbon materials that are catalytically active.

## ACKNOWLEDGEMENTS

We thank R.W. Pekala of Lawrence Livermore National Laboratory for the samples of CRF materials and Dr.F. Freund from SETI-NASA for the CDA determinations.

## DISCLAIMER

Reference in the paper to any specific commercial project, process, or service is to facilitate understanding and does not necessarily imply its endorsement or favoring by the United States Department of Energy.



## REFERENCES

1. Kaminsky, M.; Yoon, K.J.; Geoffroy, G.L.; Vannice, M.A. *J.Catal.* 1985, 91, 388. Venter, J.J.; Vannice, M.A. *J.Amer. Chem. Soc.* 1989, 111, 2377 and references therein.
2. Boehm, H.P., "Structure and Reactivity of Surfaces," C. Morterra, A. Zecchina and G. Costas Editors, Elsevier Science Publishers B.V., Amsterdam, 1989.
3. Greensfelder, B.S.; Voge, H.H.; Good, G.M. *Ind. and Eng. Chem.* 1949, 41, 2573.
4. Farcasiu, M.; Smith, C. *Prepr. Pap. Am. Chem. Soc. Div. Fuel Chem.* 1990, 35, 404.
5. Farcasiu, M.; Smith, C. *Energy & Fuels* 1991, 5, 83.
6. Grunewald, G.C.; Drago, R.S. *J.Amer. Chem. Soc.* 1991, 113, 1636.
7. Sylwester, A.P.; Aubert, J.H.; Rand, P.B.; Arnold, C.J.; Clough R.L. *ACS PMSE Preprints* 1987, 57, 113.
8. U.S. Pat. 4,832,881 (1989).
9. Pekala, R.W. *J. Mat. Sci.* 24, 1989, 3221.
10. Pekala, R.W.; Kong, F. *ACS Polym. Preprints*, 1989, 30, 221.
11. Aubert, J.H.; Sylwester A.P. *J. Mat. Sci.* 1991 (In Press).
12. Freund, M.M.; Freund, F.; Batlo, F. *Phys Rev. Lett.* 1989, 63, 2096.

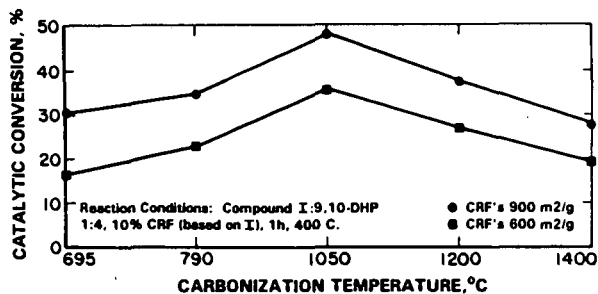


Fig.1 Influence of the Carbonization Temperature on the Catalytic Activity of CRF Carbon Materials.

Reaction conditions : I:9,10DHP 1:4 (wt), 10 % CRF (based on I), 1h, 400°C.

Table 1 Properties of Carbon Blacks form Cabot Co.

Material	Surface Area m <sup>2</sup> /g	Dry loss %	Elemental		Analysis	Dry	Basis %
			C	H	S	O	Ash
Regal 400 R	86	2.3	95.9	0.5	0.9*	1.5	0.9
Mogul L	138	3.2	94.9	0.5	1.0	3.0	0.5
Monarch 1300	560	7.9	88.9	0.5	1.1	7.5	2.8
Black Pearls 2000	1475	10.9	96.1	1.4	1.4	1.4	1.2
Black Pearls 2000, recovered*	1026	0.0	96.5	1.7	0.3	0.6	0.8

\* the recovery of the used BP2000 is described in the experimental section.

Table 2 Properties of Carbonized Polyacrylonitrile Polymers.

PAN #	Temperature of Carbonization C	Surface Area m <sup>2</sup> /g	Elemental		Analysis wt.	%
			C	H	N	O*
455	700	16	73.5	0.5	15.6	10.4**
662	800	17	75.4	0.2	13.4	10.0
1260	1100	22	94.3	<0.05	3.2	2.5**
410	1200	85	96.9	<0.05	1.8	0.6
1448	2000	48	>99.9	-	-	-

\* O by Neutron Activation Analysis

\*\* O by difference

Table 3 Properties of Carbonized Resorcinol-Formaldehyde Polymers.

CRF #	Temperature of Carbonization °C	Surface Area m2/g	Elemental Analysis,		wt.% O*	
			C	H		
654	695	900	93.69	1.45	<0.01	-4.9
626	695	700	--	--	--	-
654	790	900	94.62	0.85	0.02	-4.1
626	790	700	--	--	--	-
1029	1050	900	94.22	0.59	0.20	-5.0
613	1050	600	92.33	0.63	0.18	-6.9
654	1200	900	97.57	0.19	0.21	-2.0
626	1200	600	--	--	--	-
571	1400	900	98.88	0.30	0.06	-0.8
624	1400	600	--	--	--	-

\* Oxygen by difference

Table 4 Experiments with Various Cabot Carbon Blacks at Equivalent Surface Area of Catalyst per gram of Compound I.  
In all cases 1:4 ratio (wt) Compound I : 9,10 DHP, 1h.

Carbon Black	Cat. conc. m <sup>2</sup> cat/g I	Temp. C	overall conv. %	catalytic conv. %	selectivity %
None	-	407	5	-	(43)*
Regal	15.6	407	15.3	10.3	100
Mogul	15.6	407	15.4	10.4	97
Monarch	15.6	407	13.5	8.5	100
BP2000	15.6	407	13.6	8.6	100
None	-	428	26	-	(40)*
Regal	14	428	42	16	100
Mogul	14	428	45	19	100
Monarch	14	428	35	9	100
BP2000	14	428	46	20	100

\* The selectivity of the thermal reaction is expressed as a percent of the C-C bond cleavage of the bond adjacent to the naphthalene ring vs overall conversion.

Table 5. Catalytic Properties of Carbonized PAN Polymers.

Reaction conditions: Compound I:9,10 DHP = 1:3 (by wt), 1h, 420°C.  
Different PAN carbons were added to an equivalent surface area (4.25 m<sup>2</sup> catalyst/g of I).

Carbonization temp. of PAN C	Surface Area m <sup>2</sup> /g	Overall conv. I %	Catalytic conv. I %	Catalytic Selectivity %
700	16	15.1	0	-
800	17	14.5	0	-
1100	21	20.1	3.8	> 93
1200	85	21.0	4.7	100
2000	48	17.5	1.2	> 90
Thermal		16.2		43*

\* The selectivity of the thermal reaction is expressed as a percent of the C-C bond cleavage of the bond adjacent to the naphthalene ring vs. overall conversion.

Table 6. Catalytic Properties of Carbonized Resorcinol Formaldehyde Polymers.

Reaction conditions :  
I : 9,10 DHP (wt) 1:4, 10 % wt CRF material (based on I), 400°C, 1h.

Carbonization temp. of CRF C	Surface Area m <sup>2</sup> /g	Overall conv. I %	Catalytic conv. I %	Catalytic Selectivity %
695	900	33.4	30.4	>99
790	900	37.8	34.8	100
1050	900	51.2	48.2	98
1200	900	40.6	37.8	100
1400	900	31.0	28.0	97
695	700	19.6*	16.4	>99
790	700	25.8*	22.8	100
1050	600	38.8	35.8	99
1200	600	30.0	27.0	100
1400	600	22.1	19.1	96
Thermal		3.0		43**

• the experimental values for the overall conversion for these catalysts have been reduced by the factor of 600/700 for comparison with the catalysts that have surface areas of 600 m<sup>2</sup>/g ( samples carbonized at 1050, 1200 and 1400°C).

\*\* the selectivity of the thermal reaction is expressed as a percent of the C-C bond cleavage of the bond adjacent to the naphthalene ring vs. overall conversion.

Table 7. Activity of Fresh and Recovered\* BP2000

Reaction of I in presence of 9,10 DHP, 1h, 407°C 10% BP2000 (based on I)

Catalyst	Surface area m <sup>2</sup> /g	Overall conv. %	Catalytic conv. %	Selectivity %
None	-	5	-	44**
Fresh	1475	63	58	98
Recovered*	1026	45	40	98

\* for the recovery conditions see Experimental Section.

\*\* The selectivity of the thermal reaction is expressed as a percent of the C-C bond cleavage of the bond adjacent to the naphthalene ring vs overall conversion.

## INDUSTRIAL CATALYSTS FOR AROMATICS REDUCTION IN GAS OIL

Arpad F. Somogyvari, Michael C. Oballa and Patricio S. Herrera  
NOVA Husky Research Corporation  
2928 16 - Street N.E., Calgary, Alberta, Canada T2E 7K7

Keywords: hydrotreating, aromatics reduction, hydrocracked gas oil

### ABSTRACT

Six commercially available Ni-Mo/ $\text{Al}_2\text{O}_3$  catalysts were tested for HDN, aromatics reduction and HDS on a hydrocracked gas oil (249 - 524°C) in a fixed bed reactor operating in the upflow mode. Acceptable HDN, HDS, and aromatics reduction were obtained for three of the six catalysts. Total aromatics concentrations were determined using four different methods, two of which were also used to determine PNA concentrations. Each method gave a different aromatics concentration, however, linear correlations were established between the results obtained by each method. Contrary to expectations, superior HDN and HDS performance and comparable PNA reductions were observed in a heavier fraction (343+°C) than in the total liquid product.

### INTRODUCTION

The expected depletion of the lightest conventional feedstocks has placed a greater emphasis on upgrading technologies. These technologies generally involve hydrocracking the "bottom of the barrel" and hydrotreating the resulting distillates to reduce the amounts of sulphur and nitrogen<sup>1,3</sup>. The substitution of conventional petroleum with synthetic crudes is on the rise. This trend is expected to shift the hydrocarbon distribution toward the aromatic at the expense of the saturates in the blended feedstocks<sup>4</sup>. Studies have shown that, due to their high content of aromatic components, combustion of synthetic fuels generates higher particulate concentrations than combustion of conventional fuels in both diesel engines and heating appliances. Because of the varied health hazards associated with particulate emissions<sup>5,6</sup>, refiners are confronted with stricter regulations aimed at controlling particulate emissions and unburned hydrocarbons in diesel exhaust through reduced aromatics levels.

Thus, aromatics reduction has become a key upgrading parameter in light of stringent environmental regulations and industry trends toward low-quality component blends derived from conventional crudes and synthetic crude distillates. The optimization of product quality and product performance becomes critical both from an environmental and a marketing perspective. While regulations have focussed on aromatics determined by fluorescent indicator adsorption (FIA) in diesel fuels, the guidelines for aromatics determination in the gas oil fraction are much more ambiguous. Consequently, it is essential to have a reliable method for aromatics determination in these heavy cuts.

The work reported herein is part of a much larger study aimed at evaluating the performance of commercial catalysts during the hydrotreating of gas oil. One of the performance indicators in that study was the reduction in the amount of aromatic components. Many conventional hydrotreating catalysts (e.g., sulphided Ni-Mo/ $\text{Al}_2\text{O}_3$ ), normally designed for hydrodesulphurisation, show excellent hydrodenitrogenation activity and perform aromatics reduction as well.

This paper provides technical information related to product properties upon hydrotreating a hydrocracked gas oil. The data will focus on aromatics determination and aromatics reduction for six commercially available hydrotreating catalysts.

## EXPERIMENTAL

The hydrotreating experiments were performed in a stainless steel tubular fixed-bed reactor operating in the upflow mode. The key process parameters were  $T = 375^\circ\text{C}$ ,  $P = 1750$  psig and  $\text{LHSV} = 0.5 \text{ h}^{-1}$ . The feedstock was the fraction boiling between  $249^\circ\text{C}$  and  $524^\circ\text{C}$  obtained from hydrocracking a 50/50 volumetric blend of Cold Lake/ Lloydminster resid.

Specific gravities were determined at  $15.5^\circ\text{C}$  on a Paar DMA 48 Instrument while dynamic viscosities were determined at  $25^\circ\text{C}$  on a Brookfield DV II instrument. Sulphur was determined on a Leco SC-132 sulphur analyzer while carbon and hydrogen as well as trace nitrogen were determined commercially. Both simulated distillations (ASTM D-2887) and vacuum distillations (ASTM D-1160) were performed in-house.

Carbon-13 NMR analyses were obtained on a Bruker ACE-200 instrument. Solutions were prepared by diluting  $2.0 \text{ cm}^3$  of the sample with  $2.0 \text{ cm}^3$  of a  $0.10 \text{ mole dm}^{-3}$  solution of tris(2,4-pentanedionato)chromium(III) in  $\text{CDCl}_3$ . The instrument was operated in the inverse gated decoupled mode for NOE suppression using a  $6.5 \text{ us}$  pulse ( $90^\circ\text{C}$ ) and a repetition time of  $10 \text{ s}$ . In a typical experiment 5000 transients were collected as 8K data points which were zero filled to 16K. A Lorentzian line broadening of  $5 \text{ Hz}$  was applied to the free induction decay prior to processing. Integration for paraffins, naphthenes and aromatics was as described by Young and Galya<sup>7</sup>.

Low resolution mass spectrometric analyses for aromatic types were obtained commercially. The method of Robinson and Cook<sup>8</sup>, which has been adopted as ASTM D-3239, was used with minor modifications. As well, the weight per cent of total aromatics was determined by a column chromatographic technique as described by Watson<sup>9</sup>. The method of Fitzgerald *et al*<sup>10</sup>, for the determination of aromatic components by UV/Vis spectroscopy, was adapted in-house to account for expected differences in the sample composition.

## RESULTS AND DISCUSSIONS

The project from which these data were derived concerned the selection of hydrotreating catalysts for the Bi-Provincial Upgrader facility<sup>11</sup> currently under construction. The design specifications for hydrotreated product quality included, among others, nitrogen at 500

wppm, sulphur at 400 wppm and total aromatics by Watson's method<sup>9</sup> at 45 wt.%. The properties of the feedstock and of the products obtained from hydrotreating this material using six different catalysts have been recorded in Table 1. The data indicate that all of the products exceed the design specifications for nitrogen and total aromatics content and that three of the six products meet the sulphur specifications as well.

The aromatics content of the feedstock and the six hydrotreated products have been measured using four different methods (Table 2). Both <sup>13</sup>C NMR<sup>7</sup> and the Watson method<sup>9</sup> measure total aromatics only. With <sup>13</sup>C NMR the paraffinic and naphthenic carbon content as well as the aromatic carbon content of the sample may be determined while with the Watson method, any moiety which has not been eluted from a silica containing chromatographic column with an aliphatic hydrocarbon is considered aromatic. Consequently, in this latter technique any compound which contains an aromatic unit would be considered as aromatic. The UV/Vis method<sup>10</sup> may be used to determine both total aromatics and polynuclear aromatics (PNA). The technique requires an *a priori* assumption or knowledge of the types of aromatic components in the sample so that the absorption maximo and absorptivities of corresponding model compound types may be used to calculate the concentrations of related components in the sample of interest. The method seems to be highly dependent on the materials chosen to represent the PNA components, the sensitivity has been found to be low, and the method was found to overestimate both PNA content and total aromatics content. However, the UV/Vis method may be useful for determining trends. The last method used for aromatics determination was a modification of Robinson and Cook's mass spectrometric technique<sup>8</sup>. Saturates are separated from aromatics by column chromatography and each fraction is introduced into the mass spectrometer for classification by Z number. Because "aromatics" is loosely and operationally defined, each of the techniques determines a different quantity and consequently results in method dependent values for aromatics content.

Among the various methods, the best agreement for total aromatics content appears to be between the UV/Vis and MS methods. Bearing in mind the limitations of the UV/Vis method, this correspondence may be more fruitious than real and probably reflects the large number of tetra- and penta-aromatic standards used in the technique and that the mono-aromatics account for the major portion of the total aromatics content of the samples. Also, it may be seen that while the absolute values for total aromatics vary considerably according to method, a relationship exists between the different methods. This relationship has been further explored by plotting the total aromatics content obtained via NMR, chromatographic and UV/Vis analyses in the hydrotreated total liquid product against that obtained from mass spectrometry (Figure 1). Linear regression analysis has resulted in correlation coefficients of 0.971, 0.988 and 0.997 respectively for the following equations:

$$\text{NMR} = 0.31 * \text{MS} + 3.95 \dots\dots\dots(1)$$

$$\text{Watson} = 0.84 * \text{MS} + 10.0 \dots\dots\dots(2)$$

$$\text{UV/Vis} = 1.06 * \text{MS} - 1.44 \dots\dots\dots(3)$$



Again, the fortuitous relationship between aromatics determined by the UV/Vis method and the MS method noted above has resulted in excellent correlations between the methods. However, it is noted that the correlation coefficient drops to 0.75 if the aromatics content of the feedstock is included in the regression analyses. It is possible that the deviation of the data point for the feedstock from the regression line encompassing the hydrotreated products may be due to the sensitivity of the method to the choice of reference standards. The inclusion of the data point for the feedstock in the remaining two methods alters the correlation coefficients only slightly but results in appreciable changes in the slope of the regression line.

One interpretation of equations 1-3 above could be that on average, only 31% of the carbon atoms are in aromatic rings, the remainder being in alkyl side chains and naphthenic substituents. Consistent with this, 16% of the aromatic components in the sample could be considered saturate on the basis of polarity because of long chain alkyl substituents on the aromatic moiety.

Only the UV/Vis method can be compared to the MS method for aromatics content by ring number. Meaningful results have been obtained for only mono-aromatics, di-aromatics and total PNA (Figure II). The insensitivity of the UV/Vis method to higher ring number components precluded further correlations. The data indicate that while the correlation coefficients were acceptable, the UV/Vis technique overestimates mono-aromatics while severely underestimating higher ring number aromatics.

Lee *et al*<sup>12,13</sup> have found similar correlations between aromatics determined by mass spectrometry and NMR, FIA (ASTM D-1319) and SFC for diesel fuels and middle distillates. Since the NMR analyses methodology adopted by these authors differed from our approach, no basis for data comparison existed. However, the fact that such correlations exist for diesel and middle distillate cuts<sup>12,13</sup> and for the gas oil fraction suggests that these correlations may be part of a more general phenomenon.

The heteroatom distribution as well as the PNA (UV/Vis method) and total aromatics (Watson method) content of the 343+°C fractions of the feedstock and hydrotreated products were determined (Table 3). The data indicate that both the heteroatom content and the aromatics content have increased in the feedstock while, for the most part, these values have decreased for the hydrotreated product relative to those in total liquid product. Surprisingly, this has resulted in higher conversions in the heavier gas oil fractions (Table 4) and consequently indicates the superior catalytic activity of these catalysts for the heavier components.

## CONCLUSIONS

Although the Ni-Mo/Al<sub>2</sub>O<sub>3</sub> catalysts used in this work will not perform deep aromatics hydrogenation, they will remove 30 - 60% of the total aromatics in the hydrocracked gas oil while at the same time exhibiting a 90 - 99% conversion of sulphur and nitrogen. The catalysts investigated show superior performance with the heavier gas oil fractions. The

amount of aromatics determined, and consequently the aromatics conversions, are method dependant. This must be considered in potential environmental legislation as well as in fuel oil and catalyst marketing and underscores the requirements for standardization. The trends determined for the very narrow range of compounds reported here may be part of a broader, more general phenomenon.

#### ACKNOWLEDGEMENTS

The authors thank Mr. Leon Neumann, who ran the hydrotreater, Mr. Antonio Nicola, who was instrumental in obtaining the Watson aromatics, and Ms. Nadia Hamza, who performed our distillations and obtained the densities and viscosities, for their technical assistance and for providing most of the data reported here. As well, the authors thank the Analytical Services Group at NHRC for adapting the UV/Vis technique for internal use and for providing those and the NMR data. Part of this work was supported by a 50/50 cost shared program between Husky Oil Ltd. and CANMET, EMR under contract number 23440-8-9261/01-SQ.

#### REFERENCES

1. S. Mohanty, D.F. Saraf and D. Kunzru, *Erdol und Kohle, Erdgas Petrochemie* 1990, **43**, 359.
2. J.F. Le page, G. Martino and C. Thonon, *J. Pet. Res.* 1989, **8**, 147.
3. R.A. Corbett, *Oil Gas J.* 1989, **87**, 49.
4. M.F. Wilson, I.P. Fisher and J.F. Kriz, *Ind. Eng. Chem. Prod. Res. Dev.* 1986, **25**, 505.
5. S.T. Bagley, L.D. Gratz, D.G. Leddy and J.H. Johnson, *Prepr. Am. Chem. Soc. Div. Fuel Chem.* 1991, **36**, 311.
6. J. Lewtas, *Prepr. Am. Chem. Soc. Div. Fuel Chem.* 1991, **36**, 319.
7. D.C. Young and L.G. Galya, *Liq. Fuels Technol.* 1984, **2**, 307.
8. C.J. Robinson and G.L. Cook, *Anal. Chem.* 1969, **41**, 1548.
9. A.T. Watson, *Anal. Chem.* 1952, **24**, 507.
10. M.E. Fitzgerald, J.L. Moirano, H. Morgan and V.A. Cirillo, *Appl. Spectros.* 1970, **24**, 106.
11. S. Chase, *The Husky Bi-Provincial Design Basis*, Paper presented at the Sixth Annual Heavy Oil and Oil Sands Technical Symposium, Calgary, March 8, 1989.
12. S.W. Lee, B.J. Fuhr, L.R. Holloway and C. Reichert, *Energy and Fuels* 1989, **3**, 80.
13. S.W. Lee, S. Coulombe and B. Glavincevski, *Energy and Fuels* 1990, **4**, 20.

TABLE 1  
FEEDSTOCK AND HYDROTREATED PRODUCT PROPERTIES

	FEED-STOCK	PROD. A	PROD. B	PROD. C	PROD. D	PROD. E	PROD. F
Density (kg/dm <sup>3</sup> )	923.3	872.8	890.2	890.2	886.3	889.2	880.4
Viscosity (cP)	38	13	22	21	19	22	16
Carbon (wt%)	87.09	86.60	87.04	87.02	86.91	86.78	86.50
Hydrogen (wt%)	11.61	12.74	12.15	12.26	12.47	12.38	12.66
Sulphur (wppm)	14123	795	984	517	393	391	247
Nitrogen (wppm)	1799	102	276	204	62	129	30
Sim. Dist. (wt%)							
IPB - 177	-	4.1	1.5	1.4	1.8	1.5	2.7
177 - 249	1.6	7.4	4.3	3.8	4.7	4.2	5.9
249 - 343	31.4	39.2	35.7	36.3	36.5	35.8	37.4
343 - 524	65.4	49.3	58.5	58.5	57.0	58.5	54.0
524+	1.6	-	-	-	-	-	-

Note: A, B, C, D, E, F are commercially available catalysts.

TABLE 2  
TOTAL AROMATICS (WT.%) BY METHOD

METHOD	FEED-STOCK	PROD. A	PROD. B	PROD. C	PROD. D	PROD. E	PROD. F
<sup>13</sup> C NMR	27.0	9.8	13.9	13.9	12.2	13.6	11.1
Watson	55.1	25.7	35.2	37.3	33.8	36.3	29.3
UV/Vis	32.4	18.1	30.7	33.8	28.0	30.6	24.0
Mass Spec.	50.45	18.94	29.92	33.72	27.45	30.55	23.73

TABLE 3

HETEROATOM AND AROMATICS DISTRIBUTION IN THE 343+°C FRACTIONS

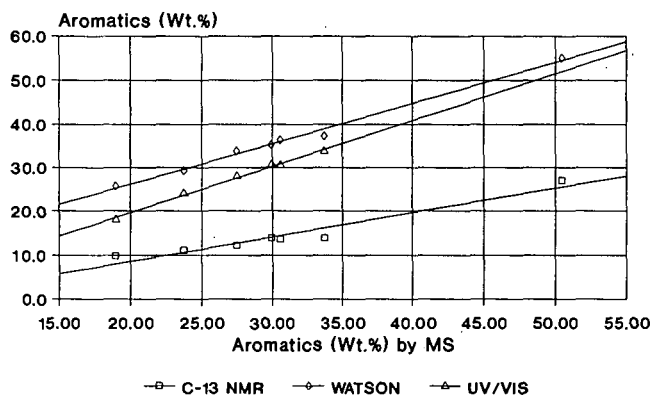
	FEED-STOCK	PROD. A	PROD. B	PROD. C	PROD. D	PROD. E	PROD. F
Density (kg/dm <sup>3</sup> )	940.6	888.7	905.4	904.2	900.7	903.4	895.4
Nitrogen (wppm)	2050	37	230	145	60	161	15
Sulphur (wppm)	16400	265	718	488	265	240	60
Aromatics, UV/Vs (wt%)							
Monoaromatics	23.3	16.7	25.1	29.9	25.7	27.0	21.5
Polynuclear Arom.	12.9	4.1	4.7	4.4	4.4	4.5	4.2
Total Aromatics	36.2	20.7	29.8	34.3	30.1	31.5	25.7
Aromatics, Watson (wt%)	57.9	22.1	35.9	38.4	33.8	37.1	28.0

TABLE 4

HETEROATOM AND AROMATICS CONVERSION (%)  
IN THE TOTAL LIQUID PRODUCT AND THE 343+°C FRACTION

TEST	CAT. A	CAT. B	CAT. C	CAT. D	CAT. E	CAT. F
Total Liquid Product						
Sulphur	94.4	84.7	88.7	96.5	92.8	98.3
Nitrogen	94.4	93.0	96.3	97.2	97.2	98.2
Aromatics, Watson (wt%)	53.3	36.1	32.3	38.7	34.1	46.8
343+ Fractions						
Nitrogen	98.2	88.8	92.9	97.1	92.1	99.3
Sulphur	98.4	95.6	97.0	98.4	98.5	99.6
Aromatics, Watson (wt%)	61.8	38.1	33.7	41.7	36.0	51.7

Figure I. Effect of Analysis Method  
on Aromatics Content in Gas Oil



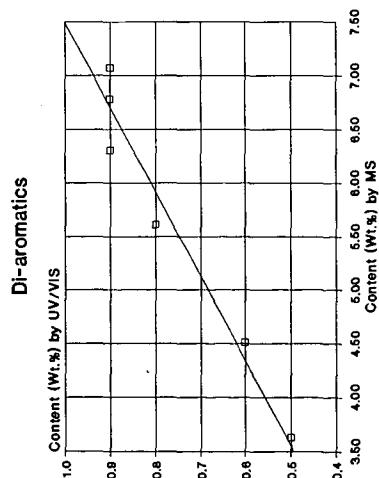
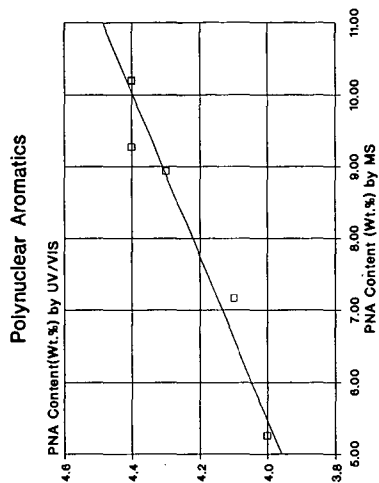
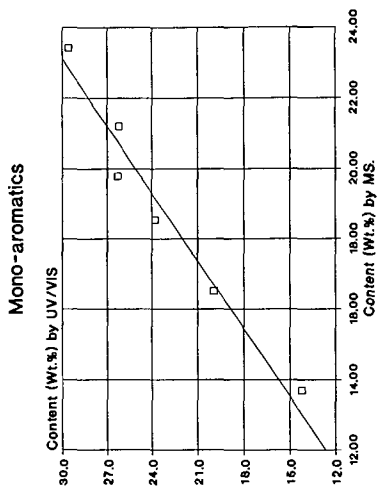


Figure II. Correlation Between UV/Vis and Mass Spectrometric Methods for Aromatics Content by Ring Number

## COAL/OIL COPROCESSING USING SYNGAS

Yuan C. Fu, Makoto Akiyoshi, Fumiaki Tanaka and Kenichi Fujiya

Department of Applied Chemistry,  
Muroran Institute of Technology,  
Muroran, Japan 050

Keywords: Coprocessing, Model Compounds, Syngas

### ABSTRACT

Coal and model compounds were hydrogenated and desulfurized in the presence of petroleum solvents and catalyst under coprocessing conditions by using syngas with steam in place of hydrogen. Nickel molybdate and cobalt molybdate catalysts impregnated with potassium carbonate exhibited good activities for hydrogenation and desulfurization of coal and model compounds (anthracene and benzothiophene) at 400-425°C with the use of syngas. Some water gas shift conversion also took place simultaneously. The extent of hydrogenation and desulfurization obtained are comparable to those obtained in coprocessing using pure hydrogen. Iron catalysts such as synthetic pyrite exhibited good activities for coal conversion in coprocessing using hydrogen, but only moderate activities in coprocessing using syngas. Results from coprocessing of model compounds indicate that these iron catalysts have relatively low activities in the desulfurization of benzothiophene.

### INTRODUCTION

In coprocessing of coal and petroleum residues to produce liquid fuels, the process economics could be improved significantly by using syngas ( $H_2+CO$ ) and steam instead of hydrogen as feed gas to the reactor. The use of syngas, even only at the first stage of the current two-stage process being developed, could substantially reduce the hydrogen consumption and improve the overall thermal efficiency. It has been demonstrated that lignite<sup>1</sup> and bituminous coal<sup>2</sup> are liquefied and coal liquid<sup>3</sup> is hydrogenated by the use of carbon monoxide or carbon monoxide-containing gas.

In this study, coal model compounds (anthracene and benzothiophene) are coprocessed with petroleum solvents in the presence of catalyst, and the results of hydrogenation and desulfurization during coprocessing using syngas and hydrogen were compared. The catalysts used include NiMo, CoMo, and disposable Fe and  $ZnCl_2$  catalysts. In general the catalyst activities are somewhat lower with the use of syngas than with hydrogen. It is shown, however, that NiMo and CoMo catalysts exhibit good activities with syngas and the performances are comparable to those obtained with hydrogen. Some coprocessing experiments using coal and petroleum solvents with syngas yielded moderately good coal conversions, but reaction conditions relating to  $H_2/CO$  ratio, steam/syngas ratio, solvent composition, catalyst, and process severity should be optimized to achieve better results.

### EXPERIMENTAL

The coprocessing reactions of model compounds were conducted in a shaking 20-ml microreactor with syngas ( $H_2:CO=1:1$ ) or  $H_2$  at initial pressures of 70 Kg/cm<sup>2</sup> and temperatures of 350-400°C for 45 minutes. Anthracene and benzothiophene were used as the model compounds, and mixtures of n-paraffin and cycloalkane and that added with tetralin were used as petroleum solvents. The ratio of solvent to coal model compounds was 5:1. With syngas, 10 weight % of  $H_2O$  based on the total amounts of the model compounds and solvent was added. The amount of ground catalyst powder added was also 10 weight %.

The conventional NiMo/Al<sub>2</sub>O<sub>3</sub> and CoMo/Al<sub>2</sub>O<sub>3</sub> catalysts and disposable synthetic pyrite (Mitsui Coal Liquefaction Co.) were used for coprocessing experiments using H<sub>2</sub>. For experiments using syngas, the NiMo/Al<sub>2</sub>O<sub>3</sub> and CoMo/Al<sub>2</sub>O<sub>3</sub> catalysts and synthetic pyrite were impregnated with aqueous potassium carbonate solution (10 wt%). Additional catalysts tested for comparison purpose included a solid superacid catalyst of sulfate-promoted iron oxide<sup>4,5</sup> and a zinc chloride catalyst<sup>6</sup> (30 wt%) supported on silica-alumina. The Fe<sub>2</sub>O<sub>3</sub>/SO<sub>4</sub><sup>2-</sup> (2 wt%) was prepared starting from iron(III) nitrate precipitated with an aqueous ammonia. The powdered precipitate was treated with ammonium sulfate, and then dried and calcined at 500°C.

Some coprocessing experiments using coal and petroleum solvents with syngas were also conducted. Illinois No. 6 bituminous coal (River King) with an ultimate analysis of C, 78.3; H, 5.4; N, 1.32; O, 11.12; S, 3.86; Ash, 10.9 (maf. basis) was used. The coal conversion was determined from tetrahydrofuran insolubles, and the solubles were analyzed by Yanaco G-6800 gas chromatograph using OV-1701 fused silica capillary column (60m x 0.25mm  $\phi$ ).

## RESULTS AND DISCUSSION

**Hydrogenation of Anthracene.** Anthracene was initially hydrogenated in the presence of petroleum solvents and synthetic pyrite using H<sub>2</sub> and syngas. The results in Table 1 show that the hydrogenation proceed well at 350°C with H<sub>2</sub> irrespective of the type of solvent used. Paraffins and cycloalkanes did not participate in the reaction and hydrogen transfer from tetralin was not an important factor. The reaction with syngas at the same temperature gave only 65.9% anthracene conversion. It is observed that the conversion increased as the temperature increased to 400°C, and that this was accompanied by the increase of CO shift conversion.

**Coprocessing of Model Compounds.** Anthracene and benzothiophene were coprocessed with petroleum solvents to study the hydrogenation and desulfurization during coprocessing. It is seen in Table 2 that anthracene was hydrogenated easily with H<sub>2</sub> in the presence of synthetic pyrite, but desulfurization of benzothiophene did not take place easily. In the presence of NiMo/Al<sub>2</sub>O<sub>3</sub> and CoMo/Al<sub>2</sub>O<sub>3</sub>, both hydrogenation and desulfurization progressed markedly. In the run using an n-dodecane/decalin mixture as the solvent, 23.8% of decalin was dehydrogenated (17.7% to tetralin and 6.1% to naphthalene). It is of interest to note that trans/cis ratio of the remaining decalin has increased to 4.6 from the original trans/cis ratio of 1.6 after the coprocessing reaction. Similar increase of trans/cis ratio was also observed in the run using an n-dodecane/decalin/tetralin solvent mixture. The occurrence of isomerization to trans decalin during extraction of coal was also observed by Clarke et al<sup>7</sup>.

For comparison purpose, a sulfate-treated iron oxide catalyst and a ZnCl<sub>2</sub>/SiO<sub>2</sub>-Al<sub>2</sub>O<sub>3</sub> catalyst were prepared and tested. Both catalysts showed moderately good activities for hydrogenation and desulfurization in coprocessing using H<sub>2</sub>.

In coprocessing using a paraffin/ethylcyclohexane/tetralin solvent with syngas, NiMo and CoMo catalysts impregnated with K<sub>2</sub>CO<sub>3</sub> exhibited good activities for both hydrogenation and desulfurization, as shown in Table 3. When a paraffin/decalin/tetralin solvent was used, the extent of hydrogenation and desulfurization decreased. It was noticed that no net conversion or dehydrogenation of decalin took place in this case. The trans/cis ratios of the remaining decalin were much lower than those observed for coprocessing using H<sub>2</sub>, indicating limited occurrence of isomerization during coprocessing with syngas. As was suggested by Clarke et al<sup>7</sup>, decalin could participate in hydrogen donation reactions in the presence of polyaromatic compounds, and this was more pronounced in the reaction with H<sub>2</sub> than with syngas. It is speculated that hydrogen donation reactions of decalin somehow relate to the occurrence of isomerization. With syngas,



synthetic pyrite, sulfate-treated iron oxide, and  $\text{ZnCl}_2/\text{SiO}_2\text{-Al}_2\text{O}_3$  exhibited moderate activities for hydrogenation, but poor activities for desulfurization. Presence of significant concentrations of hydrogen donating tetralin alone was not sufficient to give high conversion in coprocessing using syngas. It is also observed, in general, that hydrogenation and desulfurization progress with the progress of CO shift conversion.

**Coprocessing of Coal with Petroleum Solvents.** Table 4 shows the test results of coprocessing bituminous coal with paraffin/decalin/tetralin solvents. Fairly high coal conversions were obtained with  $\text{NiMo}/\text{Al}_2\text{O}_3$ ,  $\text{CoMo}/\text{Al}_2\text{O}_3$ , and synthetic pyrite using  $\text{H}_2$ . The coal conversions obtained with syngas were only moderate, but it should be emphasized that the reaction conditions have not been optimized in these runs. Improved conversions should be obtainable if variables including steam/syngas ratio,  $\text{H}_2/\text{CO}$  ratio, solvent composition, catalyst, and process severity are properly chosen.

In the run using an n-dodecane/decalin/1-methylnaphthalene mixture as the solvent, high coal conversion was obtained even without the use of tetralin. Product analysis indicates that significant amounts of 1-methylnaphthalene may have participated in hydrogen exchanges with decalin and coal. In the similar run with syngas, the active participation of 1-methylnaphthalene was not evident, and the decalin conversion decreased. For syngas runs, again the trans/cis ratio of the remaining decalin was lower, probably suggesting that only limited participation of decalin in hydrogen donation reactions has taken place.

#### ACKNOWLEDGEMENTS

We thank the support of Grant-in-Aid of Scientific Research provided by the Ministry of Education, Japan. We also thank Nippon Mining Co. and Mitsui Coal Liquefaction Co. for providing catalyst samples.

#### References

1. Appell, H. R., Miller, R. D., Wender, I., presented before the Division of Fuel Chemistry, 163rd ACS National Meeting, Boston, April 10-14, 1972
2. Batchelder, R. F., Fu, Y. C., Ind. Eng. Chem. Process Des. Dev. Vol. 18, No. 4, 599 (1979)
3. Stephens, H. P., Kottenstette, R. J., presented before the Division of Fuel Chemistry, 194th ACS National Meeting, New Orleans, August 30-September 4, 1987
4. Tanabe, K., Yamaguchi, T., Hattori, H., Matsushashi, H., Kimura, A., Fuel Processing Technology, Vol. 4, 247 (1986)
5. Pradhan, V., Tierney, J. W., Wender, I., Preprints, Div. Fuel Chem., Am. Chem. Soc. Vol. 35, No. 3, 793 (1990)
6. Sharma, R. K., Diehl, J. W., Olson, E. S., Preprints, Div. Fuel Chem., Am. Chem. Soc. Vol. 35, No. 2, 414 (1990)
7. Clarke, J. W., Rantell, T. D., Snape, C. E., Fuel, Vol. 63, 1476 (1984)

Table 1 Hydrogenation of Anthracene Using  $H_2$  and Syngas  
(Initial Pressure: 70Kg/cm<sup>2</sup>, Time: 45min)

Gas	$H_2$					Syngas ( $H_2$ :CO=1:1)	
Catalyst	FeS <sub>x</sub> <sup>a</sup>					FeS <sub>x</sub> <sup>b</sup>	
Solvent <sup>c</sup>	T	D/E	D/E/DL	D/E/T	D/E/T	D/E/T	D/E/T
Temperature, °C	350	350	350	350	400	350	400
Anthracene conversion, %	92.8	92.2	90.0	92.4	82.8	65.9	81.0
DHA formed, %	68.8	74.3	74.3	66.8	47.2	65.9	67.6
Conversion of tetralin, %	3.8	-	1.8 <sup>d</sup>	6.7	20.2	1.5	8.3
CO conversion, %	-	-	-	-	-	2.0	8.3

<sup>a</sup> Synthetic pyrite <sup>b</sup> Impregnated with K<sub>2</sub>CO<sub>3</sub> solution

<sup>c</sup> Equal wt% of each component <sup>d</sup> Conversion of decalin

D:n-Decane, E:Ethylcyclohexane, T:Tetralin, DL:Decalin, DHA:9,10-Dihydroanthracene

Table 2 Coprocessing of Model Compounds Using  $H_2$   
(Coal Model: Anthracene/Benzothiophene, Initial Pressure: 70Kg/cm<sup>2</sup>, Time: 45min)

Catalyst	FeS <sub>x</sub>	FeS <sub>x</sub>	Fe <sub>2</sub> O <sub>3</sub>	ZnCl <sub>2</sub>	NiMo	CoMo	NiMo	NiMo
			/SO <sub>4</sub> <sup>2-</sup>	/SiO <sub>2</sub> -Al <sub>2</sub> O <sub>3</sub>				
Solvent <sup>a</sup>	D/E/T	D/E/T	D/E/T	DO/E/T	D/E/T	D/E/T	DO/DL/T	DO/DL
Temperature, °C	350	400	400	400	400	400	400	400
Anthracene conversion, %	90.8	81.7	68.4	87.1	97.0	96.8	97.2	89.4
Benzothiophene conversion, %	10.2	26.0	80.8	50.2	96.2	100	100	100
Conversion of tetralin, %	11.5	13.8	13.5	33.2	38.5	33.0	16.7	-
Decalin remained, %							86.4	76.2
cis							15.0	13.7
trans							71.4	62.5
trans/cis ratio							4.8	4.6

<sup>a</sup> Equal wt% of each component

T:Tetralin, D:n-Decane, E:Ethylcyclohexane, DO:n-Dodecane, DL:Decalin

Table 3 Coprocessing of Model Compounds Using Syngas ( $H_2:CO=1:1$ )

(Coal Model: Anthracene/Benzothiophene.

Initial Pressure: 70 Kg/cm<sup>2</sup>,  $H_2O$ : 10 wt% of Reactants, Time: 45 min)

	FeS <sub>x</sub> <sup>a</sup>	FeS <sub>x</sub> <sup>a</sup>	NiMo <sup>a</sup>	NiMo <sup>a</sup>	NiMo <sup>a</sup>	CoMo <sup>a</sup>	Fe <sub>2</sub> O <sub>3</sub> /SO <sub>4</sub> <sup>2-</sup>	ZnCl <sub>2</sub> /SiO <sub>2</sub> -Al <sub>2</sub> O <sub>3</sub>
Solvent <sup>b</sup>	D/E/T	D/E/T	D/E/T	DO/DL/T	TD/DL/T	D/E/T	DO/E/T	DO/E/T
Temperature, °C	350	400	400	400	400	400	400	400
Anthracene conv., %	80.1	70.9	90.1	78.9	77.8	88.3	50.2	65.6
Benzothiophene conv., %	4.1	11.7	90.4	67.6	66.6	100	28.3	22.6
Conversion of tetralin, %	15.4	4.0	11.3	6.6	11.4	22.1	2.6	23.2
CO conversion, %	2.0	7.7	15.3	10.4	15.9	18.3	16.4	2.8
Decalin remained				102.4	102.4			
cis				33.4	30.8			
trans				69.0	71.6			
trans/cis ratio				2.1	2.32			

<sup>a</sup> Catalyst impregnated with K<sub>2</sub>CO<sub>3</sub> solution <sup>b</sup> Equal wt% of each component

D:n-Decane, E:Ethylcyclohexane, T:Tetralin, DO:n-Dodecane, DL:Decalin, TD:n-Tridecane

Table 4 Coprocessing of Bituminous Coal with Petroleum Solvents (425°C, 45 min)

(Solvent:n-Dodecane/Decalin/Tetralin, Solvent:Coal=4:1)

	H <sub>2</sub>				Syngas ( $H_2:CO=1:1$ )		
Catalyst	FeS <sub>x</sub>	NiMo	NiMo <sup>a</sup>	CoMo	FeS <sub>x</sub> <sup>b</sup>	NiMo <sup>b</sup>	NiMo <sup>a,b</sup>
Coal conversion, %	89.3	87.6	84.9	83.7	63.7	79.8	62.6
H <sub>2</sub> consumption, wt% of maf coal	3.1	3.1	3.9	5.3	0.8	-0.3	-0.2
CO conversion, %	-	-	-	-	6.2	22.1	19.3
Conversion of tetralin, %	17.3	10.1	-	12.9	14.1	8.2	-
Conversion of 1-methylnaphthalene, %	-	-	17.4	-	-	-	1.2
Decalin remained, %	98.6	90.7	88.6	95.8	95.7	87.2	94.5
cis	16.8	27.4	25.3	27.3	22.2	30.3	32.4
trans	81.8	63.3	63.3	68.5	73.5	56.9	62.1
trans/cis ratio	4.9	2.3	2.5	2.5	3.3	1.9	1.9

<sup>a</sup> Solvent:n-Dodecane/Decalin/1-Methylnaphthalene <sup>b</sup> Impregnated with 10% K<sub>2</sub>CO<sub>3</sub>

## CATALYSIS OF METAL-ION EXCHANGED Y-ZEOLITES AND MODIFIED Ni-Mo/Al<sub>2</sub>O<sub>3</sub> FOR HYDROCRACKING OF PHENANTHRENE AND COAL-DERIVED DISTILLATES

Chunshan SONG\*, Harold H. SCHOBERT\*, and Hisaji MATSUI†

\*Fuel Science Program, Department of Materials Science and Engineering  
The Pennsylvania State University, University Park, PA 16802, USA

†Research and Development Center, Osaka Gas Co., Ltd., Osaka 554, Japan

**Keywords:** Y-Zeolite catalyst, Hydrocracking, Phenanthrene, Coal-Derived distillates

### INTRODUCTION

The liquids derived from liquefaction, pyrolysis and gasification of coals have high contents of condensed polyaromatic compounds and polar compounds. Even in the middle distillate fraction (MD) produced from the advanced two-stage coal liquefaction plant at Wilsonville, Alabama, there are considerable amounts of polyaromatics such as pyrene [1]. These liquids require catalytic hydroprocessing before they can be used as clean transportation fuels such as gasoline and jet fuels. During the last two decades, emphasis in selecting catalysts for coal liquids upgrading has always been given to the Ni-Mo and Co-Mo combinations, which are used extensively in the petroleum industry. Research has focused mainly on catalyst screening and evaluation, and little attention has been given to investigating novel formulations [2].

In regard to catalytic materials, the use of zeolites is of both fundamental and practical importance because of their higher surface area and unique catalytic property as compared to conventional catalysts supported on alumina or silica-alumina. There are numerous reports on the application of various zeolites in the catalytic reaction processes related to petroleum industry [3-4]. Introducing transition metals into zeolites by appropriate methods could make the zeolite suitable for hydrocracking, and the metals can also serve to hydrogenate the coke precursors rapidly and to prevent their conversion to coke deposit on the zeolite [3]. There are also commercial hydrocracking processes using zeolite-based catalysts for converting petroleum distillates [3], and more recently, for converting residues [5-6]. However, the research work on zeolite catalysts in hydrocracking of polyaromatics and coal liquids is still very limited. Haynes et al. [7] studied hydrocracking of prehydrogenated polycyclic hydrocarbons over Ni-W impregnated on a Y-zeolite. They showed that mixtures of hydrogenated pyrenes can be hydrocracked over Ni-W/Y catalyst. Kikuchi et al. [8] studied hydrocracking of phenanthrene using LaY catalyst in the presence of H-donor tetralin solvent. They showed that this catalyst can significantly promote phenanthrene conversion if tetralin was present, otherwise Ni-Mo/Al<sub>2</sub>O<sub>3</sub> was much more active than LaY. Our preliminary work has shown that some transition metal-ion exchanged Y-zeolites show some unique catalytic activity for hydrocracking of polyaromatics [9-10] as compared to other catalysts [10-12]. The work reported here aimed at clarifying the effects of loading small amounts of metals on the catalytic activity of Y-zeolite. In this work, we prepared several metal-loaded Y-zeolites by ion-exchange and evaluated the effects of these zeolite catalysts and of two third-generation commercial Ni-Mo catalysts in hydrocracking of phenanthrene, which is a typical polyaromatic component in liquids from pyrolysis and liquefaction of coals. Some of the catalysts were further examined in hydrocracking of a coal-derived middle distillate fraction which is rich in polyaromatics.

### EXPERIMENTAL

The metal-ion exchanged Y-zeolites were prepared by mixing ammonium-exchanged Y-zeolite, NH<sub>4</sub>-Y (SiO<sub>2</sub>/Al<sub>2</sub>O<sub>3</sub> mol ratio: 4.6) and 0.25 M aqueous solutions of Ni(NO<sub>3</sub>)<sub>2</sub>·6H<sub>2</sub>O, Fe(NO<sub>3</sub>)<sub>3</sub>·9H<sub>2</sub>O, or La(NO<sub>3</sub>)<sub>3</sub>·6H<sub>2</sub>O. The mixtures were agitated at 85°C for 2 h and then filtered. The ion-exchanged zeolites were washed with distilled water, dried at 120°C for 2 h and then calcined in air at 500°C for 4 h. Two commercial Ni-Mo catalysts were sulfided with 6% CS<sub>2</sub> in n-dodecane at 250°C for 2 h and 300°C for 3 h under 100 psi H<sub>2</sub>, and used in phenanthrene hydrocracking. The chemical composition of both the metal-ion exchanged zeolites and supported Ni-Mo or Co-Mo catalysts was determined by inductively coupled plasma - atomic emission spectrometry (ICP-AES, Seiko Denshi Kogyo, JY-48P-SPS1100). The surface analyses of the zeolite catalysts, unsulfided and sulfided Ni-Mo catalysts were also conducted by X-ray photoelectron spectroscopy (XPS; Shimadzu ESCA-850, MgKα) and scanning electron microscope - electron probe microanalysis (SEM-EPMA; Nihon Denshi, JXA-733).

Hydrocracking of phenanthrene was carried out at 400°C for 1 h with 1000 psi H<sub>2</sub> (cold) in a 100 ml autoclave with phenanthrene (4 g), n-heptane solvent (10 ml) and a catalyst (2 g). The gaseous products were analyzed by GC. The liquid and solid products were analyzed by capillary GC-MS (Shimadzu QP-1000) and capillary GC (Shimadzu 9A). The used catalysts were washed by methylene chloride solvent, dried in vacuum oven at 100°C, and analyzed for carbonaceous deposits by combustion method.

We also used a coal-derived distillate sample (b.p. 204-343°C), which was produced from two-stage liquefaction of Ireland Mine coal at Wilsonville two-stage liquefaction plant using Shell 324 Ni-Mo catalyst [1]. Hydrocracking of Wilsonville middle distillates (WI-MD) was carried out at 400°C for 1 h with 1500 psi H<sub>2</sub> (cold) in 20 ml microautoclaves with 2 g feedstock and 0.4 g catalyst. The zeolite catalysts (NiH-Y, FeH-Y) were exposed to the feedstock in the microautoclave for about 20 hours before the reaction. The gas products were analyzed by GC. The liquid products were characterized by capillary GC-MS using a Kratos MS80 GC-MS system.

## RESULTS AND DISCUSSION

### Catalyst Characterization

In general, the extent of metal-ion exchange depends on the conditions and the samples used. In this work, the contents of metals of the prepared catalysts, and the change in chemical composition of the Y-zeolite framework before and after the metal-ion exchange were determined by using the ICP-AES technique. As shown in Table 1, the introduction of Ni, Fe and La into the NH<sub>4</sub>-Y zeolite by ion-exchange was successful and the contents of these three metals in the finished catalysts are 3.6 (NiO), 4.4 (Fe<sub>2</sub>O<sub>3</sub>) and 8.4 (La<sub>2</sub>O<sub>3</sub>) wt%, respectively. For NiH-Y and LaH-Y catalysts, the SiO<sub>2</sub>/Al<sub>2</sub>O<sub>3</sub> ratios of the zeolites are similar to the original NH<sub>4</sub>-Y or H-Y. However, in the case of FeH-Y, the content of Al<sub>2</sub>O<sub>3</sub> is significantly less and the SiO<sub>2</sub>/Al<sub>2</sub>O<sub>3</sub> ratio is substantially higher than the other two catalysts. This indicates that the preparation of FeH-Y was accompanied by remarkable dealumination from zeolite framework, probably due to the higher acidity of the aqueous solution with Fe(NO<sub>3</sub>)<sub>3</sub>·9H<sub>2</sub>O and NH<sub>4</sub>-Y. In fact, we measured the pH of the aqueous solutions of the Fe, Ni and La salts before ion exchange, which were 1.1, 3.5, and 4.2, respectively. It is known that steam or acid treatment can cause dealumination of Y-zeolite [13].

SEM indicated that the size and shape of the three metal-ion exchanged zeolites are very similar to that of H-Y (un-exchanged). XPS spectra of NiH-Y and FeH-Y clearly showed a strong signal of Ni and Fe on the zeolite surface. The binding energies for Al 2p or Si 2p of NiH-Y and LaH-Y are similar, while the intensity of Al 2p for FeH-Y is very low (with high noise signals), 72 cps as compared to 730 cps for Al in NiH-Y and 636 cps for Al in LaH-Y. This is considered to be due to the very low content of Al in FeH-Y, being consistent with the finding from ICP-AES. Surprisingly, ICP-AES indicated that LaH-Y contains 8.4 wt% La<sub>2</sub>O<sub>3</sub>, but XPS showed that the intensity of La on the surface is very low. However, it was found that when the etching technique was applied in XPS (for the depth distribution from surface to the bulk), the intensity of the peak of La increased remarkably with increasing etching time from 0.4 to 1.2 min, whereas there was little change in the relative intensity of peaks for Al and Si in LaH-Y with etching from 0 to 1.2 min. These results clearly indicate that the concentration of La in the bulk or framework is higher than that on the zeolite surface. We also examined two alumina-supported NiMo catalysts obtained from two catalyst companies, which are currently being used in many commercial plants for hydroprocessing of petroleum feedstocks. Detailed analyses by ICP-AES, SEM-EDPA and other techniques revealed that one of the third-generation NiMo catalysts contains P, and the other contains B. It is clear from the figures in Table 1 that B or P was intentionally added to improve the catalyst property or performance. XPS analysis showed that spectra pattern of the Mo 3d doublets of the two catalysts is similar to each other, but the Ni 2p peak for the P-modified NiMo is relatively sharper, suggesting a better dispersion of Ni.

### Phenanthrene Hydrocracking

In this work, we examined the catalytic effects of the metal-ion modified Y-zeolites (NiH-Y, FeH-Y, LaH-Y) and H-Y for hydrocracking of phenanthrene. The catalytic activity of these zeolites was also evaluated by comparing with two commercial Ni-Mo catalysts. Numerous products were formed during the catalytic hydrocracking of phenanthrene. These products can be classified into the following groups: 1) C<sub>1</sub>-C<sub>4</sub>

gases; 2) C5-C7 aliphatics; 3) alkylbenzenes; 4) alkyltetralins and alkylindans; 5) alkylnaphthalenes; 6) alkylbiphenyls; 7) unsym-octahydrophenanthrene and octahydrophenanthrene isomers; 8) sym-octahydrophenanthrene; 9) methylbenzoinindanes; 10) tetrahydrophenanthrene; 11) dihydrophenanthrene; 12) phenanthrene; 13) alkylphenanthrenes; 14) carbonaceous deposits; and the others. Figure 1 shows some typical results of GC-MS and GC analysis of products from hydrocracking of phenanthrene with different catalysts. Table 2 is a summary of the results with all the catalysts. As can be seen from Figure 1 and Table 2, the product distribution and phenanthrene conversion strongly depend on the metal introduced into the Y-zeolites. When H-Y is used, alkylbenzenes and alkylnaphthalenes were obtained as major hydrocracked products together with C1-C4 gases. The La-exchanged zeolite, LaH-Y (Figure 1B), gave similar results to those with H-Y. Yields of alkyltetralins were very low but more than 10wt% of methyl and dimethylphenanthrene were formed with LaH-Y and H-Y, probably due to transalkylation between alkylnaphthalenes or alkylbenzenes and phenanthrene. Interestingly, introducing Ni to Y-zeolite significantly promoted the hydrocracking activity, as can be seen from comparison of Figures 1A with 1B. In fact, NiH-Y afforded much higher conversion and higher yields of BTX, especially toluene. Moreover, not only alkylnaphthalene but also tetralin and methylindanes were obtained as two-ring hydrocracked products with NiH-Y. On the other hand, FeH-Y showed quite a different catalytic behavior as compared to H-Y, NiH-Y and LaH-Y. While naphthalene was also produced with FeH-Y, the major products are dihydro- and tetrahydro-phenanthrene. The formation of alkylphenanthrenes and carbonaceous deposits was suppressed significantly with FeH-Y. These results indicate that FeH-Y has a very low acidity as compared to the other zeolites, probably due mainly to the dealumination as revealed by ICP-AES. The runs over supported Ni-Mo catalysts afforded partially hydrogenated phenanthrene as main products (Figure 1 and Table 2), and the major cracking products are alkyltetralins, cyclohexylphenylethane, cyclohexylbenzene, and alkylbiphenyls together with small amounts of alkylnaphthalenes. While the two catalysts from different sources have different metal contents, it appears that the P-modified catalyst shows higher hydrogenation activity than the B-modified one but the latter has a relatively higher cracking ability than the former (Table 2). We have observed a similar trend for P- and B-modified Co-Mo/Al<sub>2</sub>O<sub>3</sub> catalysts [9-10]. Comparison of Figure 1A with Figure 1C reveals that NiH-Y has much higher hydrocracking activity than the industrial Ni-Mo hydroprocessing catalyst.

The differences in product distribution also reflect the occurrence of different reaction paths. It is worthwhile noting from Figure 1 and Table 2 that yields of alkylbiphenyls are considerably lower with the Y-zeolite catalysts, probably because the ring-opening cracking of dihydrophenanthrene is difficult with the catalysts having strong acidity, such as H-Y, NiH-Y and LaH-Y. This consideration is also supported by the fact that considerable amounts of biphenyl and cyclohexylbenzene were formed with the relatively less acidic Ni-Mo/Al<sub>2</sub>O<sub>3</sub> (Figure 1, Table 2), probably via the hydrocracking of the central ring in 9,10-dihydrophenanthrene. The relatively higher yields of alkylnaphthalenes with LaH-Y and H-Y suggests a major hydrocracking path via tetrahydrophenanthrene, whereas the higher yields of alkyltetralins and cyclohexylphenylethane (Figure 1) with the Ni-Mo catalysts implicate the paths of hydrocracking via sym- and unsym-octahydrophenanthrene. It seems that both these two paths exist for the hydrocracking with NiH-Y catalyst, probably because it has both high acidic cracking ability and high hydrogenation activity. Since the critical diameter of phenanthrene is 7.9 Å [7] which is similar to the diameter of Y-zeolite (about 8 Å), the hydrocracking reactions with H-Y may have been associated mainly with the external surface of the zeolite. The metal-ion exchange may induce some dealumination, which could generate some mesopores in the zeolite [6]. ICP-AES clearly indicated the dealumination during the preparation of FeH-Y. At the present stage, it is not clear whether this occurred during the preparation of NiH-Y and LaH-Y, but the "apparent" SiO<sub>2</sub>/Al<sub>2</sub>O<sub>3</sub> ratios of these two zeolites are similar to that of H-Y.

#### Hydrocracking of Wilsonville Middle Distillates

From the above results, it is clear that the zeolite ion-exchanged with Ni or Fe exhibits distinctly different catalytic activity as compared to LaH-Y and H-Y. We further examined NiH-Y and FeH-Y for hydrocracking of WI-MD, which has a boiling range of 204-343°C. Because it was produced from direct liquefaction of coal and because of the co-boiling phenomena, it has high contents of polyaromatic materials [1]. The hydrocracking of WI-MD was conducted at 400°C with 1500 psi H<sub>2</sub>. In order to derive useful data on the applicability of the zeolitic catalysts for converting WI-MD, the FeH-Y and NiH-Y were immersed in the WI-

MD for over 20 hours before the reaction. This was intended to deactivate the active sites in the zeolite catalysts which would be poisoned upon contact with coal-derived distillates in a continuous reactor. In this way we might be able to see the activity level of the active sites which are not poisoned by the adsorption of polar and polyaromatic materials. Figure 2 shows the GC-MS total ion chromatograms of the liquids from a non-catalytic run and catalytic runs. The GC-MS profile of the liquids from a noncatalytic run of WI-MD (Figure 2A) is very similar to the original sample [1]. Both samples contain very limited amounts of aliphatics, and are rich in polyaromatics. The most predominant peak appeared in GC-MS total ion chromatogram in Figure 2A (scan No. 3683, retention time: 59:31 min) is pyrene. The use of FeH-Y, after its 20 h exposure to WI-MD prior to reaction, did not alter the liquid composition to any significant extent. On the other hand, using NiH-Y catalyst significantly promoted the hydrocracking reactions, and resulted in a dramatic change in the composition of liquid products. The major products identified by GC-MS include alkylcyclohexanes, alkylbenzenes, tetralin and naphthalene and their homologues.

## CONCLUSIONS

In summary, it has been found that NiH-Y, the proton form Y-zeolite loaded with Ni by ion exchange, shows much higher activity for phenanthrene hydrocracking than LaH-Y, H-Y, FeH-Y and commercial, B- or P-modified NiMo/Al<sub>2</sub>O<sub>3</sub> hydroprocessing catalysts. The test with WI-MD also revealed that NiH-Y has high hydrocracking activity for converting the middle distillates derived from direct coal liquefaction. While some problems such as coking and pore size limitations remain to be solved, the preliminary results showed that some metal-ion exchanged zeolites can be promising hydrocracking catalysts. In future we hope to explore novel zeolitic catalysts with desired activity and performance for converting coal-derived distillates into transportation fuels.

## ACKNOWLEDGEMENTS

We wish to acknowledge the Analytical Laboratory of the Osaka Gas Research Center for providing the analyses, and the personnel of the Special Project Team for assistance in conducting some of the experiments. We are pleased to thank Dr. Richard F. Hickey of the Pittsburgh Energy Technology Center for the sample of Wilsonville Middle Distillate.

## REFERENCES


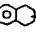
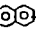
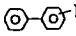
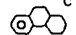
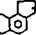
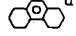
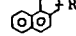
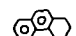
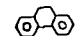
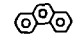
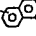
1. Song, C.; Eser, S.; Schobert, H.H.; Hatcher, P.G. et al., *Technical Progress Report 42-3462-TPR-2*, DOE/Sandia National Laboratory, February 1991, 96 pp.
2. Derbyshire F. J., *Energy and Fuels*, 1989, 3, 273.
3. Bolton A. P., "Hydrocracking, Isomerization, and Other Industrial Processes", in "Zeolite Chemistry and Catalysis" (Ed. J. A. Rabo), ACS Monograph 171, Washington D.C., 1976, pp.714-780
4. Karge, H.G.; Weitkamp, J. (Eds), "Zeolites as Catalysts, Sorbents and Detergent Builders", Elsevier, Amsterdam, 1989, Part I, pp. 1-428.
5. Sue, H.; Fujita, M.; *Oil and Gas J.* 1986, 51
6. Yamamoto T., *Petrotech*, 1989, 12, 621
7. Haynes Jr. H. W., Parcher J. F. and Helmer N. E., *Ind. Eng. Chem. Process Des. Dev.*, 1983, 22, 401
8. Kikuchi E., Tsunoda A., Katsumata H. and Morita Y., *J. Japan Petrol. Inst.*, 1984, 27, 296
9. Song, C. "Catalytic Hydrogenation and Cracking of Phenanthrene over Y-Zeolite Catalysts", Final Report, The Research Center of Osaka Gas Co., October 1989.
10. Ueda, K.; Matsui, H.; Song, C.; Xu, W. *J. Japan Petrol. Inst.*, 1990, 33, 413.
11. Song, C.; Hanoka, K.; Ono, T.; Nomura, M. *Bull. Chem. Soc. Japan* 1988, 61, 3788.
12. Song, C.; Nomura, M.; Ono, T.; *ACS Fuel Chem. Prepr.* 1991, 36(2), 586.
13. Humphries, A.; Yanik, S.J.; Gerritsen, L.A.; Desai, P.H. *Hydrocarbon Processing*. 1991, 70, 69.

**Table 1.** Chemical Composition of the Metal-Ion Exchanged Y-zeolites and Supported Ni-Mo/Al<sub>2</sub>O<sub>3</sub> Catalysts Determined by ICP-AES

wt%, dry	NH <sub>4</sub> -Y	H-Y	NiH-Y	FeH-Y	LaH-Y	P-Modified NiMo/Al <sub>2</sub> O <sub>3</sub>	B-Modified NiMo/Al <sub>2</sub> O <sub>3</sub>
NiO			3.6			3.7	2.4
Fe <sub>2</sub> O <sub>3</sub>				4.4			
La <sub>2</sub> O <sub>3</sub>					8.4		
MoO <sub>3</sub>						18.5	9.2
SiO <sub>2</sub>	71.6	73.3	70.6	91.5	66.5		
Al <sub>2</sub> O <sub>3</sub>	26.7	26.2	25.5	2.2	24.7	68.2	71.8
Na <sub>2</sub> O	0.9	0.4	0.3	0.1	0.3		
P <sub>2</sub> O <sub>5</sub>						7.8	
B <sub>2</sub> O <sub>3</sub>							12.2
SiO <sub>2</sub> /Al <sub>2</sub> O <sub>3</sub>	4.55	4.76	4.70	69.46	4.56		
SA, m <sup>2</sup> /g	719	646	665	342	662	162	268



**Table 2.** Results of Catalytic Hydrocracking of Phenanthrene at 400°C with 6.9 MPa H<sub>2</sub>

Catalyst	H-Y	NiH-Y	FeH-Y	LaH-Y	S-NiMo/ Al <sub>2</sub> O <sub>3</sub> -B <sub>2</sub> O <sub>3</sub>	S-NiMo/ Al <sub>2</sub> O <sub>3</sub> -P <sub>2</sub> O <sub>5</sub>
Products <sup>a)</sup> (wt%)						
C <sub>1</sub> -C <sub>4</sub>	2.4	8.5	0.2	2.2	0.5	0.4
C <sub>5</sub> -C <sub>7</sub>	0.4	0.4	tr.	0.6	0.2	tr.
R <sub>1</sub> -  -R <sub>2</sub> <sup>b)</sup>	1.0	6.9	0.1	1.4	1.5	1.7
R <sub>1</sub> -  -R <sub>2</sub>	0.7	4.4	0.2	0.7	4.4	3.3
R <sub>1</sub> -  -R <sub>2</sub>	4.4	6.3	1.0	3.8	1.8	0.8
 -R	0.2	0.4	0.1	0.1	1.3	1.8
 <sup>c)</sup> +  -R	0.7	2.9	0.2	1.4	8.1	9.0
 <sup>d)</sup>	0.5	2.4	tr.	0.5	6.2	11.8
 -R <sup>e)</sup>	2.0	3.6	0.7	1.9	1.9	1.0
	1.3	2.7	4.6	1.2	16.7	17.0
	1.8	2.4	6.2	1.9	7.6	10.1
	53.3	19.3	80.4	54.0	31.6	30.5
R <sub>1</sub> -  -R <sub>2</sub>	11.2	8.7	1.1	10.3	1.0	0.4
C deposits <sup>f)</sup>	11.5	11.3	2.5	11.3	3.6	3.2
Conversion (wt%)	46.7	80.7	19.6	46.0	68.4	69.5

a) R, R<sub>1</sub> and R<sub>2</sub> mean alkyl groups or hydrogen. b) Including cyclohexyl phenylethane and cyclohexylbenzene. c) Unsym-octahydrophenanthrene. d) Sym-octahydrophenanthrene. e) Including some unknown components with molecular weight (by GC-MS) of 182. f) Amount of carbonaceous deposits on catalyst as determined by combustion method.

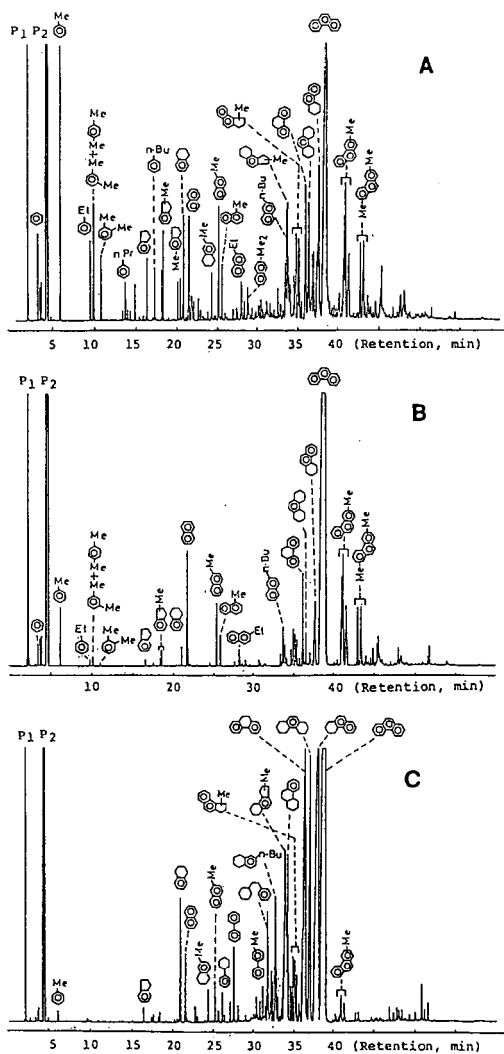


Figure 1. Composition of products from hydrocracking of phenanthrene over NiH-Y (A), LaH-Y (B) and commercial, B-modified NiMo/Al<sub>2</sub>O<sub>3</sub> (C) catalysts (P<sub>1</sub>: CH<sub>2</sub>Cl<sub>2</sub> solvent; P<sub>2</sub>: n-heptane solvent)

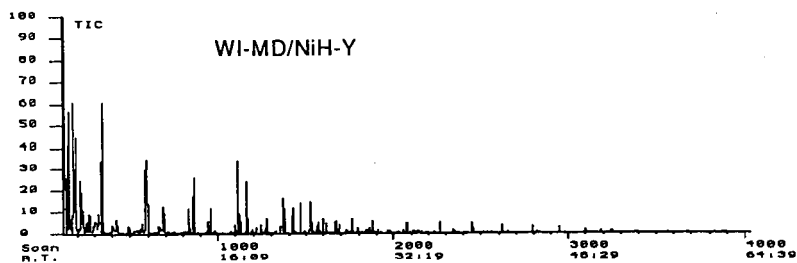
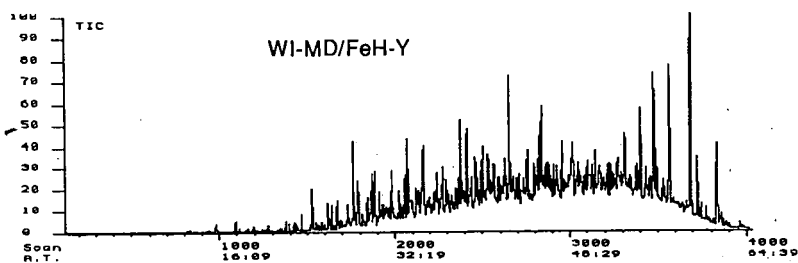
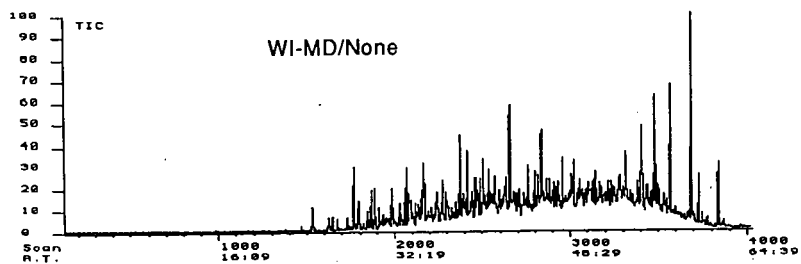


Figure 2. GC-MS TIC of liquid products from hydrocracking of Wilsonville middle distillates

## ULTRAFINE IRON CARBIDE AS LIQUEFACTION CATALYST PRECURSOR

G T Hager, X-X Bi\*, F J Derbyshire, P C Eklund\*, and J M Stencel

University of Kentucky

Center for Applied Energy Research

3572 Iron Works Pike, Lexington, KY 40511-8433

\*Department of Physics and Astronomy

**KEYWORDS:** Ultrafine Particles, Coal Dissolution, Iron Carbide

### ABSTRACT

Novel ultrafine particles (UFPs) of iron carbide have been synthesized and evaluated for their catalytic activity in coal liquefaction. The particles, with average diameters of 5 - 10 nm, were prepared by the laser driven pyrolysis reactions of ethylene and iron pentacarbonyl. Two different crystalline phases,  $\text{Fe}_7\text{C}_3$  and  $\text{Fe}_3\text{C}$ , have been prepared and these unsupported catalysts have been characterized using a range of analytical techniques. Results of microautoclave studies indicate the high catalytic activity of these UFPs for coal liquefaction compared to iron added as iron pentacarbonyl, and to a thermal baseline. The transformation of the catalyst under liquefaction conditions in the presence of sulfur is reported. The presence and catalytic role of monolayer pyrolytic carbon coatings formed on the catalyst surface during laser synthesis will also be addressed.

### INTRODUCTION

The primary use of highly dispersed slurry phase catalysts is in the first stage of a two stage liquefaction process. The preferred catalyst is one that will aid in the conversion of the coal to soluble products which may then be further upgraded in the second stage to more useful products using conventional supported catalysts. A successful slurry phase catalyst should improve product selectivity, allow increased throughput, and yield a first stage product which will reduce the rate of catalyst deactivation in the second stage. The effective use of a slurry phase catalyst may also offer an efficient means of liquefying low rank western U. S. coals which can produce more desirable products [1,2] and reduce second stage catalyst deactivation [3]. Subbituminous coals are generally found,

however, to convert at a lower rate and to a lesser extent than higher rank coals. This is purported to be caused by an imbalance in the rates of bond cleavage and hydrogenation. Dissolution promoted by an effective slurry phase catalyst may be able to correct this imbalance.

Historically, the oxides and sulfides of molybdenum, tungsten and the iron group metals were among the first catalysts used in coal liquefaction. Molybdenum compounds are generally considered to exhibit higher activity in dissolution and hydrogenation than iron compounds. However, due to the higher cost of the molybdenum and the fact that dissolution catalysts are not easily recovered, iron based catalysts are usually preferred for industrial operations.

Since the catalytic process takes place at the surface-liquid interphase, the amount of surface area available for reaction is critical. By increasing the surface area per unit volume the relative activity of a catalyst may be increased. In supported catalysts this is often done by depositing the catalyst over a high surface area porous substrate such as alumina or a zeolite. Unsupported catalysts, on the other hand, can present a high surface area by maintaining a high dispersion. The majority of the active catalyst surface is on the outside of the particles and therefore is not subject to pore diffusion limitations. Further, ultrafine particles, measuring only a few nanometers in diameter, may exhibit markedly different properties than bulk particles of the same composition and may therefore present a means to improve the activity.

The current research program is concerned with the production of ultrafine iron carbide particles by laser pyrolysis and their catalytic behavior as related to composition, structure, size, and other properties.

## EXPERIMENTAL

### PARTICLE SYNTHESIS

The use of laser pyrolysis for ultrafine particle synthesis was first performed by Haggerty and co-workers [4] for the production of silicon-containing ceramics. The technique was later adopted by researchers at Exxon who used it to produce transition metal carbide particles for use as catalysts in synthesis gas reactions [5,6]. One such carbide described in an Exxon patent was  $\text{Fe}_3\text{C}$ . To produce this carbide a stream of the

reactant gases, ethylene and iron pentacarbonyl ( $\text{Fe}(\text{CO})_5$ ), was intersected with a tunable cw  $\text{CO}_2$  laser. The same method was used in the present research. Approximately 5% of the incident energy from the laser is adsorbed by the ethylene. The added heat causes the thermal decomposition of the iron pentacarbonyl which leads to the formation of ultrafine (2-20 nm) spherical iron carbide particles. The exact mechanism of the particle formation is still under investigation.

The apparatus used for the synthesis of these particles has been described previously [7]. The reaction cell is shown in Figure 1. Particles generated in the reaction volume were originally collected on a teflon membrane filter. In this system the production limiting factor was the pressure drop across the filter.

The collection mechanism has since been improved to allow for production of large (>1g) batches of particles. A large magnet, placed upstream of the previously used teflon membrane filter, effectively traps most of the particles in a sample chamber. This sample chamber may be sealed and removed from the system when full and the particles may then be passivated (see Results and Discussion). The use of the magnetic trap is possible due to the ferromagnetic properties of the particles. However, this ferromagnetism leads to particle agglomeration which may adversely affect dispersion in liquefaction experiments.

## LIQUEFACTION

Since it has been reported that some transition metal carbide catalysts resist sulfiding under liquefaction conditions [8,9], coal-free experiments were conducted to determine the catalyst behavior under both sulfiding and nonsulfiding conditions. These experiments were carried out in 18 mL batch microautoclaves, in the absence of coal, with 4 wt%  $\text{Fe}_7\text{C}_3$  in 5 g of tetralin, with and without sulfur added as dimethyldisulfide (DMDS) at twice the stoichiometric ratio required for formation of  $\text{FeS}_2$ . The reaction conditions used in this study were 385 °C with 800 psig (cold) hydrogen pressure and the reaction time was 30 minutes.

The liquefaction experiments were conducted in the same batch microautoclaves using 3 g of a subbituminous Wyodak coal and 5 g of tetralin. The reaction conditions were the same as the coal-free runs and

the reaction time was 15 minutes. Two passivated iron carbide catalysts,  $\text{Fe}_7\text{C}_3$  and  $\text{Fe}_3\text{C}$ , were used in the study. A thermal run and a catalytic run using  $\text{Fe}(\text{CO})_5$  were also made for comparison. The catalyst loading was 1 wt % Fe, as determined from precursor stoichiometry, and dimethyldisulfide (DMDS) was added in 20 % excess for the formation of  $\text{FeS}_2$ . The addition of DMDS was based on the results of the previous coal-free experiments with added sulfur. The conversions (daf) of the coal liquefaction runs were determined using solubility in pyridine (preasphaltenes), benzene (asphaltenes), and pentane (oils). Gas yields were determined by gas chromatography.

## RESULTS AND DISCUSSION

Two distinct phases of iron carbide particles, orthorhombic  $\text{Fe}_3\text{C}$  and metastable hexagonal  $\text{Fe}_7\text{C}_3$ , have been synthesized. These particles have been characterized by XRD, transmission electron microscopy, electron diffraction, and Mössbauer spectroscopy. The phase and size of the particles is controlled by the gas flow rate, pressure and laser intensity. Adjustment of these parameters allows the control and reproducible production of different size ranges and both phases.

The particles are formed with a thin layer of pyrolytic carbon coating the surfaces of the particles. The particles are also pyrophoric which necessitates their passivation prior to exposure to air. The passivation process involves the gradual introduction of 10%  $\text{O}_2$  in helium with constant temperature monitoring to prevent runaway reaction. While the effect of the process on the carbon coating is unclear, X-ray photoelectron spectroscopy (XPS) has shown that the passivated particles possess a surface layer of  $\text{Fe}_3\text{O}_4$ .

The results of the coal-free experiments showed that the iron carbide particles will sulfide under liquefaction conditions in the presence of added sulfur to form pyrrhotite. While it is believed that the addition of coal will not prevent this transformation from occurring, Mössbauer spectroscopy of the liquefaction residues are being done to provide evidence of the final state of the catalyst after reaction. Particle growth, as shown by SEM micrographs and the narrowing of X-ray diffraction lines (Figure 2), is seen in both the coal-free runs. TEM micrographs of the particles formed in the absence of sulfur confirm the increase in size due to the agglomeration of the smaller particles. The

larger particles have a relatively narrow size distribution and appear to be made up of the small particles which have agglomerated to form spheres around a hollow or carbon center. The XRD analysis indicates that in the absence of added sulfur the catalyst undergoes a phase change to an iron carbide, or mixture of carbides, and some  $\text{Fe}_3\text{O}_4$ . It seems unlikely that this oxide phase could have been produced in the reducing atmosphere present in the reactor. Its presence may be due to the fact that the surface oxide layer on the passivated particles was not effectively reduced or it may be an artefact of sample handling. In the presence of added sulfur the  $\text{Fe}_7\text{C}_3$  is converted to pyrrhotite and sintering is again observed by SEM and XRD. TEM micrographs show that the sulfided catalyst exists as both small particles and as larger agglomerated crystals. Energy dispersive X-ray analysis indicates an approximate stoichiometry of  $\text{Fe}_{0.85}\text{S}$ , or approximately  $\text{Fe}_7\text{S}_8$ , for the pyrrhotite. The rate of the conversion to pyrrhotite is not known. The effect of coal on this transformation is under investigation.

Based on the results from the coal-free experiments with sulfur, excess sulfur was added in the liquefaction experiments to allow for the catalyst transformation to pyrrhotite, since pyrrhotite has widely been reported to be the active form of iron catalysts. Table 1 shows the results of the liquefaction experiments. When compared to the thermal run and a run using iron carbonyl as the catalyst precursor, both carbide forms showed enhanced total conversion. This increase in conversion may be more significant than these results indicate since the pyrolytic carbon coating has been suggested by the results of thermogravimetric analysis (TGA) to account for approximately 30 % of the particle weight. The exact quantity of carbon in the coating is being determined by current experiments. The corrected iron loading for the catalytic runs with iron carbide precursors was then approximately 0.75 wt. %. This shows higher conversion at lower iron loading for the heterogeneous iron carbide precursors compared to the homogeneous iron pentacarbonyl precursor. The result corresponds with other research [10-12] which has shown that aerosol iron oxide precursors produce higher activity than organometallic or salt precursors. This may be due to the unexpectedly large (70 -110 nm) crystallites which are reportedly formed by the soluble precursors and the relative stable size of the particle precursor. The reason for the larger crystallite formation by the soluble precursors is not understood at present. In addition to the higher overall conversion, there are also some differences in the product selectivity. The catalytic effect, if any,



of the carbon coating has not been determined.

Comparing the data from these experiments to the work of Keogh and Davis [13] plotted on a Wei-Prater diagram (Figure 3), a similar, but slightly different, pathway from the subbituminous pathway seems to be shown. The reason for this deviation is unclear at present. Since the deviation in the trend is present in the thermal baseline as well as the catalytic runs, it is expected that a difference in the coal and/or reactor, rather than the catalyst, is the cause. However, it is clearly seen in this plot that the addition of the iron carbide catalyst precursors increase the rate of progress along the proposed pathway with  $\text{Fe}_7\text{C}_3$  progressing furthest in the 15 minute runs. The high conversion is particularly promising since no efforts have been made to maximize or stabilize the precursor dispersion in the slurry.

## REFERENCES

1. Wu, W.R.K., Storch, H.H., 1968, Hydrogenation of Coal and Tar. Bulletin 633, Washington, DC, USA, US Department of the Interior, Bureau of Mines, 195pp.
2. Derbyshire, F.J., Stansberry, P.G., Fuel, 1987, 66, 1741-2
3. El Sawy, A., Gray, D., Talib, A., Tomlinson, G., 1986, Report SAND86-7103, Albuquerque, NM, USA, Sandia National Laboratories, 198pp.
4. Haggerty, J.S., Cannon, W.R., 1981, in Laser-Induced Chemical Processes (Ed. J I Steinfeld), Plenum Press, New York, NY, USA
5. Fiato, R.A. et al, 1987, US pat. 4,637,753
6. Rice, G.W. et al, 1987, US pat. 4,659, 681
7. Eklund, P.C., Stencel, J.M., Bi, X.X., Keogh, R.A., and Derbyshire, F.J., American Chemical Society. Div. of Fuel Chemistry. Preprints, 1991, 36(2) 551-60
8. Lee, J.S., Boudart, M., Applied Catalysis, 1985, 19, 207-210
9. Markel, E.J., Van Zee, J.W. Journal of Catalysis, 1990, 126, 643-657

10. Andres, M., Charcosset, H., Chiche, P., Davignon, L., Djega-Mariadasson, G., Joly, J-P., Peregermain, S. Fuel, 1983, **62**, 69-72
11. Andres, M., Charcosset, H., Chiche, P., Djega-Mariadasson, G., Joly, J-P., Peregermain, S. Preparation of Catalysts III (Eds. G. Poncelet and P. Grange) Elsevier 1983, 67 -682
12. Vergon, P.G., Landonisi, H.B., Industrial and Engineering Chemistry, 1980, **19**, 147-151
13. Keogh, R.A., Davis, B.H., American Chemical Society, Div. of Fuel Chemistry, Preprints, 1991, **36(2)** 438-444

Table 1 Conversion Analysis of Liquefaction Experiments

	YOM	Pre-asphaltenes	Asphaltenes	Oil & Gas	Total Conversion
Thermal	58.13	15.02	15.14	11.71	41.87
$\text{Fe}(\text{CO})_5$	53.15	9.34	23.43	14.08	46.85
$\text{Fe}_3\text{C}$	48.88	18.74	21.07	11.32	51.12
$\text{Fe}_7\text{C}_3$	43.74	22.29	18.01	15.96	56.26

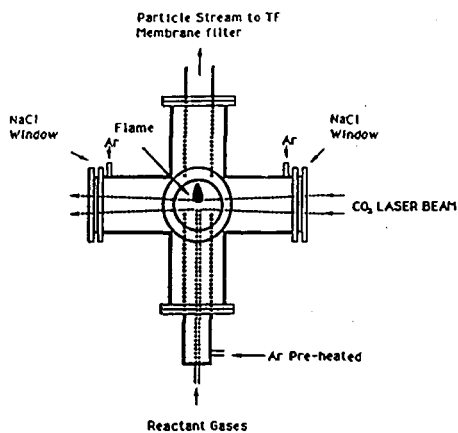


Fig. 1. Schematic Laser Pyrolysis Cell.



## CATALYTIC HYDROTREATMENT OF COAL-DERIVED NAPHTHA

Liguang Xu, Robert A. Keogh, Chen-Shi Huang,  
Robert L. Spicer, Dennis E. Sparks, Scott Lambert,  
Gerald A. Thomas and Burtron H. Davis

Center for Applied Energy Research  
University of Kentucky  
3572 Iron Works Pike  
Lexington, KY 40511

**Keywords:** Coal-derived Naphtha, Catalytic Hydrotreatment

### ABSTRACT

A naphtha derived from the liquefaction of a subbituminous (Black Thunder) and a bituminous coal (Ill. #6) was hydrotreated on a pilot plant scale, to provide a feedstock sufficiently low in heteroatoms for further studies in reforming. Two commercial catalysts, a Ni/Mo and Co/Mo on alumina, were employed in the processing of the naphtha samples. The Black Thunder naphtha was processed for over 120 hours for two passes using a Co/Mo catalyst and once using a Ni/Mo catalyst. For this naphtha, the nitrogen removal was extremely difficult using the catalysts and conditions employed in this study. An average of 51.6% of the nitrogen was removed for the three passes. The oxygen compounds in this naphtha were relatively easily removed. During the first pass over the Co/Mo catalyst, 94.0% of the oxygen was removed. Further processing during the next two passes using a Co/Mo and a Ni/Mo catalyst further reduced the oxygen content by 54% and 40% respectively.

### INTRODUCTION

The dominance of gasoline as a transportation fuel in the United States dictate that any viable coal liquefaction technology must produce a naphtha feedstock that can be upgraded for gasoline production. The concept of what a "good" gasoline is has changed over the decades depending on availability of crudes, environmental concerns, etc. One of the major problems associated with a naphtha derived from processing coal is the high heteroatom content. In order to reform a coal-derived naphtha, the heteroatom content must be further reduced by hydrotreating.

HDN and HDO has been studied extensively using model compounds to determine the mechanism (1-3) and for evaluation of catalysts (4). However, few studies have addressed the upgrading of coal-derived naphtha on a pilot plant scale (5). In the present study, the hydrotreatment of a subbituminous coal-derived naphtha was catalytically hydrotreated in the CAER pilot plant. Two commercial hydrotreating catalysts (Ni/Mo and Co/Mo on alumina) were employed in this study.

## EXPERIMENTAL

### Naphtha Feedstock

Three, 55 gallon drums of the naphtha were obtained from the Wilsonville, Alabama Advanced Integrated Two Stage Liquefaction pilot plant. The naphtha hydrotreated was obtained from processing a Black Thunder coal (subbituminous).

### Pilot Plant Operations

The naphtha was hydrotreated in the reconfigured CAER 1/8 tpd liquefaction pilot plant. The process diagram is shown in Figure 1. The plant consists of the following sections: (a) feed delivery (naphtha,  $H_2$ ), (b) reactor, and (c) high and low pressure separators. The reactor was charged with 2 kg of catalyst and operated in a fixed bed down-flow configuration for the hydrotreating operations.

The first catalyst employed was a commercial Co/Mo on alumina catalyst (American Cyanamid HDS-1442A, 1/16" x 1/4" pellets). The second catalyst studied was a commercial Ni/Mo on alumina catalyst (Akzo KF-840 1.3Q).

Both catalysts were presulfided using a mixture of 3%  $H_2S$  in hydrogen prior to the beginning of hydrotreating operations. During the presulfiding operation, a flowrate 30  $ft.^3/h$  of the  $H_2S/H_2$  mixture was used. The reactor temperature was rapidly increased to 175°C followed by a 25°C/h ramp. During these operations, the composition of the gas stream exiting the plant was continuously monitored for the  $H_2S$  breakthrough by an on-line gas chromatograph. During the ramping of the reactor temperature, the data obtained from the GC indicated that no additional  $H_2S$  was being absorbed by the catalyst. At this point, the temperature was increased to 375°C and held at this temperature for 90 minutes. The reactor temperature was then cooled to 300°C and the inlet gas stream was switched to hydrogen using a flowrate 5  $ft.^3/h$  prior to the start of naphtha processing. The same presulfiding procedure was used for operations with the Ni/Mo catalyst.

The processing conditions for the three pilot runs are given in Table 1. During naphtha processing, daily samples from the low pressure separator (V-451) were obtained for analysis. The pilot plant was placed under nitrogen at a system pressure of 360 psig prior to the beginning of the second hydrotreating run. Prior to the third pilot plant run, the Co/Mo catalyst was replaced by the Ni/Mo catalyst.

During the hydrotreating operations, two barrels of the Black Thunder naphtha was processed. Collection of the hydrotreated naphtha from each pass into the product barrel was initiated upon the attainment of steady state conditions as indicated by the process variables and the nitrogen content of the daily samples. The feedstock for the second pass using the Black Thunder naphtha was the product barrels obtained during the first pass. The feedstock for the third pass using the Ni/Mo catalyst was the hydrotreated product from the second pass.

Oxygen analyses were performed using the FNA method and were provided by the University of Kentucky Radioanalytical Services. Trace level nitrogen was analyzed using a Xertex DN-10 total nitrogen analyzer equipped with a chemiluminescence detector.

## RESULTS AND DISCUSSION

### Black Thunder Hydrotreatment

The nitrogen content of the hydrotreated naphtha (daily samples) obtained during the three passes are shown in Figure 2. The data clearly show the difficulty in removing the nitrogen from the naphtha using either the Co/Mo or Ni/Mo catalysts using these process conditions. During the initial pass, only 43% of the nitrogen was removed from the naphtha. The amount of nitrogen during the second pass was only marginally better (51%). Switching to a Ni/Mo catalyst and using the same process conditions did increase the nitrogen removal to 61%. However, after three passes, the nitrogen content of the hydrotreated naphtha remained at an average level of 383 ppm. The average nitrogen removal was only 52% for all three passes. Based on these data, it was projected that to obtain a hydrotreated product containing 2 ppm nitrogen, the naphtha would have to be processed 10 times (Figure 3). Clearly, hydrotreatment of the Black Thunder naphtha will require more severe conditions than are normally employed in petroleum refining to obtain a final product in which the nitrogen content is sufficiently low for further upgrading by reforming.

The amount of oxygen in the hydrotreated Black Thunder naphtha is shown in Figure 4. Although the oxygen content of the original naphtha is high (2.01%), 94% of the oxygen was removed during the first pass to yield a product containing .11% oxygen. The second and third pass (Ni/Mo) removed an additional 54% and 40% of the oxygen to produce a final hydrotreated naphtha containing .03% oxygen. The results indicate that the majority of the oxygen was easily removed during the first pass using the Co/Mo catalyst and low oxygen content of naphtha feedstock not substantially improve the amount of nitrogen removed during the second pass.

It is apparent from these data, that oxygen is easily removed from the Black Thunder (subbituminous coal) naphtha. The nitrogen compounds found in this naphtha are more difficult to remove during hydrotreating using a WHSV of 1 and a reaction temperature of 403°C. The data also suggests that the HDN process did not substantially inhibit the HDO process using either the Co/Mo or Ni/Mo catalysts under these conditions.

## CONCLUSIONS

The resulting data from the hydrotreatment of a Black Thunder naphtha indicate that the removal of nitrogen is difficult. To obtain a nitrogen content of less than 10 ppm require process conditions which are more severe than normally associated with petroleum hydrotreating. In contrast to the difficulty in obtaining a low nitrogen product, oxygen is relatively easy to remove from the Black Thunder naphtha. It is apparent from these data that new catalysts will have to be developed for the processing of coal-derived

naphtha to obtain a sufficiently heteroatom free product using common industrial process conditions.

#### ACKNOWLEDGMENT

This work was supported by the Commonwealth of Kentucky and DOE contract No. DE-AC22-90PC90049. The authors thank Dr. Charles Cantrell for providing the Wilsonville naphtha samples.

#### REFERENCES

1. McIlvried, H. G., Ind. Eng. Chem. Process Des. Dev., **10**, 125 (1971).
2. Furinsky, E., Appl. Catal., **6**, 159 (1983).
3. Ledoux, M. J., Appl. Catal., **9**, 31 (1984).
4. Furinsky, E., I & EC, Prod. Res. & Dev., **22**, 34 (1983).
5. Fischer, R. H. and Hildebrand, R. E., ACS Symp. Series, No. 156 (1981).

TABLE 1

#### Process Summary

#### Black Thunder Hydrotreatment

<u>Pass #</u> <u>(Run Hours)</u>	<u>Catalyst</u>	<u>Feed Rate</u> <u>(#/hr)</u>	<u>WHSV</u> <u># feed/# catalyst/hr</u>	<u>Temp</u> <u>(°C)</u>	<u>Pressure</u> <u>(psig)</u>
1 (0-165)	CoMo	4.0, 4.5	.9, 1.0	418	2010
2 (0-143)	CoMo	4.0, 4.5	.9, 1.0	418	2010
3 (0-127)	NiMo	4.5	.8	403	2000



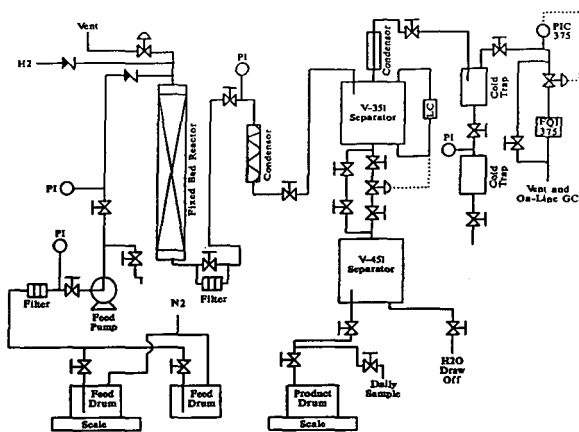


Figure 1. CAER Pilot Plant configuration for naphtha hydrotreating.

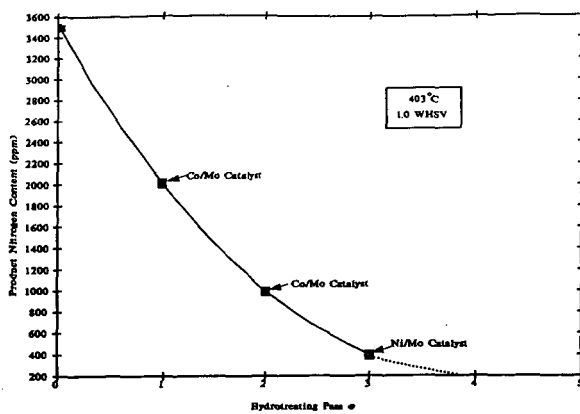


Figure 2. Summary of HDN for Black Thunder hydrotreatment.

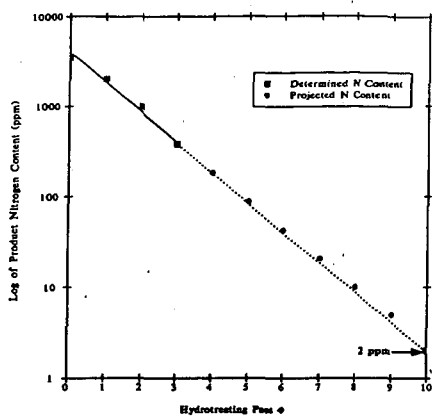


Figure 3. The projected number of passes to obtain a Black Thunder product containing 2 ppm nitrogen.

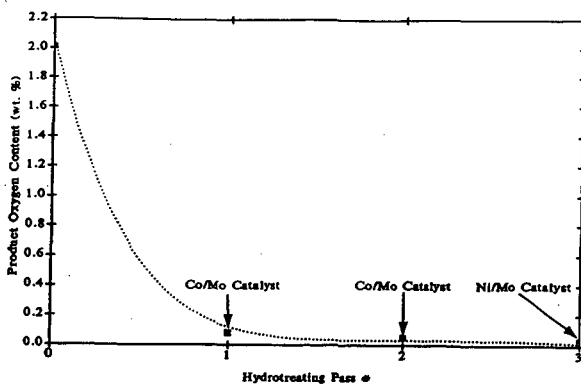


Figure 4. Summary of HDO for Black Thunder hydrotreatment.

## **DISTILLATE SELECTIVITY AND QUALITY OF BITUMINOUS COALS IN THE CATALYTIC TWO-STAGE LIQUEFACTION PROCESS**

J. M. Lee, C. E. Cantrell, S. V. Gollakota  
O. L. Davies, M. M. Corser, and P. Vimalchand  
Southern Electric International, Inc.  
P. O. Box 1069, Wilsonville, Alabama 35186

**Keywords:** catalytic liquefaction, distillate selectivity

### **INTRODUCTION**

The Clean Coal Research Center at Wilsonville, Alabama, has been operating for over 17 years to develop alternate technologies for producing low cost fuels from coal. Process developments of close-coupled integrated (CC-ITSL) configurations using the thermal/catalytic or catalytic/catalytic mode of operation were discussed in an earlier article<sup>1</sup>.

This paper is primarily focused on the high-volatile bituminous coal performance at steady-state operation with catalyst replacement in the catalytic/catalytic mode. Process developments results from eight runs are discussed: Runs 251-I, 252, 253, 254, 256, 257, 259 and 261. Runs 251-I, 252, 253, 257 and 261 processed a normally mine-washed high-ash Illinois No. 6 coal with four bimodal and one unimodal catalysts (Amocat 1A, Amocat 1C, Shell 317, EXP-AO-60 and Shell 324). Runs 254 and 256 processed an additionally cleaned Ohio No. 6 coal with Shell 317 and 324. Run 259 processed an additionally cleaned low-ash Pittsburgh No.8 coal with Shell 324 and Amocat 1C.

The primary objective of this study is to maximize the distillate production with good quality in order to improve the process economics. The distillate production can be enhanced by improving coal reactivity, catalyst conversion activity, and distillate selectivity. Typical analyses of feed coals processed for this study are summarized in Table 1. The coal cleaning procedure was reported elsewhere<sup>2</sup>. Properties of EXP-AO-60, Amocat and Shell Ni-Mo catalysts tested are shown in Table 2.

### **PROCESS DESCRIPTION**

The current catalytic close-coupled integrated two-stage liquefaction (CC-ITSL) process consists of two H-OIL<sup>®</sup> ebullated-bed reactors and a Residuum Oil Supercritical Extraction-Solids Rejection (ROSE-SR<sup>sm</sup>) unit<sup>3</sup>. Both the reactor designs utilize "H-OIL<sup>®</sup>" technology supplied by Hydrocarbon Research, Inc. The ebullated-bed design helps to maintain a uniform temperature distribution in the reactor. The ROSE-SR<sup>sm</sup> is a proprietary extraction process at conditions close to the critical point of the deashing solvent. It was developed and licensed by the Kerr-McGee Corporation.

### **RUN EXPERIMENTS**

Key process variables studied are listed below to maximize the distillate yield and production.

- (1) Combined activity of coal and catalyst  
- Illinois, Ohio, Pittsburgh

- unimodal Shell 324
- bimodal EXP-AO-60, Amocat 1C(/1A), Shell 317
- additionally cleaned low-ash coal
- (2) Steady-state operation with catalyst replacement
  - 1.5 to 4 lb/ton MF coal per stage
- (3) Recycle resid concentration in the process solvent
  - 40-50 wt %
- (4) Low/high and high/low thermal severity modes
- (5) Vacuum gas oil recycle
- (6) Coal space velocity
  - 28-76 lb MF coal/hr/cuft-cat per stage
- (7) Reaction temperature
  - 760-835°F in the first stage
  - 750-825°F in the second stage
- (8) Inlet hydrogen partial pressure
  - 2500-2700 psia in the first stage
  - 2400-2600 psia in the second stage
  - 2100 psia in the first stage in 253H
- (9) Slurry composition
  - 29-34 wt % coal (40 wt % in 253C)
  - 12 wt % CI (9 in 251-IA-IB, 4 wt % in 253C)
- (10) No interstage separation
- (11) Catalyst cascading in Run 252
- (12) Reactor operation parameters
  - temperature profiles, exotherms
  - ebullation rate, gas flow, slurry flow
  - slurry viscosity, etc.

Several steady-state operation periods were selected for comparisons of the distillate production, the effect of recycle resid concentration, and the effect of catalyst replacement rate, and are summarized below along with the distillate production projected for the "all-distillate" product slate with resid extinction<sup>4</sup>.

run	catalyst	tempera.	cat. rep.	recycle	projected
		(°F)	(lb/t MF)	resid	distillate
		1st/2nd	1st/2nd	(wt %)	product. <sup>d</sup>
(1) distillate production					
w/ Illinois coal					
257DE	Amo 1C	790/760	3/1.5	50	28.8
257H	Amo 1C	760/810	1.5/3	40	24.8
257J <sup>a</sup>	Amo 1C	810/760	3/1.5	50	42.2
251-IE	Amo 1A/1C	810/760	2 <sup>b</sup> /1 <sup>b</sup>	40	23.6
261B	EXP-AO-60	790/810	3/3	40	37.1
261D	EXP-AO-60	790/810	1.5/1.5	50	29.8
w/ Ohio coal					
254B	She 317	810/760	4 <sup>b</sup> /4 <sup>b</sup>	40	25.3
254G <sup>c</sup>	She 317	810/790	3/3 <sup>b</sup>	50	33.3
w/ Pittsburgh coal					
259H	She 324	825/790	3.6/3.6	50	28.6
259DE <sup>c</sup>	She 324	825/790	4/4	50	23.8
(2) effect of recycle resid concentration					
w/ Illinois coal					
257DE				50	28.8
257F				40	22.3
w/ Pittsburgh coal <sup>c</sup>					
259DE				50	23.8
259F				40	19.3

(3) effect of catalyst replacement			
w/ Illinois coal			
261B	3/3	40	37.1
261D	1.5/1.5	50	29.8
w/ Ohio coal <sup>c</sup>			
254G	3/3 <sup>b</sup>	50	33.3
254H	3/2.1 <sup>b</sup>		28.8
254I	3/1.5 <sup>b</sup>		26.8
254J	3/1.3 <sup>b</sup>		30.4
w/ Pittsburgh coal <sup>c</sup>			
259DE	4/4	50	23.8
259I	3 <sup>b</sup> /3 <sup>b</sup>		19.4
259J	2.5 <sup>b</sup> /2.5 <sup>b</sup>		15.8

<sup>a</sup> Half-volume reactors operation.  
<sup>b</sup> Estimated at steady-state operation from batch aging.  
<sup>c</sup> Additionally cleaned low-ash coal.  
<sup>d</sup> Unit: lb/hr/cuft-cat per stage.  
<sup>e</sup> Runs 254 and 257 operated without interstage separation.

## RESULTS AND DISCUSSION

### DISTILLATE PRODUCTION COMPARISON

#### Combined Activity of Coal and Catalyst

The distillate production was significantly improved in period 261B processing Illinois with EXP-AO-60 (37.1 lb/hr/cuft-cat per stage); 29-57% increases compared to 257DE, 257H and 251-IE. However, the distillate production was 12% lower than 257J. With additional coal cleaning with heavy media the distillate production significantly improved processing Ohio with Shell 317, by 16% in comparison of periods 254G and 257DE, while in contrast lowered 17% processing Pittsburgh with Shell 324 in comparison of periods 259DE, 259H and 257DE.

#### Effect of Recycle Resid Concentration

The effect of recycle resid concentration on distillate production was projected in both Runs 257D-F and 259D-F. Results are illustrated in Figure 1. The recycle resid level increase from 40 to 50 wt % improved 29% distillate production in 257D-F and improved 23% in 259D-F. 257D-F was with Illinois and Amocat 1C and 259D-F was with Pittsburgh and Shell 324. Both runs were in the high/low severity.

#### Effect of Catalyst Replacement Rate

The effect of catalyst replacement rate on distillate production was projected in Runs 261BD, 254G-J, and 259DEIJ. Results are illustrated in Figure 2. If the effect of resid recycle increase from 40 to 50 wt % observed in 257D-F with Illinois and Amocat 1C is considered in comparison of 261B and 261D (29% increase in the distillate production), then the catalyst replacement effect becomes more significant, approximately 61% increase in coal throughput by 3 lb/ton MF coal total replacement increase in 261B compared to 261D with Illinois and EXP-AO-60. The distillate production becomes 48 lb/hr/cuft-cat per stage, higher than that in 257J (42.2). The effect of catalyst replacement increase on coal throughput and distillate production was also significant in 254G-J with Ohio and Shell 317, and in 259DEIJ with Pittsburgh

and Shell 324. Both coals were cleaned with heavy media to lower the ash content and operated at 50 wt % resid recycle level. 254G-J with 1-1.5 lb/ton MF coal total catalyst replacement increase showed 16-24% increase in the distillate production; 259DEIJ with 2-3 lb/ton MF coal total catalyst replacement increase showed 23-51% increase in the distillate production.

Data for 251-IE and 257DEJ in the high/low mode were also included for comparison in Figure 2. Recycle resid concentration was 40 wt % in 251-IE and 50 wt % in 257DEJ. Operating conditions for these runs are listed in the previous section. 257J had the highest distillate production, primarily due to half-volume reactors operation resulting in more isothermal temperature distribution and better mixing, and a higher resid recycle level at 50 wt %, while 251-IE and 257DE with full-volume reactors operation had lower distillate production, because 251-IE operated at a lower resid recycle level, 40 wt % and 257DE operated at a lower first stage reaction temperature, 790°F.

259H with high-ash Pittsburgh and Shell 324 had a similar distillate production to that in 257DE with high-ash Illinois and Amocat 1C (28-29 lb/hr/cuft-cat per stage); 17% higher production than 259DE with low-ash Pittsburgh and Shell 324 (Figure 2). 259H operated at 33°F higher reaction temperature and 60% higher total catalyst replacement than 257DE in the high/low mode. Recycle resid concentration for these periods was same at 50 wt %.

#### EFFECT OF COAL CLEANING ON MAXIMUM DISTILLATE YIELD

Ohio coal was cleaned with heavy media to reduce the ash content from 10 to 6 wt % and Pittsburgh coal was cleaned from 15 to 4-5 wt %. Coal cleaning significantly improved the coal conversion for both Pittsburgh and Ohio coals. As a result, the organic rejection significantly reduced and the C4+ distillate yield significantly increased. Process performance improvements by the coal cleaning are summarized below.

<u>run</u>	<u>254</u>		<u>259</u>	
<u>coal</u>	<u>Ohio</u>		<u>Pittsburgh</u>	
base period(s)	B	GI	AH <sup>a</sup>	E
cleaning	normal	addit.	normal	addit.
ash in coal (wt%)	10	6	15	5
pyritic sulfur (wt% MF)	1.9	1.5	1.6	0.6
reactives (petrograp.)	94	97	92	93
potential liquid yield				
C4+ resid (wt% MAF)	70	78	69-70	78
coal conversion				
(wt % MAF coal)	94	97	92-93	96
organics rejected to				
solids prod. (wt% MAF)	16	8	19-20	9
C4+ distillate yield				
(projected) (wt% MAF)	68	78	67-70	78
C4+ dist. selectivity				
to resid+UC conv.	0.81	0.84	0.83-0.88	0.85

<sup>a</sup> 259A was unstable.

The coal conversion improvement was probably due to removal of less reactive coal components such as inertinites by cleaning with heavy media<sup>5</sup>. As reported earlier<sup>6</sup>, the linear regression analyses for bituminous coals projected that fully cleaned coals with zero ash content could achieve 100 wt % MAF coal conversion; could produce 83 wt % MAF coal C4+ distillate. The distillate yield higher than 83 wt % is possible, if the distillate selectivity further increases to higher than 0.85, which was observed with the cleaned low-ash coals (4-6 wt % ash content) with heavy media. The effect of coal conversion on organic rejection appeared to be very similar for the three coals. A good linear correlation between organic rejection (Y) and coal conversion (X) was derived for these coals by a linear regression analysis and is shown below.

$$Y = 265.7 - 2.67 X$$

$$r^2 = 0.94 \text{ (determination coefficient)}$$

#### DISTILLATE SELECTIVITY COMPARISON

##### Distillate Selectivity vs Yield

Figure 3 shows that the C4+ distillate selectivity to resid + UC conversion increases, as the distillate yield increases. High-ash Illinois, low-ash Ohio and low-ash Pittsburgh coals are compared. Processing Illinois in Runs 251-I, 252, 253, 257 and 261, the distillate selectivity was not significantly affected by four different catalysts tested (EXP-AO-60, Amocat 1C, Amocat 1A and Shell 317). The variation was 4%. For simplicity of the illustration the linear regression line with Illinois is included without showing the actual data points. Although two different thermal severity modes of low/high and high/low were investigated in runs with Illinois, it seemed that the selectivity was slightly increased by 1-3%, when operated at 790/760°F in the high/low mode (257A-FIK), 760/790-810°F in the low/high mode (257GH) and 790/810°F in the low/high mode with 3 lb/ton MF coal catalyst replacement per stage (261AB). The lower first stage reaction temperature improved the selectivity with less gas make.

Processing additionally cleaned low-ash Ohio and Pittsburgh in Runs 254 and 259, Pittsburgh and Shell 324 had 2% higher selectivity than that with the combination of Illinois and bimodal catalysts, and 4-5% higher than that with Ohio and Shell 317, although operated higher reaction temperatures, 810-825/790°F (Figure 4). Runs 254 with Ohio and Shell 317 and 257 with Illinois and Amocat 1C operated without interstage separation, which might have affected the selectivity. Coal cleaning appeared to improve the selectivity to 0.85-0.86 by producing more distillate about 78 wt % MAF coal (highest). Normally mine-washed high-ash Illinois with bimodal catalysts had a lower selectivity, 0.82-0.83 by producing less distillate about 68-70 wt % (highest). Inconsistent selectivity data were obtained with high-ash Ohio (•) and Pittsburgh (◊), that is, 0.86 in 254A, 0.81 in 254B, 0.83 in 259A and 0.88 in 259H.

##### Distillate Yield vs Hydrogen Consumption

Figure 4 shows with the three coals that the C4+ distillate yield increases, as the hydrogen consumption increases. The effects of catalyst type and reaction temperature were not apparent

processing Illinois. A linear correlation was observed with 4 wt % variation upto 70 wt % MAF coal distillate yield, which is the highest achieved so far with high-ash Illinois at Wilsonville. Required coal conversion and organic rejection to achieve this yield were 94 and 15 wt %, respectively. Processing low-ash Ohio and Pittsburgh, the distillate yield increased to 78 wt % MAF coal due to higher coal conversion (96-97 wt %) and lower organic rejection (7-9 wt %). Hydrogen efficiency (lb distillate/lb hydrogen consumed) in 254 with low-ash Ohio and Shell 317 increased at higher distillate yields above 70 wt %, compared to that with high-ash Illinois at lower distillate yields below 70 wt %. This trend indicated a possibility of two different hydrogenation routes with different reactants and products. Data from low-ash Pittsburgh showed a high scattering; inconclusive trend. Data from high-ash Ohio (\*) and Pittsburgh (e) are also included in the figure for comparison.

#### Hydrogen Efficiency vs Reaction Temperature

Figure 5 compares hydrogen efficiencies from Runs 251-I with high-ash Illinois and Amocat 1A/1C (a regression curve without showing the actual data points), 257 with high-ash Illinois and Amocat 1C, 259 with low-ash Pittsburgh and Shell 324, and 261 with high-ash Illinois and EXP-AO-60. Reaction temperature in the high severity stage was selected as x-coordinate variable. The hydrogen efficiencies for Runs 257, 259 and 261 were significantly higher than that obtained in Run 251-I with high-ash Illinois and Amocat 1A/1C; were similar to that with low-ash Ohio and Shell 317 at 810/790°F (Run 254 data are not included in the figure). Although two different thermal severity modes of low/high and high/low were investigated in these runs, it seemed that the efficiency was increased by 10% processing Illinois coal, when operated at 790/760°F in the high/low mode (257A-FIK), 760/790-810°F in the low/high mode (257GH (\*)), and 790/810°F in the low/high mode (261A-D). The lower first stage reaction temperature improved the selectivity with less gas make. Low-ash Pittsburgh and Shell 324 in Run 259 had a higher hydrogen efficiency with wide variation from 10 to 12 compared to Run 251-I, although operated higher reaction temperatures, 810-825/790°F. Coal cleaning with heavy media might be partially contributed to this efficiency improvement by producing more distillate with comparable gas make. Runs 254 with Ohio and Shell 317 and 257 with Illinois and Amocat 1C operated without interstage separation, which might have affected the hydrogen efficiency. Coal cleaning appeared to improve the efficiency by producing more distillate to 78 wt % MAF coal (highest). Two data obtained with high-ash Pittsburgh (e) showed an inconsistent trend, that is, a higher efficiency was observed at a higher temperature operation (12 vs 10.5 lb distillate/lb hydrogen consumed).

#### C<sub>1</sub>-C<sub>3</sub> Gas Selectivity vs Reaction Temperature

Figure 6 compares gas selectivities from Runs 251-I (a regression curve without showing the actual data points), 257, 259, and 261. Reaction temperature in the high severity stage was selected as x-coordinate variable. The gas selectivities for Runs 257 and 261 with high-ash Illinois were significantly lower than those obtained in Run 251-I with high-ash Illinois and Amocat 1A/1C and Run 254 with low-ash Ohio and Shell 317 at 810/790°F (Run 254 data are not included in the figure). The selectivity for Run



259 with low-ash Pittsburgh and Shell 324 was similar to that for Run 254 with low-ash Ohio and Shell 317, although operated at higher reaction temperatures, 810-825/790°F. It seemed that the gas selectivity was decreased with Illinois coal, when operated at 790/760°F in the high/low mode (257A-FIK), 760/790-810°F in the low/high mode (257GH (•)), and 790/810°F in the low/high mode (261A-D). The lower first stage reaction temperature reduced the gas selectivity with less gas make. Low-ash Pittsburgh and Shell 324 in Run 259 had a higher gas selectivity with wide variation from 11 to 15, when operated at a higher first stage reaction temperature, 825°F. Coal cleaning with heavy media seemed no significant impact on the gas selectivity. Runs 254 with Ohio and Shell 317, and 257 with Illinois and Amocat 1C operated without interstage separation, which might have affected the gas selectivity. Two data with high-ash Pittsburgh (e) showed an inconsistent trend having a similar gas selectivity observed at a higher temperature operation.

#### CATALYST ACTIVITY IN RESID + UC CONVERSION

Catalyst activities were calculated assuming that the resid + UC conversion reaction follows first-order kinetics for a continuous stirred tank reactor<sup>3</sup>. Cracking activity (resid conversion) is not the only function of the catalyst. Hydrogenation activity of the catalyst was not considered in these catalyst activity analyses. Catalyst activity analysis should be considered as the overall activity of combined catalytic and thermal conversion.

Figure 7 compares first stage activities in Runs 261, 257 and 259. Runs 261 and 257 processed Illinois with two different catalysts, EXP-AO-60 and Amocat 1C. The calculated rate constant value at 790°F for 261 with EXP-AO-60 was much higher than that for 257 with Amocat 1C. The rate constant values at 810 and 825°F for 259 processing Pittsburgh with Shell 324 were much lower than those at 790°F for 261 and 257 processing Illinois with EXP-AO-60 and Amocat 1C, respectively. The rate constant value at 810°F for 254 processing Ohio with Shell 317 was higher than those at 810 and 825°F for 259 processing Pittsburgh with Shell 324; lower than those at 790°F for 261 and 257 processing Illinois with EXP-AO-60 and Amocat 1C<sup>2</sup>.

Figure 8 compares second stage activities in Runs 261, 257 and 259. The calculated rate constant value at 810°F for 261 with EXP-AO-60 was higher than those at 760 and 790°F for 257 with Amocat 1C in the high/low mode; similar to that at 810°F for 257H with Amocat 1C in the low/high mode. However, the deactivation rate at 810°F was higher than that at 760°F. The rate constant values became similar for these temperatures at high catalyst ages above 50,000 lb MF coal/cuft-cat. The rate constant values at 760 and 790°F for 259 processing Pittsburgh with Shell 324 were much lower than those at 810°F for 261 and 257H processing Illinois with EXP-AO-60 and Amocat 1C, respectively; similar to those at 760 and 790°F for 257 processing Illinois with Amocat 1C. The rate constant values at 760 and 790°F for 254 processing Ohio with Shell 317 were lower than those at 760 and 790°F for 259 processing Pittsburgh with Shell 324; lower than that at 760°F for 257 processing Illinois with Amocat 1C. The value at 810°F for 254 processing Ohio with Shell 317 appeared to be similar to that at 810°F for 261 processing Illinois with EXP-AO-60, when the deactivation curves were extrapolated for comparison.

at similar catalyst ages.

#### COAL REACTIVITY COMPARISON IN RESID + UC CONVERSION

High-ash coal reactivity in the resid + UC conversion reaction was compared and reported in an earlier article<sup>2</sup>, by adjusting the responses measured in Runs 253, 254, 257 and 259. Results are summarized below.

<u>coal</u>	<u>run</u>	<u>C4+dist</u>	<u>resid w/OR=20%</u>	<u>resid+UC conv.</u>
Illinois	257J	66	0	80
Pitts.	259A	50	19	61
Ohio	254B/253D	59	7	73

#### DISTILLATE PRODUCT QUALITY

Table 3 summarizes distillate product qualities in Runs 251-IE, 257FGI, 261BD, 254G and 259DH. During Run 259 with Pittsburgh and Shell 324 which was the first run tested with a better distillation separation system, the distillate product quality improved by reducing the boiling end point of the distillate product (715°F in 259D and 760°F in 259H)<sup>7</sup>. In Run 261BD with Illinois and EXP-AO-60, the boiling end point was 772°F in 261B and 780°F in 261D. 257FGI end point data were estimated by assuming steady recycle of heavy distillate as in Runs 259 and 261. In many respects, the properties of distillates from Illinois, Ohio and Pittsburgh with different Ni-Mo catalysts are similar. This is not unexpected, since they were converted to liquids under similar operating conditions. Hydrogen content was high, 11.3-12.2 wt %. Heteroatom contents were low, 0.1-0.3 wt % nitrogen and <0.1 wt % sulfur. Oxygen content varied 0-2.5 wt %, since it was calculated by the difference. °API gravity was 19-28. Improvements in product quality were recognized by upgrading studies performed with coal-derived liquids by Chevron Oil Company<sup>8</sup>. Reduced boiling end point, lower nitrogen and sulfur contents and increased hydrogen content would make the upgrading task easier for the usage of commercial-type transportation fuels. Some improvements have been made during the past several years and efforts continue at Wilsonville to improve the product quality for the better process economics.

#### CONCLUSIONS

- Processing high-ash Illinois, the distillate production improved by 30-50%. The low/high severity mode with EXP-AO-60, increased catalyst replacement, increased resid recycle, and half-volume reactors operation significantly improved the distillate production.
- Processing low-ash Ohio and Pittsburgh, the distillate yield improved to 78 wt % MAF coal by coal cleaning with heavy media, primarily due to increased coal conversion to 97 wt % and reduced organic rejection to 8 wt %. The distillate production was improved with Ohio and Shell 317 by 16%; was reduced with Pittsburgh and Shell 324 by 17%. The reduction of distillate production with the cleaned Pittsburgh and Shell 324 seemed partly due to a lower pyrite content of the cleaned coal and/or a lower resid conversion activity of the cleaned coal and catalyst.
- The increased gas oil recycle improved the distillate

product quality by reducing the boiling end point of the distillate product. The boiling end point was 715-760°F with Pittsburgh and Shell 324; 770-780°F with Illinois and EXP-AO-60.

- The low/high severity operation seemed improving the distillate selectivity and hydrogen efficiency with less gas make.
- The additional coal cleaning with heavy media seemed improving the distillate selectivity and hydrogen efficiency by increasing the distillate yield to 78 wt % MAF coal.
- The theoretical maximum distillate yield of fully cleaned coals with zero ash content was projected to be 83 wt % MAF coal for high-volatile bituminous coals. The distillate yield higher than 83 wt % is possible, if the distillate selectivity further increases to higher than 0.85, which was observed with the cleaned coals (4-6 wt % ash content) with heavy media.
- Resid derived from Illinois was easier to convert to distillate than from Ohio and Pittsburgh; resid from Pittsburgh was harder to convert than Ohio. Higher reaction temperatures were required to achieve the "all-distillate" product slate with combinations of low-ash Ohio-Shell 317 and Pittsburgh-Shell 324; hydrogen efficiencies were similar with higher gas selectivities due to higher distillate yields.

#### ACKNOWLEDGEMENTS

This work was supported by the U. S. Department of Energy under Contract DE-AC22-82PC50041, and the Electric Power Research Institute under Contract RP1234-1-2, and was managed by the Southern Company Services, Inc. Mr. Bill Weber is EPRI project manager and Dr. Ed Klunder is DOE project manager. The authors gratefully appreciate the assistance of Mrs. Mary Jane Sherbert and Mrs. Mary Dunnaway in preparation of this paper.

#### REFERENCES

1. R. V. Nalitham, J. M. Lee, C. W. Lamb, and T. W. Johnson. Fuel Processing Technology, Vol. 17, 1987, pp. 13-27.
2. J. M. Lee, S.V. Gollakota and O.L. Davies. Proceedings of the Fifteenth Annual EPRI Conference on Fuel Science, June 1990.
3. Catalytic, Inc., Topical Report. DOE Contract No. DE-AC22-82PC50041, EPRI Contract No. RP1234-1-2, Document No. DOE/PC/50041-82.
4. J. M. Lee, C. E. Cantrell, S. V. Gollakota, O. L. Davies, M. M. Corser, and P. Vimalchand. Proceedings of the Sixteenth Annual EPRI Conference on Fuel Science, June 1991.
5. R. P. Anderson, B. F. Alexander, C. H. Wright, and J. Freel. Fuel, Vol. 64, November, 1985, pp. 1558-1563.
6. J. M. Lee and C. E. Cantrell. Proceedings of the Fourteenth Annual EPRI Conference on Fuel Science, May 1989.
7. Southern Electric International, Inc., Technical Progress Report. DOE Contract No. DE-AC22-82PC50041, EPRI Contract No. RP1234-1-2, Document No. DOE/PC/50041-. (Not published)
8. R. F. Sullivan and H. A. Frumkin. ACS National Meeting, Div. Fuel Chem., New York, NY, April, 1986.

TABLE 1

## FEED COAL ANALYSIS

Coal	Illinois No.8	Ohio No.8	Pittsburgh No.8
Mine	Burning Star	Crooksville (cleaned)	Ireland (cleaned)
Runs	251-1,252,253	254,258	259
Rank (ASTM)	257,261		
FC (mf wt %)	hvbB	hvbB	hvaB
HV (Btu/lb mf)	51	53	54
Ultimate (mf wt %)	12,600	13,300	14,200
Carbon	70.8	75.3	76.6
Hydrogen	4.8	5.3	5.7
Nitrogen	1.5	1.4	1.4
Sulfur	3.4	2.8	3.2
Ash	11.5	6.6	4.6
Oxygen (dif.)	8.2	8.8	5.8
Petrographic (mmf vol %)			
Reactive	94	97	93
Pyritic Sulfur	1.1	1.5	0.6

TABLE 2

## WILSONVILLE NI-MO CATALYST PROPERTIES

Catalyst Run	Shell 324 256,259	Amocat 1C 251-253	EXP-AO-60 261	Shell 317 253,254
	261	257,259		258
Shape	Cylindrical			Trilobe
Size (in)	1/16	1/16, 1/12	1/16	1/20
Ni (wt%)	2.7	2.3	2.5	2.7
Mo	13.2	10.4	10.7	11.6
Surface Area (sqm/g)	165	190,165	241	235
Pore Volume (cc/g)	0.48	0.85,0.88	0.78	0.75
Pore Size Dist.	Unimodal	Bimodal		
Comp. B. Density (lb/cuft)	54	42,36	33	38

TABLE 3. TOTAL DISTILLATE PRODUCT QUALITY COMPARISON

Run Coal	257F	257G	257I	251-IE	261B	261D	254G	259D	259H
	Illinois						Ohio	Pitts.	
Wt % C	87.5	87.8	87.4	87.2	87.3	87.5	88.3	86.7	87.0
H	12.2	12.1	12.1	11.6	11.4	11.3	11.3	12.0	11.7
N	0.2	0.1	0.1	0.2	0.2	0.3	0.3	0.2	0.2
S	0.0	0.0	0.0	0.0	0.0	0.0	0.0	0.0	0.0
O	0.1	0.0	0.4	1.0	1.1	0.9	0.1	1.1	1.1
								(2.5)	
°API	21	21	21	26	23	22	19	28	25
Wt % Naphtha	22	21	18	26	19	14	25	20	19
Mid.D1	11	10	11	12	11	16	9	18	13
Mid.D2	50	53	64	32	40	40	35	43	43
Gas Oil	17	16	7	30	30	30	32	19	25
End point °F (D1160)	680	700	665	-	772	780	-	715	760
	- estimated -								

FIGURE 1  
EFFECT OF RECYCLE RESID CONCENTRATION  
ON DISTILLATE PRODUCTION

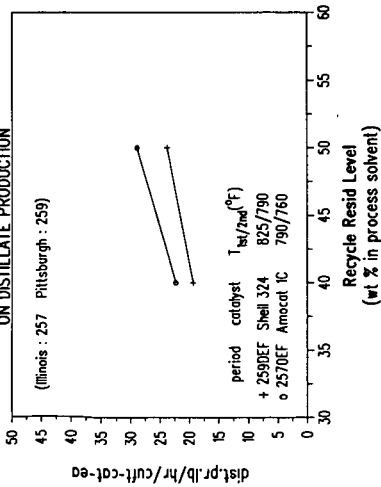


FIGURE 2  
EFFECT OF CATALYST REPLACEMENT  
ON DISTILLATE PRODUCTION

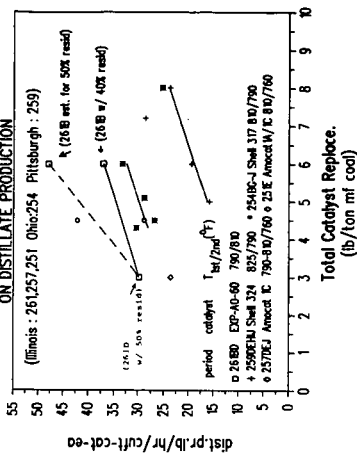


FIGURE 3  
DISTILLATE SELECTIVITY VS YIELD  
(Ohio and Pittsburgh Coals - Low Ash)

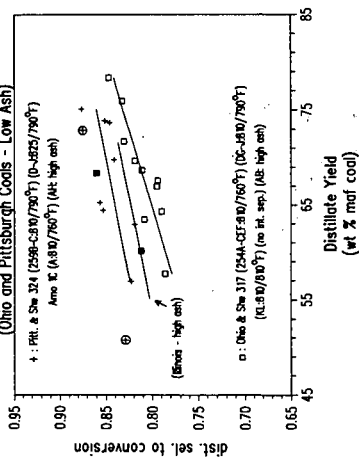


FIGURE 4  
DISTILLATE YIELD VS H<sub>2</sub> CONSUMPTION  
(Ohio and Pittsburgh Coals - Low Ash)

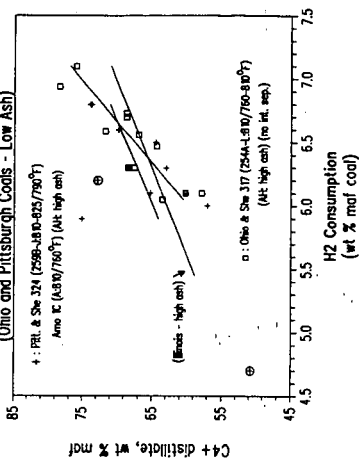


FIGURE 5 HYDROGEN EFFICIENCY VS TEMPERATURE

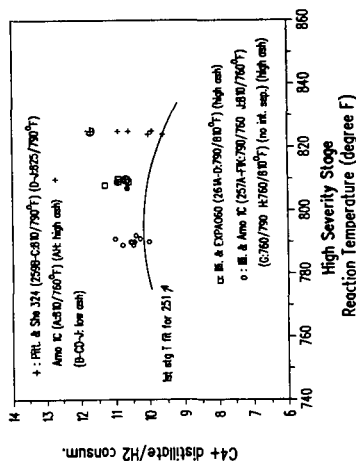


FIGURE 6 C1-C3 GAS SELECTIVITY VS TEMPERATURE

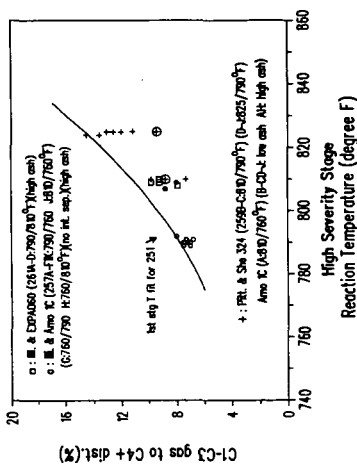


FIGURE 7 1ST STAGE CATALYST ACTIVITY COMPARISON  
257 (O) vs 259 (+) vs 261 (□)

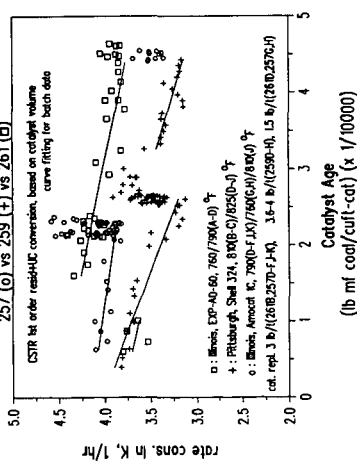
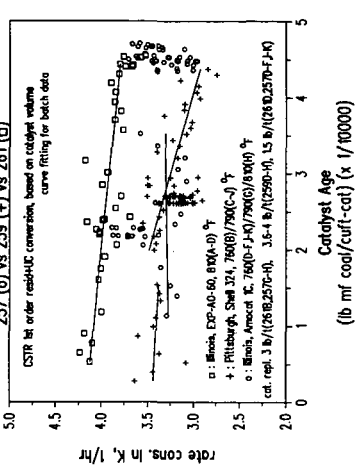


FIGURE 8 2ND STAGE CATALYST ACTIVITY COMPARISON  
257 (O) vs 259 (+) vs 261 (□)



## TWO STAGE GASIFICATION : EFFECT OF HYDROPYROLYSIS CONDITIONS

G. Skodras and G.P. Sakellariopoulos  
Department of Chemical Engineering and  
Chemical Process Engineering Research Institute  
Aristotle University of Thessaloniki  
Thessaloniki, Greece 54006

### SUMMARY

Two-stage hydrocarbon gasification and  $\text{CO}_2$  gasification has been investigated with Greek lignite at various temperatures and residence times in order to identify optimal conditions for switching between the two steps. Optimality was based on carbon conversion and product formation. Such optimum conditions are obtained for hydrocharring at  $900^\circ\text{C}$  for 2 to 5 min and subsequent  $\text{CO}_2$  gasification of the resulting chars at  $900^\circ\text{C}$  and 10 min.

### INTRODUCTION

Hydrogasification is a relatively slow process [1,2], with most hydrocarbons formed in the early hydrocarbon step [2,3]. Carbon dioxide gasification of chars is faster than hydrogasification and can improve conversion and carbon atom utilization. Char gasification in  $\text{CO}_2$  has been investigated with respect to carbon reactivity [4,5], kinetic behavior [6], and promotion by catalysis [7]. However, most chars used in  $\text{CO}_2$  gasification have been prepared, almost exclusively, in non-reactive atmospheres, such as  $\text{N}_2$  or He [4-6]. Little is known about the effect of the initial charring step (pyrolysis or hydrocarbon gasification) on the reactivity in the second stage and on total carbon conversion and gaseous product formation.

In this work Greek lignite was gasified in a reactive hydrogen atmosphere and subsequently in  $\text{CO}_2$ , to explore lignite behavior under two stage, ambient pressure gasification. The effect of temperature and solids residence time in each stage on total carbon conversion and on gaseous product yields and selectivity was studied.

### EXPERIMENTAL

Greek lignite from the Ptolemais reserve (4  $10^6$  t) was used, with particles in the range of 150 to 250  $\mu$ . This lignite is high in calcium carbonate ash and humidity and has a volatiles content of 47.16% (on dry basis).

The gasification test reactor was equipped with gas and solids feeding controls and with product collection and analysis devices, Fig. 1. The U-shape reactor design permitted rapid quenching of the reactor, thus, hydrocarbon gasification or  $\text{CO}_2$  gasification reactions could be interrupted at any desirable time.

Lignite samples were initially hydrocarbon gasified ( $800^\circ\text{C}$  or  $900^\circ\text{C}$ , at 2, 5 or 10 min) and the produced chars were gasified under a  $\text{CO}_2$  atmosphere ( $800^\circ\text{C}$  or  $900^\circ\text{C}$ , at up to 15 min). Gaseous products were collected in both stages, and were analyzed mainly for  $\text{CH}_4$  and  $\text{CO}$  by G.C. (Varian Vista 6000). Chars obtained in the hydrocarbon gasification and the  $\text{CO}_2$  gasification step were analyzed by a LECO C-H-N 800 analyzer, in order to determine elemental compositions and conversions in each step.

### RESULTS AND DISCUSSION

During the first stage (hydrocarbon gasification), the devolatilization and hydrocracking reactions which take place [3,8] cause significant

weight loss. On a dry and ash free basis, weight losses are of the order of 62% at 800°C, reaching about 67% at 900°C and long residence times. Since the initial volatile matter of lignite is 47% w/w on a dry basis, devolatilization appears to be the main reaction during this first stage [3,8,9]. The heterogeneous carbon-hydrogen gas-solid reaction becomes significant only at longer solid residence times (>10 min).

Methane, CO and CO<sub>2</sub> are the main gaseous products during this first stage. Tables 1 and 2. Maximum CH<sub>4</sub> formation is observed at 900°C and 10 min, via the heterogeneous hydrogen-carbon gas-solid reaction. In contrast, CO+CO<sub>2</sub> yields are less affected by the hydrolysis residence time, since these are products of hydrolysis and hydrocracking reactions during the initial 2 min of pyrolysis. The yield of CO, however, increases appreciably (about 60%) with temperature, from 800°C to 900°C, while that of CO<sub>2</sub> drops to about one third, due to enhancement of the CO<sub>2</sub> reduction to CO in a H<sub>2</sub> atmosphere [3]. Other hydrocarbons (C<sub>2</sub>H<sub>4</sub>, C<sub>2</sub>H<sub>6</sub>, etc) are also produced in small quantities (1 to 12 cc/g lign. daf), Table 1 and 2.

In order to evaluate the significance of each product at the various conditions tested a "selectivity index" has been used, shown in Table 1 and 2. To calculate the selectivity of the gaseous products, other higher molecular weight products have been assumed to be insignificant compared to CO, CO<sub>2</sub>, CH<sub>4</sub>, C<sub>2</sub>H<sub>4</sub>, and C<sub>2</sub>H<sub>6</sub>. Increase of solid residence time at low hydrolysis temperature (800°C) almost doubles the CH<sub>4</sub> "selectivity index" (8.15% at 2 min, and 15.7% at 10 min), Table 1. Similar behavior is also exhibited by CO selectivity for both hydrolysis temperatures. In contrast, CO<sub>2</sub> selectivity decreases with an increase of hydrolysis time and temperature. This is particularly evident by the relative selectivity of CO and CO<sub>2</sub>, expressed as the ratio CO/CO<sub>2</sub>, Tables 1 and 2. Thus, high T and long times minimize CO<sub>2</sub> formation while total (CO+CO<sub>2</sub>) selectivity decreases somewhat.

The elemental analyses of chars prepared at 800°C and 2.5 or 10 min show that elemental carbon conversion is rather low in this stage, Table 3. Increase of hydrolysis temperature to 900°C improves the elemental carbon conversion, which reaches 51.5% for 10 min solid residence time, Table 3. This improvement results from enhancement of the devolatilization and hydrocracking reactions with temperature. Elemental H and O conversions, are in all cases high (84-96% w/w), Table 3. Thus, during hydrolysis, cleavage of oxygen containing groups occurs. In the same period, cleavage and release of aliphatic and aromatic groups take place [8], resulting in high hydrogen conversion (84-96% w/w). The chars formed are, hence, rich in carbon and ash.

In the second stage, the carbon-carbon dioxide gas-solid reaction is practically the only one taking place, since the volatile matter has been almost completely removed during hydrolysis [8,9]. Traces of hydrocarbons detected in this stage, come from residual volatiles of the original lignite.

Conversion of organic matter (essentially C-conversion) in the second stage depends on the history of the char and on the conditions of CO<sub>2</sub> gasification, i.e. temperature and residence time. Increase of the solids residence time at low temperature (800°C) hydrolysis, increases conversion in the second stage, Fig 2. In contrast, at high



hydropyrolysis temperature (900°C) and solid residence time, conversion in CO<sub>2</sub> gasification decreases, Figs 2 and 3. Thus, chars prepared by hydropyrolysis at low T and residence time (800°C/2-5 min) yield 22% C-conversion when gasified in CO<sub>2</sub> at 800°C and 5 min, Fig 2. As the residence time in hydropyrolysis stage increases, more active sites are formed in the char, capable of further reaction with CO<sub>2</sub>, thereby increasing C-conversion, Fig 2,3. For the same hydropyrolysis char, conversion increases by 20 to 30% with increasing residence time in CO<sub>2</sub> gasification.

Similar behavior is also exhibited by hydrochars prepared at 900°C. However, CO<sub>2</sub> gasification of these chars yields lower conversions in the second stage, as compared with chars prepared at 800°C and 10 min, Fig 2,3. Conversion in CO<sub>2</sub> gasification decreases further with an increase in hydropyrolysis solid residence time, for chars prepared at 900°C, Fig 2. This is probably due to active site deactivation, occurring at high hydropyrolysis temperatures (900°C) and long residence times, [10-12] of Fig 2,3.

Formation of CH<sub>4</sub> and other hydrocarbons practically stops during CO<sub>2</sub> gasification of the chars. Hydropyrolysis chars react in the second stage according to the Boudouard reaction, and produce CO which is the main gaseous product, Figs 4 and 5. We should note here that second-stage product yields are presented per gram of initial lignite (daf), permitting direct comparison of yields between the two stages. Carbon monoxide formation in the second stage, improves with hydrochars obtained at 800°C and long residence time, Fig 4 and 5. However, chars prepared at 900°C and long residence times yield low CO product by CO<sub>2</sub> gasification, Fig 4 and 5, due to active site deactivation under such conditions. These results are in good agreement with the observed C-conversions discussed previously. Such agreement should be anticipated since CO is formed by char reaction with CO<sub>2</sub> in the second stage.

Elemental carbon conversion of CO<sub>2</sub> gasification chars at 800°C or 900°C and 5 min residence time, is rather low and incomplete (29-46% w/w), Fig 6. The increase of second stage solid residence time improves elemental C-conversion for both CO<sub>2</sub> gasification temperatures (800°C & 900°C), Fig 6. It should be noted here that second stage elemental C-conversion values at 900°C are higher than at 800°C, Fig 6, due to enhancement of the Boudouard reaction rate with increasing temperature.

Similar to weight loss, elemental C-conversion in the second stage depends on the history of the char, ie hydropyrolysis temperature and residence time. Increase of the solid residence time at low temperature (800°C) hydropyrolysis, increases elemental carbon conversion in the second stage, Fig 6. In contrast, at high hydropyrolysis temperature (900°C), and long solid residence time, second stage elemental C-conversion decreases, Fig 6. This behavior is in agreement with the previously discussed active carbon deactivation at high hydropyrolysis temperatures and times.

From Figs 2-5 it is apparent that an optimum hydropyrolysis temperature and residence time should exist, which, combined with CO<sub>2</sub> gasification, leads to maximum carbon conversion. The optimum corresponds to hydrogasification at 900°C and 2 to 5 min. Thus, a hydropyrolysis char, obtained at 900°C/2 min, reacted with CO<sub>2</sub> at 800°C and 10 min, gives a maximum total carbon conversion of about

88%. For  $\text{CO}_2$  gasification at  $900^\circ\text{C}$  and 10 min total C-conversion reaches 98%. At other temperatures and residence times, overall conversions are somewhat lower (84-95%), at longer times (15-20 min).

These results suggest that hydropyrolysis at  $900^\circ\text{C}$  and 2 to 5 min generates more active sites in the lignite matrix than hydropyrolysis at  $800^\circ\text{C}$  at the same residence time, resulting in higher second-stage char conversions. However, prolongation of the residence time (10 min) at lower hydropyrolysis temperature ( $800^\circ\text{C}$ ) improves C-conversion in the second stage, Fig 2. Thus, total C-conversion of hydrochars prepared at  $800^\circ\text{C}/10$  min is comparable to that of chars obtained at  $900^\circ\text{C}/2$  min. This indicates that similar amounts of active sites exist in the lignite matrix of these two chars, further supporting the notion of deactivation at high hydropyrolysis temperature and long time.

The above comments on optimality are based solely on total carbon conversion. However, selection of optimum operating conditions should also take into account the yields of gaseous products. Thus, maximum  $\text{CH}_4$  production is observed for samples hydropyrolyzed at  $900^\circ\text{C}$  and 10 min. This maximum should be anticipated, since  $\text{CH}_4$  formation via the heterogeneous carbon-hydrogen gas-solid reaction becomes significant for long hydropyrolysis times. Maximum  $\text{CO}$  production is observed for chars hydropyrolyzed at  $900^\circ\text{C}$  and 2 min and subsequently gasified in  $\text{CO}_2$  at  $900^\circ\text{C}$  and 10 min (about  $1700 \text{ cm}^3 \text{ CO/g lignite daf}$ ). Maximum total carbon conversion (97.8% w/w) is also observed at these conditions. Thus, optimum conditions for carbon conversion coincide with these for  $\text{CO}$  formation. However, maximum  $\text{CH}_4$  production appears at somewhat different conditions.

#### ACKNOWLEDGEMENT

The authors wish to thank the European Coal and Steel Community and the Chemical Process Engineering Research Institute for financial support of this work.

#### REFERENCES

1. Kokorotsikos, P.S., Stavropoulos, G.G., Sakellariopoulos, G.P., Proc. 1985 Int. Conf. Coal Science, Sydney, Oct. 1985, 253.
2. Kokorotsikos, P.S., Stavropoulos, G.G., Sakellariopoulos, G.P., Proc. Int. Symp. on "Fundamentals of Catalytic Carbon and Coal Gasification", FUNCAT COGAS 86, Rolduc, The Netherlands, May 1986, 327.
3. Sakellariopoulos, G.P., Kokorotsikos, P., Korili, S., Stavropoulos, G., "Catalytic Gasification of Lignites for Synthetic Fuels", Final Report, Contr. No 7220, EC/701, Thess/niki, October 1987.
4. Adanez, J., Miranda, J.L. and Gavilan, J.M., Fuel, 1985, 64, 801.
5. Koenig, P.C., Squires, R.G. and Laurendeau, N.M., Fuel, 1986, 65, 412.
6. E. Hippo and D.L. Walker, Jr., Fuel, 1975, 54, 245.
7. Sams, D.A. and Shadman, F., AIChE J., 1986, 32, 1132.
8. Anthony, D. and Howard, J.B., AIChE J., 1976, 22, 625.
9. Gavalas, G.R., "Coal Pyrolysis", Elsevier, NY 1982.
10. Johnson, J.L., "Kinetics of Coal Gasification", J. Wiley & Sons Inc, NY 1979.
11. P. Ehrburger, F. Louys and J. Lahaye, Carbon, 1989, 27, 389.
12. Elliot, M.A. "Chemistry of Coal Utilization", Second Supplementary Volume, J Wiley and Sons, NY 1981.

Table 1 : Total gaseous products during hydrolysis at 800°C

Product	cm <sup>3</sup> /g lignite d.a.f. *					
	800°C/2 min		800°C/5 min		800°C/10 min	
	Yield	Selectivity(%)	Yield	Selectivity(%)	Yield	Selectivity(%)
CH <sub>4</sub>	26.6	8.2	42.5	11.8	68.4	15.7
C <sub>2</sub> H <sub>6</sub>	6.5	2.0	8.0	2.2	14.0	3.3
C <sub>3</sub> H <sub>8</sub>	1.5	0.5	2.0	0.6	2.3	0.5
CO	128.0	39.1	139.0	38.4	236.0	54.3
CO <sub>2</sub>	164.0	50.3	170.0	47.1	114.0	26.2
CO+CO <sub>2</sub>	292.0	89.4	309.0	85.5	350.0	80.5
CO/CO <sub>2</sub>		0.8		0.8		2.1

Table 2 : Total gaseous products during hydrolysis at 900°C

Product	cm <sup>3</sup> /g lignite d.a.f. *					
	900°C/2 min		900°C/5 min		900°C/10 min	
	Yield	Selectivity(%)	Yield	Selectivity(%)	Yield	Selectivity(%)
CH <sub>4</sub>	52.3	11.6	72.2	14.4	77.1	14.8
C <sub>2</sub> H <sub>6</sub>	11.8	2.6	12.0	2.4	12.7	2.4
C <sub>3</sub> H <sub>8</sub>	0.8	0.2	1.0	0.2	1.2	0.2
CO	306.0	67.7	337.0	67.2	378.0	72.4
CO <sub>2</sub>	81.0	17.9	80.0	15.9	53.0	10.2
CO+CO <sub>2</sub>	387.0	85.6	417.0	83.0	431.0	82.8
CO/CO <sub>2</sub>		3.8		4.2		7.1

Table 3 : Composition and conversion of hydrolysis chars

Sample Code	Temp/Time (°C,min)	Weight loss (% w/w)	Char Composition (% w/w)					Elemental conversion (Ci)% w/w			
			C	H	N	ASH	O	C <sub>g</sub>	C <sub>h</sub>	C <sub>o</sub>	C <sub>u</sub>
TS1a	800/2	48.10	55.74	1.21	1.18	31.97	9.30	36.60	86.60	51.80	83.50
TS2a	800/5	49.20	57.80	0.93	1.19	32.69	8.92	37.90	89.90	52.40	88.00
TS3a	800/10	51.70	55.04	1.22	0.66	34.35	8.13	43.60	87.40	74.90	86.60
TS4a	900/2	54.10	54.21	0.42	1.27	36.15	7.35	47.20	95.90	54.10	88.50
TS5a	900/5	55.00	54.72	0.51	1.01	36.92	6.24	48.80	95.10	64.20	90.40
TS6a	900/10	56.70	52.84	0.44	1.15	38.33	6.24	51.50	95.90	60.80	90.20

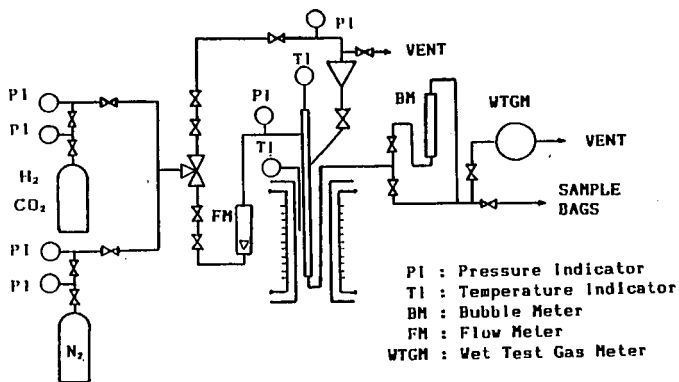


Figure 1 : Flow diagram of a rapid quenching gasification system.

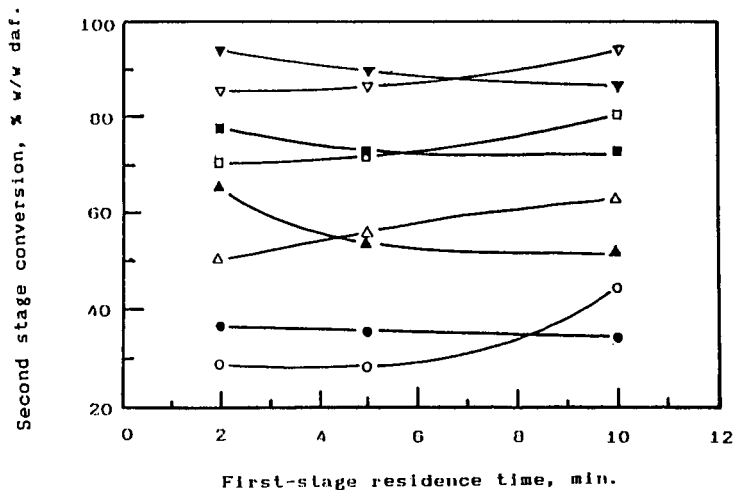


Figure 2 : Effect of hydropyrolysis temperature and residence time on weight loss during  $\text{CO}_2$  gasification. Open points: hydropyrolysis at  $800^\circ\text{C}$ ; closed points: hydropyrolysis at  $900^\circ\text{C}$ .  $\text{CO}_2$  gasification:  $\circ$  :  $800^\circ\text{C}/5$  min,  $\Delta$  :  $800^\circ\text{C}/10$  min,  $\square$  :  $900^\circ\text{C}/5$  min,  $\nabla$  :  $900^\circ\text{C}/10$  min.

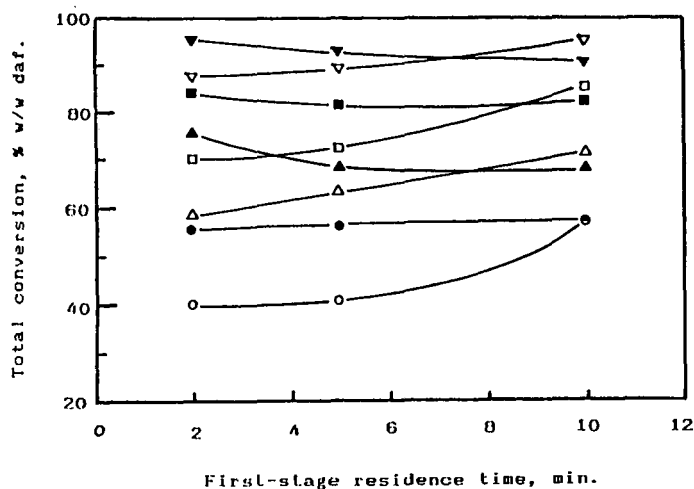


Figure 3 : Effect of hydropyrolysis temperature and residence time on total weight loss. Open points: hydropyrolysis at 800°C; closed points: hydropyrolysis at 900°C. CO<sub>2</sub> gasification: ○ ● : 800°C/5 min, △ ▲ : 800°C/10 min, □ ■ : 900°C/5 min, ▽ ▼ : 900°C/10 min.

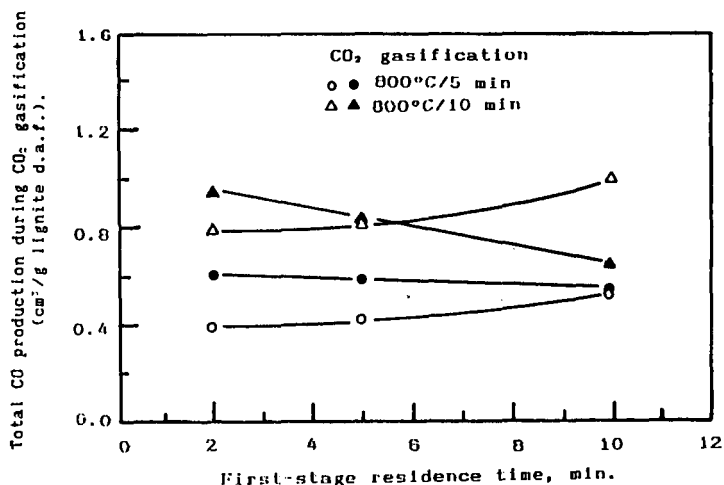


Figure 4 : Effect of hydropyrolysis temperature and residence time on total CO production, during CO<sub>2</sub> gasification at 800°C. Open points: hydropyrolysis at 800°C; closed points: hydropyrolysis at 900°C.

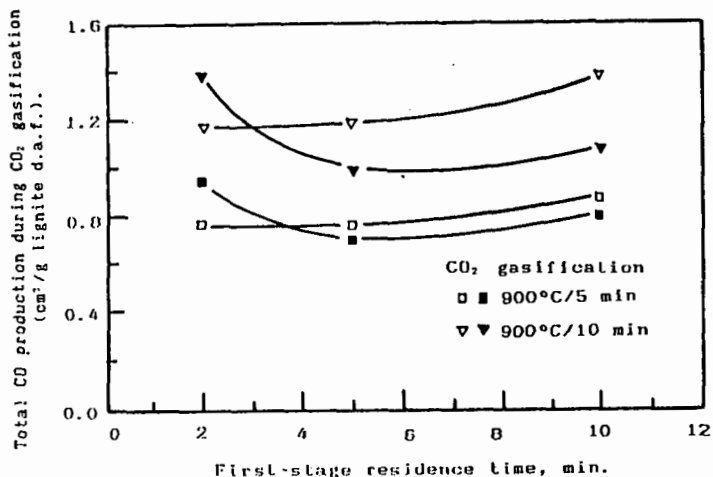


Figure 5 : Effect of hydrolysis temperature and residence time on total CO production, during CO<sub>2</sub> gasification at 900°C. Open points: hydrolysis at 800°C; closed points: hydrolysis at 900°C.

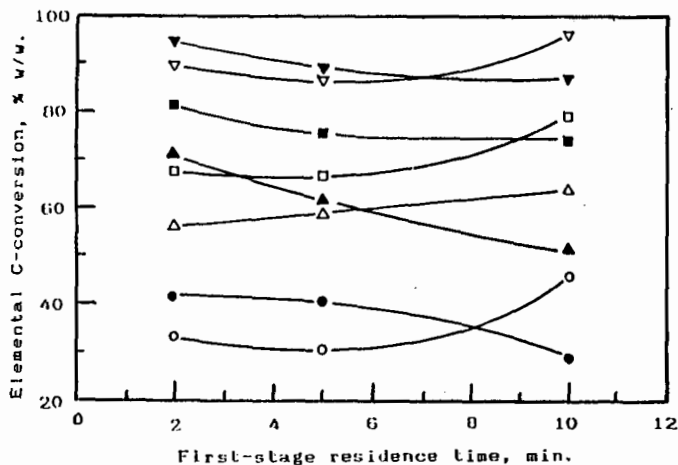


Figure 6 : Effect of hydrolysis temperature and residence time on elemental C-conversion during CO<sub>2</sub> gasification. Open points: hydrolysis at 800°C; closed points: hydrolysis at 900°C. CO<sub>2</sub> gasification: ○ ● : 800°C/5 min, △ ▲ : 800°C/10 min, □ ■ : 900°C/5 min, ▼ ▽ : 900°C/10 min.